IN VIVO MULTI-MODAL NEUROIMAGING IN MOUSE MODELS OF DYT1 DYSTONIA

By

JESSE C. DESIMONE

A DISSERTATION PRESENTED TO THE GRADUATE SCHOOL
OF THE UNIVERSITY OF FLORIDA IN PARTIAL FULFILLMENT
OF THE REQUIREMENTS FOR THE DEGREE OF
DOCTOR OF PHILOSOPHY

UNIVERSITY OF FLORIDA

2019

To my mother, Julie

ACKNOWLEDGMENTS

This work would not have been possible without the support of many individuals. I have had the distinct pleasure of being mentored by Dr. David Vaillancourt, who exemplifies the qualities of research, leadership, and professionalism to which I aspire. I thank Dr. Vaillancourt for his esteemed guidance and teaching. I thank current and former members of the Laboratory for Rehabilitation Neuroscience for fostering a positive and intellectually stimulating research environment. A special thank you to Dr. Roxana Burciu and Dr. Luis Colon-Perez, who dedicated significant time towards my training in advanced neuroimaging. I thank my dissertation committee members, Dr. Stephen Coombes, Dr. Rachael Seidler, and Dr. Yuqing Li for their respective guidance and input. I thank my loving parents, Julie and Billy, who have always been my biggest source of encouragement and support in both personal and academic life. I thank them for instilling the qualities and values that have allowed me to be successful in pursuit of higher education. Finally, I thank Kaleigh for her endless love, support, and encouragement. Her selflessness and passion for helping others provides added inspiration each day to be a great scientist.

TABLE OF CONTENTS

page

LIST OF TABLES

Table page

LIST OF FIGURES

LIST OF ABBREVIATIONS

ΔE	Removal of a single glutamic acid residue
ΔGAG	Trinucleotide deletion in the DYT1/TOR1A gene
ACh	Acetylcholine
AUC	Receiver operating characteristic area under the curve
BOLD	Blood-oxygen-level dependent
cKO	Conditional knockout: Site-specific gene deletion using Cre-loxP flanking system
CNS	Central nervous system
CSF	Cerebrospinal fluid
d2KO	Mouse model with conditional knockout of torsinA from D2R-expressing neurons in striatum
D2R	Dopamine type-2 receptor
Dlx-cKO	Mouse model with conditional knockout of torsinA from forebrain cholinergic and GABAergic progenitor neurons
DTI	Diffusion tensor imaging
DYT1/Dyt1	Human/mouse nomenclature for gene encoding torsinA
FA/FA_T	Fractional anisotropy/tensor-corrected fractional anisotropy
FDR	False discovery rate
fMRI	Functional magnetic resonance imaging
FWER	Family-wise error rate
hMT	Transgenic mouse model overexpressing human mutant torsinA
ICA	Independent component analysis
KI	Knock-in mouse model characterized by targeted insertion of a transgene at a specific gene locus via homologous recombination
KO	Knockout mouse characterized by targeted gene deletion via homologous recombination

LTD	Long-term depression
MD/MD_T	Mean diffusivity/tensor-corrected mean diffusivity
MSN	Medium spiny neuron
NODDI	Neurite orientation dispersion and density imaging
ODI	Orientation dispersion index
PET	Positron emission tomography
rsfMRI	Resting-state functional magnetic resonance imaging
SCI	Striatal cholinergic interneuron
stimfMRI	Sensory-evoked functional magnetic resonance imaging
TOR1A/Tor1a	Human/mouse nomenclature for gene encoding torsinA; analogous to DYT1/Dyt1
V_{ic}	Intracellular compartment volume
V_{iso}	Isotropic free-water compartment volume
WT	Wild-type

Abstract of Dissertation Presented to the Graduate School
of the University of Florida in Partial Fulfillment of the
Requirements for the Degree of Doctor of Philosophy

IN VIVO MULTI-MODAL NEUROIMAGING IN MOUSE MODELS OF DYT1 DYSTONIA

By

Jesse C. DeSimone

August 2019

Chair: David E. Vaillancourt
Major: Health and Human Performance – Biobehavioral Science

Dystonia musculorum deformans (early-onset generalized dystonia or DYT1 dystonia) is a neurological movement disorder that causes a loss of muscle control, unintentional movements, and disabling postures. The genetic hallmark includes a 3-bp deletion in the DYT1/TOR1A gene encoding the protein torsinA. The pathophysiology of dystonia is not well understood, which presents an obstacle to the development of effective symptomatic and disease-modifying therapies. Convergent evidence from human and animal studies has led to the conceptual view that dystonia represents a network disorder involving dysfunction of connected motor regions of the cortex, basal ganglia, and cerebellum. What is missing from this perspective is a deep understanding of how torsinA deficiency within specific cell types of these regions cause changes in dystonia-related phenotype and systems-level brain pathophysiology. Developing an *in vivo* perspective of brain pathophysiology related to cell-specific loss of torsinA is fundamental to our understanding of the neural substrates underlying dystonia and developing effective therapeutic strategies. In the present work, high-field (11.1 Tesla) multi-modal neuroimaging was performed in three mouse models of dystonia characterized by distinct cellular insults to the torsinA protein. Adaptations in brain

function and microstructure were examined using functional and diffusion MRI, respectively. The results from these experiments yielded several important findings. First, mice carrying the corresponding gene mutation to human DYT1 dystonia or exhibiting the conditional knockout of torsinA within forebrain cholinergic and GABAergic cells exhibited widespread changes in the spatio-temporal correlation between low-frequency fluctuations in resting-state brain signal (i.e., functional connectivity). Second, the conditional knockout of torsinA from striatum-specific dopamine type-2 receptor expressing cells impaired blood-oxygen-level dependent signal activation and connectivity of sensorimotor regions, which correlated with motor performance deficits. Lastly, evidence from these studies establish the utility of advanced multi-compartment diffusion models as a potentially sensitive method to monitor microstructural adaptations *in vivo*.

CHAPTER 1
GENERAL INTRODUCTION

Classification of DYT1 Dystonia

Dystonia represents a group of neurological movement disorders characterized by sustained muscle contractions and antagonistic co-contractions, which give rise to unintentional movements and severe disabling postures. Dystonic movements are typically patterned and twisting, may be tremulous, often initiated or worsened by voluntary movement, and associated with an overflow of muscle activation (Albanese *et al*., 2013). Clinical expression ranges from focal dystonia affecting a single body region to generalized whole-body distribution. This regional manifestation can be linked to an established genetic cause or occur idiopathically. The most common and severe form of inherited dystonia is early-onset generalized dystonia (DYT1 dystonia: OMIM 128100), with an estimated prevalence of 111 per million and 0.7-50 per million in Ashkenazi Jewish and non-Jewish populations, respectively (Risch *et al*., 1990; 1995; Defazio *et al*., 2004). DYT1 dystonia typically begins as a focal entity during childhood or early adolescence and regional expression in many patients with early onset will progress to severe generalized distribution (Zilber *et al*., 1994; Greene *et al*., 1995; Bressman, 2000; O'Riordan *et* al., 2004; Svetel *et al*., 2007). The genetic hallmark of DYT1 dystonia includes the autosomal dominant inheritance of a three base-pair deletion (ΔGAG) in exon 5 of the TOR1A/DYT1 gene on chromosome 9q34, resulting in the elimination of a single glutamic acid residue in the carboxy terminal domain at position 302 or 303 of the encoded protein torsinA (ΔE-torsinA) (Ozelius *et al*., 1997).

TorsinA

TorsinA is an AAA+ (ATPase) neuronal protein resident of the endoplasmic reticulum (ER)/nuclear envelope (NE) complex (Hewett *et al*., 2000; Kustedjo *et al*., 2003; Liu *et al*., 2003) and is involved in a myriad of molecular and cellular functions (for review see Granata and Warner, 2010; Dauer, 2014). Homozygous knock-in (KI) of ΔE-torsinA (Tor1a ΔGAG/ΔGAG) cannot rescue the early postnatal lethality phenotype exhibited by mice lacking wild-type torsinA (Tor1a -/-), suggesting that ΔGAG encodes a loss-of-function allele (Dang *et al*., 2005; Goodchild *et al*., 2005). This loss-of-function may manifest within multiple mechanisms of the ER/NE system including impaired torsinA ATPase activity (Zhao *et al*., 2013), changes in binding affinity with ER/NE transmembrane proteins LAP1 and LULL1, which regulate enzymatic function (Goodchild and Dauer, 2004; Naismith *et al*., 2009; Vander Heyden *et al*., 2009; Zhao *et al*., 2013), and reduced production of wild-type torsinA (Torres *et al*., 2004; Goodchild and Dauer, 2004; Naismith *et al*., 2004). Furthermore, overexpression of ΔE-torsinA may induce NE structural perturbations (Hewett *et al*., 2000; Kustedjo *et al*., 2000; Bragg *et al*., 2004; Gonzalez-Alegre and Paulson, 2004; Goodchild *et al*., 2005; Liang *et al*., 2014), and the redistribution of NE proteins essential to nucleo-cytoskeletal dynamics (Nery *et al*., 2008; Vander Heyden *et al*., 2009; Jungwirth *et al*., 2011).

The exact pathogenic mechanism by which ΔE-torsinA regulates phenotypic manifestation of dystonia is not yet clear. Modifying or deleting the Dyt1 gene in murine models using gene targeting based on homologous recombination is opportune for uncovering the link between torsinA and dystonia. For example, the targeted insertion [knock-in (KI)] of ΔGAG at the Dyt1 gene locus will alter the functional domain of torisinA and cause partial loss of torsinA expression (e.g., Dang *et al*., 2005; Goodchild

et al., 2005), whereas torsinA cannot be expressed following the targeted deletion [knockout (KO)] of Dyt1 via frame-shift mutation. Moreover, Cre-loxP technology can assess effects of site-specific loss of torsinA expression by isolating and conditionally deleting Dyt1 within a specific subset of cell types [i.e., conditional KO (e.g., Yokoi *et al*., 2011; Pappas *et al*., 2015)]. Mouse studies provide *in vivo* support linking torsinA loss/dysfunction and recapitulation of motor features consistent with dystonia. Indeed, the insertional mutation of ΔGAG-Dyt1 transgene [Dyt1 +/ΔGAG: Dyt1 KI (Dang *et al*., 2005; Goodchild *et al*., 2005)], conditional KO of torsinA within cholinergic neurons (Sciamanna *et al*., 2012*b*; Pappas *et al*., 2018), and conditional KO of torsinA within cell types of the cerebral cortex (Yokoi *et al*., 2008; Liang *et al*., 2014), forebrain (Pappas *et al*., 2015), striatum (Yokoi *et al*., 2011; Yokoi *et al*., *in preparation*), and hind brain/cerebellum (Zhang *et al*., 2011; Yokoi *et al*., 2012; Liang *et al*., 2014; Fremont *et al*., 2017) have resulted in motor deficits ranging from subtle changes in motor coordination, balance, learning, and muscle co-contractions to severe overt twisting movements and postures. Missing from this perspective is an understanding of the systems-level changes in brain pathophysiology that relate to the loss of torsinA within specific cell types. Developing quantifiable *in vivo* assays of brain function and microstructure related to cellular-localized lesions of torsinA is fundamental to understanding the neural substrates of dystonia and developing effective symptomatic and disease-modifying therapies.

Network Model of Dystonia

Dystonia comprises a clinically heterogeneous group of disorders characterized by a various array of etiological, molecular, and cellular CNS insults. The *network model* represents a conceptual view that these various arrays of initial CNS insults must

converge upon a shared downstream systems-level pathway to ultimately produce the involuntary movements and disabling postures common to all forms of dystonia (Prudente *et al*., 2014; see also Neychev at al., 2011; Jinnah *et al*., 2017). It has become increasingly clear from neuropathology, neurophysiology, and neuroimaging studies that DYT1 dystonia manifests within widespread dysfunction at multiple levels of the brain, including the cortex, thalamo-basal ganglia circuit, and cerebellum/brainstem. Neuroanatomical tracing studies in rodents and non-human primates have revealed dense multi-synaptic integration pathways connecting the cortex, basal ganglia, and cerebellum (Bostan *et al*., 2013; Bostan and Strick, 2018; Bostan *et al*., 2018). The so-called cerebello-thalamo-cortical pathway has received considerable attention as conduit for convergence of dysfunctional motor network signals causing dystonia (Argyelan *et al*., 2009; Uluğ *et al*., 2011; Chen *et al*., 2014; Vo *et al*., 2015*a, b*). What remains less clear is whether network-level brain dysfunction underlying the expression of dystonia originates from a specific cell type or brain region.

Basal Ganglia

It is widely accepted that dystonia involves dysfunction of the basal ganglia, including striatal dopaminergic and cholinergic pathways (Perlmutter and Mink, 2004; Wichmann, 2008; Albanese and Lalli, 2012; Eskow Jaunarajs *et al*., 2015). In human studies, positron emission tomography (PET) has revealed reduced levels of dopamine type-2 receptor (D2R) binding in the striatum of DYT1 mutation carriers (Asanuma *et al*., 2005; Carbon *et al*., 2009). Changes in levels of dopamine metabolites have been reported in post-mortem DYT1 brains (Furukawa *et al*., 2000; Augood *et al*., 2002; Rostasy *et al*., 2003; Pappas *et al*., 2015). Anticholinergic drugs (e.g., trihexyphenidyl) can alleviate dystonic symptoms in patients (Jankovic, 2013; Termsarasab *et al*., 2016;

Luc and Querubin, 2017) and deep brain stimulation targeting of the globus pallidus internus (GPi) has emerged as an effective treatment option for medicinally refractory or clinically severe dystonia patients (Cif *et al*., 2010; Panov *et al*., 2013; Vidailhet *et al*., 2013).

In mouse models of dystonia, an imbalance between dopaminergic and cholinergic neurotransmission of the striatum has been implicated as a key pathophysiological feature. Dyt1 KI mice, which carry one ΔGAG-Dyt1 allele (genocopy of human DYT1 dystonia), exhibit reduced levels of 4-hydroxy, homovanillic acid and reduced D2R binding in the striatum (Dang *et al*., 2005; 2012). Dyt1 knock-down mice show reduced striatal 3,4-Dihydroxyphenylacetic acid levels (Dang *et al*., 2006), and striatal D2R-expressing conditional Dyt1 KO mice (Dyt1 d2KO) exhibited a selective reduction of striatal cholinergic interneurons (SCI) and reduced production of acetylcholine (ACh) and dopamine metabolites (Yokoi *et al*., *in preparation*). These models exhibit subtle behavioral abnormalities including deficits in fine motor coordination, balance, and learning (Dang *et al*., 2005; 2006; Yokoi *et al*., *in preparation*) and Dyt1 KI mice exhibit sustained contractions and intermittent co-contractions of hind limb muscles, which is a core feature of dystonia (DeAndrade *et al*., 2016). Notably, acute administration of muscarinic anticholinergic drugs can restore normal motor control in various mouse models of dystonia (Dang *et al*., 2012; Pappas *et* al., 2015; DeAndrade *et al*., 2016) and is therefore a major source of predictive validity.

Dyt1 KI mice exhibit impaired synaptic plasticity in the striatum in response to high-frequency stimulation of cortico-striatal glutamatergic afferents, including long-term depression (LTD) deficit and enhanced long-term potentiation (LTP) (Dang *et al*., 2012;

Martella *et al*., 2014). Similar abnormalities in cortico-striatal synaptic plasticity have also been observed in transgenic mice and rats overexpressing human mutant torsinA hMT (Martella *et al*., 2009; Grundmann *et al*., 2012). In hMT mice, SCIs exhibit paradoxical excitation in response to the D2R agonist quinpirole (Pisani *et al*., 2006; Sciamanna *et al*., 2011). This effect has also been observed in mice with conditional KO of torsinA within cholinergic neurons (Sciamanna *et al*., 2012*b*). Abnormal cortico-striatal synaptic plasticity is hypothesized to reflect a hypercholinergic state caused by defective D2R binding and disinhibited release of endogenous ACh from SCIs that acts on indirect pathway MSN muscarinic ACh receptors (mAChR) (Calabresi *et al*., 1992*a, b*; 1994; Wang *et al*., 2006; Calabresi *et al*., 2014; Lim *et al*., 2014; Scarduzio *et al*., 2017). In hMT and Dyt1 KI mice, repetitive stimulation of thalamo-striatal axons produced a shortened pause response in SCIs and altered pre- and post-synaptic activation of MSNs through involvement of M1 and M2 mAChRs (Martella *et al*., 2009; Grundmann *et al*., 2012). Conditioned pauses in the tonic activity of SCIs in response to environmental stimuli are thought to play a central role in action selection and motor learning (Graybiel *et al*., 1994; Maurice *et al*., 2004; Cragg, 2006; Wang *et al*., 2006; Apicella, 2007; Aosaki *et al*., 2010; Lim *et al*., 2014).

The maintenance and function of SCIs are particularly vulnerable to the loss of torsinA within a set of neuronal cell types. For example, conditional KO of torsinA from forebrain (i.e., striatum, cortex, globus pallidus, basal forebrain, and reticular thalamic nucleus) cholinergic and GABAergic progenitor neurons (Dlx-cKO mice) engenders SCI-specific consequences, including a 40% reduction in cell count, somatic swelling, and dysfunctional electrophysiological properties. These changes overlap with a period

of high brain development and cause juvenile onset of overt dystonic-like twisting movements, which are responsive to anticholinergic therapies (Pappas *et al*., 2015). Similarly, conditionally deleting torsinA from cholinergic neurons throughout the neuraxis resulted in a 34% reduction in SCI number and overt postural abnormalities including spinal kyphosis and trunk twisting (Pappas *et al*., 2018). Collectively, the aforementioned work points to the regulation of dopaminergic and cholinergic pathways of the striatum as a key target for treating dystonia.

Cerebellum

It has become increasingly clear that dysfunction of the cerebellum may also contribute to dystonia pathogenesis (Shakkottai *et al*., 2017). Genetic, pharmacological, and surgical intervention studies in animal models in particular, have provided strong evidence linking abnormal cerebellar signaling output and phenotypic expression consistent with dystonia. For example, cerebellar torsinA knock-down mice developed uncoordinated movements and frequent dystonic postures that related to abnormal high-frequency burst firing patterns of Purkinje cells and deep cerebellar nuclei (Fremont *et al*., 2017; see also Fremont *et al*., 2014; 2015). The dystonic (dt) rat model is genetically characterized by an autosomal recessive insertional mutation of the Atcay allele that encodes Caytaxin, a critical mediator in Purkinje cell climbing fiber input (Xiao and LeDoux, 2005; Xiao *et al*. 2007). The dt rat demonstrates progressive axial and appendicular dystonia that correlates with abnormal burst firing of Purkinje cells (LeDoux *et al*., 1998; LeDoux and Lorden, 2002). Tottering (tg) mice, which are generated via recessive mutation of Cacna1a encoded granule and Purkinje cell $Ca_v2.1$ calcium channels, exhibit paroxysmal dyskinesia and episodic dystonic attacks that relate to abnormal cerebellar activity (Fletcher *et al*., 1996; Doyle *et al*., 1997; Walter *et*

al., 2006; Chen *et al*., 2009). Inducing cerebellar hyperexcitability via microinjections of kainate and AMPA glutamate receptor agonists triggered generalized dystonia in normal mice (Pizoli *et al*., 2002; Neychev *et al*., 2008; Fan *et al*., 2012). In contrast, cerebellectomy abolishes dystonia in dt and tg models (LeDoux *et al*., 1993; Neychev *et al*., 2008), as does genetic eradication of Purkinje cell efferents in tg mice (Campbell *et al*., 1999; Hisatsune *et al*., 2013; Raike *et al*., 2013).

Other findings in animal models of dystonia point to a systems-level interaction between the cerebellum and basal ganglia. Zhao *et al*. (2011) reported increased gluco-utilization in the inferior olive and substantia nigra pars compacta and decreased gluco-utilization in the medial and lateral putamen, indicating a shift in metabolic demand between the cerebellum and basal ganglia. In tg mice, cerebellectomy abolished dystonic attacks, whereas dystonic attacks were exaggerated by subclinical striatal lesions using 6-hydroxydopamine or quinolinic acid (Neychev *et al*., 2008). Chen *et al*. (2014) reported a correlation between electromyographic activity and abnormal neuronal activity in the dorsolateral striatum in a mouse model of rapid onset dystonia parkinsonism caused by selective partial block of cerebellar sodium pumps (see also Calderon *et al*., 2011). Furthermore, cerebellar-induced dystonia in these animals was rapidly alleviated via electrical lesions or optogenetic silencing of the contralateral nucleus of the thalamus.

Neuroimaging in Dystonia

Functional MRI in Dystonia

Brain imaging studies have provided strong support for the conceptual view that dystonia represents a large-scale network disorder involving cortical and subcortical regions. For example, a series of studies by Eidelberg and colleagues using [^{18}F]-FDG

PET imaging at rest revealed abnormal gluco-metabolism in the lentiform nuclei (posterior putamen, globus pallidus), supplementary motor area, and cerebellum irrespective of clinical penetrance in DYT1 mutation carriers (Eidelberg *et al*., 1998; Trošt *et al*., 2002; Carbon *et al*., 2004). A distinct spatial covariance pattern of abnormal metabolism was revealed in the pre-supplementary motor area, parietal cortex, precuneus, thalamus, cerebellum, and brainstem in manifesting compared to non-manifesting DYT1 mutation carriers (Carbon and Eidelberg, 2009). Assays of task-related impairments in the motor domain using $H_2{}^{15}O$-PET were revealed in sensorimotor cortex, supplementary motor area, pre-motor cortex, and inferior parietal lobule in manifesting DYT1 patients during a kinematic limb control task (Carbon *et al*., 2010). Clinically unaffected DYT1 mutation carriers revealed abnormalities of pre-frontal, auxiliary motor, associative parietal and occipital, and cerebellar regions during a motor sequence learning task (Ghilardi *et al*., 2003; Carbon *et al*., 2008*a*). Furthermore, rest- and task-related activation and connectivity changes have been consistently reinforced in focal dystonia studies (Simonyan and Ludlow, 2010; 2012; Delnooz *et al*., 2013; 2015; Battistella *et al*., 2016; 2017; Burciu *et al*., 2017; Filip *et al*., 2017; Li *et al*., 2017; Battistella and Simonyan, 2019). In agreement with large-scale network-level changes, a set of studies using *in vivo* [^{18}F]-FDG micro-PET in Dyt1 KI and Dyt1 KO mice revealed abnormal metabolic changes in sensorimotor cortex, striatum, globus pallidus, subthalamic nucleus, and cerebellar vermis (Uluğ *et al*., 2011; Vo *et al*., 2015*a*).

Diffusion MRI in Dystonia

Although subtle neuropathological changes have been reported – including enlargement of dopaminergic neurons and midbrain containing ubiquitin-inclusions

(Rostasy *et al*., 2003; McNaught *et al*., 2004; Paudel *et al*., 2014) – brains of patients with DYT1 dystonia typically lack consistently identifiable changes in gross brain structure. It is, however, important to highlight the increasing evidence of adaptations in brain microstructure that may contribute to dystonia. Studies in Dyt1 KI mice have revealed morphological changes of SCIs and MSNs (Song *et al*., 2013), shorter primary dendrites and reduced spines of Purkinje cells (Zhang *et al*., 2011; Song *et al*., 2014), and brainstem ubiquitin- and torsinA-positive aggregation (Dang *et al*., 2005). Diffusion tensor imaging (DTI) studies have provided evidence of microstructural adaptations within segments of the cerebello-thalamo-cortical pathway. Fractional anisotropy (FA), a conventional DTI measure of axonal coherence, was reduced in sensorimotor cortical white matter in a cohort of manifesting and non-manifesting DYT1 mutation carriers (Carbon *et al*., 2004*b*), as well as sensorimotor cortical white matter and the pontine brainstem adjacent to the superior cerebellar peduncle in a clinically affected cohort comprising both DYT1 and DYT6 patients (Carbon *et al*., 2008*b*). Similarly, *ex vivo* DTI in Dyt1 KO mice showed reduced FA of the sensorimotor cortex, striatum, and brainstem (Vo *et al*., 2015*a*). Using probabilistic tractography, microstructural connectivity of the cerebello-thalamic tract was reduced in DYT1 mutation carriers irrespective of clinical penetrance and the degree of connectivity of this pathway was inversely related to activation of the sensorimotor cortex and SMA (Argyelan *et al*., 2009). Clinically unaffected carriers, however, were associated with an additional tract lesion within distal thalamo-cortical projections to the cerebral cortex. The proposed *tandem lesion model* (Arygelan *et al*., 2009; Niethammer *et al*., 2011) argues that a “second hit” of the distal portion of the cerebello-thalamo-cortical pathway, in tandem

with more proximal lesions of cerebellar outflow segments, mitigates clinical penetrance by regulating the transmission of aberrant cerebello-thalamic signals to somatotopically relevant cortical sensorimotor regions (Niethammer *et al*., 2011; see also Vo *et al*., 2015*b*). *Ex vivo* DTI in Dyt1 KI mice, which may better serve as a model of the non-manifesting DYT1 carrier state, provided translational support of this assertion. Dyt1 KI mice exhibited reduced fiber tract counts in the rostral and caudal pontine-cerebellar pathway, as well as reduced FA in proximal and distal segments of the cerebello-thalamo-cortical tract (Uluğ *et al*., 2011).

Objectives and Significance

Brain imaging studies in humans and animal models of DYT1 dystonia have collectively supported the conceptual view that dystonia represents a network disorder comprising cortical, basal ganglia, and cerebellar regions. In rodent studies, the loss of torsinA within multiple cell types of the cortex, basal ganglia, and cerebellum can cause behavioral abnormalities and motor features consistent with dystonia. It is not yet clear how the deficiency or dysfunction of torsinA within specific cell types of these regions and associated phenotype relates to systems-level changes in brain pathophysiology *in vivo*. Developing an *in vivo* perspective of brain function related to cellular-localized loss of torsinA is fundamental to our understanding of dystonia and developing effective therapeutic strategies. Three mutant mouse models characterized by distinct cellular insults to the dystonia protein torsinA were used in these studies. Specifically, Chapter 2 examined Dyt1 KI mice (Dang *et al*., 2005), which exhibit the heterozygous 3-base pair deletion analogous to human ΔGAG-DYT1 carriers. Chapter 3 examined an overtly symptomatic mouse model with conditional KO of torsinA within forebrain cholinergic

and GABAergic neurons in one allele and unconditional KO of torsinA within the other allele (Dlx-cKO mice: Pappas *et al*., 2015). Lastly, Chapter 4 examined a mouse model characterized by conditional Dyt1 homozygous KO of torsinA within D2R-expressing neurons of the striatum [Dyt1 d2KO (Yokoi *et al*., *in preparation*)].

High-field strength (11.1 Tesla) functional and diffusion MRI was used to examine systems-level changes brain function and microstructure. Resting-state fMRI (rsfMRI) in combination within either maximum spatial separation independent component analysis (ICA) (McKeown *et al*., 1998*a, b*; Calhoun *et al*., 2001*a, b*) or seed-based correlation (e.g., Biswal *et al*., 1995; Fox *et al*., 2005) was used to examine whole-brain functional connectivity based on the inter-regional temporal coherence in low frequency (0.01 to 0.1 Hz) blood-oxygen-level dependent (BOLD) signal fluctuations during rest. A drawback of rsfMRI is that it does provide consideration of task-positive network properties. Identifying brain regions functionally modulated by task conditions may provide better insight into the functional topology underlying sensorimotor control deficits in dystonia. To overcome this limitation, BOLD activation and functional connectivity of task-related sensorimotor regions was examined using fMRI in combination with exogenous thermal stimulation of the hind limb [sensory-evoked fMRI (stimfMRI)] in Dyt1 d2KO mice. Lastly, diffusion MRI in combination with advanced multi-compartment modeling was used to provide an *in vivo* perpective of brain microstructural adaptations. Multi-compartment techniques provide an advantage over conventional single-tensor DTI indices because they can better account for sources of partial volume bias such as CSF contamination (Metzler-Baddeley *et al*., 2012; Jones *et al*., 2013) and high neurite orientation distribution (Zhang *et al*., 2012). To account for

potential partial volume confounds, tissue and non-tissue compartments were modeled separately using either single-shell diffusion MRI combined with a two-compartment free-water model (Pasternak *et al*., 2009) or multi-shell high-angular-resolution diffusion imaging (HARDI) combined with a three-compartment neurite orientation dispersion and density imaging model [NODDI (Zhang *et al*., 2012)].

CHAPTER 2
IN VIVO IMAGING REVEALS IMPAIRED CONNECTIVITY ACROSS CORTICAL AND SUBCORTICAL NETWORKS IN A MOUSE MODEL OF DYT1 DYSTONIA

Chapter Summary

Developing *in vivo* functional and microstructural neuroimaging assays in Dyt1 ΔGAG heterozygous knock-in (Dyt1 KI) mice can provide insight into the pathophysiology underlying DYT1 dystonia.* The current study examined *in vivo* functional connectivity of large-scale cortical and subcortical networks in Dyt1 KI mice and wild-type (WT) control mice using resting-state functional magnetic resonance imaging and an independent component analysis. Diffusion MRI was used to examine how microstructural integrity across the basal ganglia and cerebellum directly relates to impairments in functional connectivity. Compared to WT mice, Dyt1 KI mice exhibited increased functional connectivity across the striatum, thalamus, and somatosensory cortex; and reduced functional connectivity in the motor and cerebellar cortices. Further, Dyt1 KI mice demonstrated elevated free-water in the striatum and cerebellum compared to WT mice and increased free-water was correlated with impairments in functional connectivity across basal ganglia, cerebellum, and sensorimotor cortex. The current study provides the first *in vivo* MRI-based evidence in support of the hypothesis that the deletion of a 3-base pair (ΔGAG) sequence in the Dyt1 gene encoding torsinA has large-scale effects on *in vivo* functional connectivity and microstructural integrity across the sensorimotor cortex, basal ganglia, and cerebellum.

* A version of this chapter has been published as DeSimone JC, Febo M, Shukla P, Ofori E, Colon-Perez LM, Li Y, Vaillancourt DE. In vivo imaging reveals impaired connectivity across cortical and subcortical networks in a mouse model of DYT1 dystonia. Neurobiol Dis 2016; 95: 35-45. Reprinted as per Elsevier Author's Rights.

Introduction

Early-onset generalized dystonia (DYT1) is an autosomal dominant movement disorder with reduced penetrance that typically presents during early childhood through adolescence (Fahn, 1988; Ozeluis and Lubarr, 1999). Motor impairments are characterized by involuntary and sustained hyperactive muscle contractions resulting in uncontrolled upper and lower extremity movements and disabling postures (Breakefield *et al*., 2008; Albanese *et al*., 2013). In humans, DYT1 represents the most common genetic hallmark of the primary dystonias, and is caused by a trinucleotide (ΔGAG) deletion in one allele of the DYT1/TOR1A gene, and corresponding removal of a single glutamic acid residue (ΔE) in the carboxyl terminal region of the torsinA protein (Ozelius *et al*., 1997; Breakefield *et al*., 2008). TorsinA is a member of AAA+ family of ATPases and is associated with a plethora of cellular functions including the provision of protein folding, neuroprotective refuge of oxidative stress, and prevention of protein aggregate formation (Goodchild and Dauer, 2005; Hewett *et al*., 2007; Goodchild *et al*., 2015).

Magnetic resonance imaging (MRI) in Dyt1 ΔGAG heterozygous knock-in (KI) mice (Dang *et al*., 2005; Goodchild *et al*., 2005) provides a translational basis for understanding the pathophysiology underlying DYT1 dystonia. In particular, the Dyt1 KI mouse model represents a genetically derived experimental corollary akin to most human DYT1 dystonia patients (Ozelius *et al*., 1997). As well, although they do not display an overt dystonia-like phenotype (Breakefield *et al*., 2008), Dyt1 KI mice exhibit abnormally sustained muscle contractions paired with intermittent co-contractions (DeAndrade *et al*., 2016), which is a core feature of dystonia (van der Kamp *et al*., 1989; Berardelli *et al*., 1998). Previous work using [^{18}F]-FDG micro positron emission tomography (PET) *in vivo* has demonstrated increased regional metabolic activity in the

cerebellar vermis of Dyt1 KI mice (Uluğ *et al*., 2011) and Tor1a heterozygous knockout (Dyt1 KO) mice (Vo *et al*., 2015*a*). Similar regional cerebellar metabolic changes have been evidenced in a Dyt1 transgenic mouse model over-expressing human mutant torsinA [hMT mice (Zhao *et al*., 2011)]. An interesting question arising from this work is whether impaired functional connectivity exists in the cerebellum and other connected networks such as sensorimotor cortical and basal ganglia regions. The basis for this question stems from previous work employing high-frequency stimulation (HFS) and striatal field potential recordings *in vitro* showing that Dyt1 KI and hMT mice exhibit impaired inhibitory modulation and plasticity of cortico-striatal synaptic transmission [i.e., long-term depression: LTD (Dang *et al*., 2012; Martella *et al*., 2009; Wang *et al*., 2006)]. Moreover, although PET provides a robust measure of glucose utilization, it does not describe how functional networks are temporally correlated and functionally connected (Calhoun *et al*., 2001*a, b*). Since dystonia has been described as a functional circuit disorder (for reviews see Berardelli *et al*., 1998; Breakefield *et al*., 2008; Tanabe *et al*., 2009), it is important to determine how the ΔGAG mutation impairs functional connectivity across cortical and subcortical networks. The present study sought to examine functional connectivity in Dyt1 KI mice using high field (11.1 Tesla) resting-state functional magnetic resonance imaging (rsfMRI) and an independent component analysis [ICA (McKeown *et al*., 1998*a, b*; Calhoun *et al*., 2001*a, b*; Calhoun and Adali, 2012)]. The sensorimotor cortex, basal ganglia, and cerebellum were hypothesized to have altered functional connectivity patterns in Dyt1 KI compared to wild-type (WT) mice. A secondary goal of the current study was to determine how changes in structural integrity in the basal ganglia and cerebellum relate to functional connectivity. *In vivo*

diffusion MRI and a two-compartment free-water model (Pasternak *et al*., 2009) was used to disentangle diffusion properties of water in brain tissue from that of the free-water measurement in the extracellular space. It was hypothesized that elevated free-water in both basal ganglia and cerebellar regions directly relate to functional connectivity impairments across basal ganglia, cerebellar, and cortical networks.

Methods

Animals and Housing

Twenty adult male ΔGAG heterozygous knock-in mice (Dyt1 KI) and 20 male neurologically intact wild-type (WT) littermate controls (age range: 3–6 months) were used in this experiment. Dyt1 KI mice were prepared and genotyped using the PCR protocol as described by Dang *et al*. (2005). Mice were housed in groups of three in a temperature and humidity-controlled environment, maintained on an alternating 12 h light-dark cycle (i.e., lights off at 18:00 h), and were provided *ad libitum* food and water access. Animals were acquired and cared for in accordance with the ethical standards set forth by the Guide for the Care and Use of Laboratory Animals (8th edition, 2011) and the American Association for Laboratory Animal Science guidelines. All experimental protocols and procedures were approved and monitored by Institutional Animal Care and Use Committee (IACUC) at the University of Florida.

MRI Preparation and Data Acquisition

Mice were anesthetized for the duration of the experiment. Isoflurane anesthesia was delivered using compressed air through a Surgivet vaporizer (Dublin, OH, USA) connected to a charcoal trap. Mice were initially induced at 3–4% isoflurane for 1–2 min in an enclosed knock-in chamber. Anesthesia was reduced to 2% for animal setup and 1.0–1.5% for MRI acquisition. Anesthesia was periodically adjusted to accommodate a

respiration rate between 40 and 60 breaths per minute. Animals were placed in a prone position on a custom designed plastic mouse bed equipped with a bite bar to immobilize head motion during scanning. An in-house 2.5×3.5 cm quadrature surface transmit/receive coil was affixed to the top of the skull and tuned to 470.7 MHz (^{1}H resonance) for B^{1} excitation and signal detection (AMRIS Facility, University of Florida, Gainesville, FL, USA). Respiration rate was monitored using a respiration pad placed beneath the abdomen and core body temperature was maintained between 37 and 38°C using a recirculating waterbed heating system (SA Instruments, Stony Brook, NY).

MRI data were acquired using an 11.1 Tesla Magnex Scientific horizontal magnet (Agilent, Inc., Santa Clara, CA, USA, 205/120HD gradient set with 120 mm inner gradient bore size; maximum gradient strength 600 mT/m and rise time of 130 μs) at the McKnight Brain Institute, University of Florida. MRI preparation and data acquisition were controlled using Agilent Technologies VNMRJ software (Version 3.1). Preparation of the imaging protocol included localized whole-brain voxel shimming for magnetic field homogeneity and acquisition of reference anatomical scans for real-time visual depiction of animal positioning. The ordering of the MRI protocol consisted of one diffusion weighted scan (1 h 30 min), two rsfMRI scans (8 min each), and one reference anatomical T_2-weighted scan (5 min).

Diffusion weighted images were acquired using an 8-shot echo planar imaging (EPI) sequence with the following parameters: repetition time (TR) = 2,500 ms, echo time (TE) = 25.88 ms, field of view (FOV) = 19.2×19.2 mm, flip angle = 90°, max b-value = 900 s/mm^2, averages = 3, dummy scans = 2. Geometry was set up as follows: slices =

12, coronal orientation, thickness = 0.75 mm, gap = 0 mm, data matrix = 128×128 in-plane.

Functional MRI was performed using a 2-shot EPI sequence with the following parameters: TR = 1,000 ms, TE = 20 ms, FOV = 19.2×19.2 mm, flip angle = 90°, dummy scans = 4, slices = 12, coronal orientation, thickness = 0.75 mm, gap = 0 mm, data matrix = 64×64 in-plane.

Anatomical images were acquired using a fast-spin echo, T_2-weighted imaging sequence with the following parameters: TR = 2,000 ms, FOV = 19.2×19.2 mm, slices = 12, coronal orientation, thickness = 0.75 mm, gap = 0 mm, data matrix = 192×192 in-plane.

Functional MRI Data Preprocessing

Functional MRI data preprocessing was performed using the FMRIB Software Library (FSL: Oxford, UK) and custom-designed Unix shell scripts in AFNI (Cox, 1996). First, the first five volumes of both EPI sequences were discarded for magnetization equilibrium. The remaining volumes were concatenated into a single EPI image consisting of 410 volumes. The preprocessing analysis pipeline further included manual skull stripping for the removal of non-brain tissue and head motion correction. To standardize the data, the EPI image of each mouse brain was co-registered to their respective T_2-weighted image. The T_2-weighted image of each mouse was then registered to that of a single mouse brain and the resultant data matrix was applied to the EPI image via affine transformation with limited degrees of freedom and trilinear interpolation using FSL FLIRT. Additionally, spatial normalization and in-plane smoothing was performed on the EPI image using a FWHM Gaussian kernel of 0.4 mm^2

(x-y planes) and data was temporally filtered using a band pass filter with a cut-off frequency between 0.01 and 0.1 Hz.

Resting-state functional connectivity was examined using an independent component analysis [ICA (McKeown *et al*., 1998*a, b*; Calhoun *et al*., 2001*a, b*; Calhoun and Adali, 2012)] and the GIFT toolbox extension in MATLAB (http://www.nitrc.org/projects/gift) with Infomax algorithm. To quantify the maximum number of components, a stability analysis using ICASSO bootstrap mode was used – and this analysis determined that 50 mutually exclusive components be extracted for between-group analyses. Once the ICA component was identified, a back reconstruction was performed for each subject between each voxel time-series and the identified component time-series. The Pearson's correlation coefficient was then transferred to a z-value, and the z-value extracted from each voxel provides a standardized measure of the degree of connectivity with the identified component.

Diffusion MRI Data Preprocessing

Diffusion MRI preprocessing and analysis of free-water were performed using previously described methods (Ofori *et al*., 2015*a, b*; Planetta *et al*., 2016). A two-compartment free-water model (Pasternak *et al*., 2009) was used and the algorithm used in humans was modified for rodents. FSL and custom designed Unix shell scripts in AFNI were used to correct for eddy current/head motion artifacts and for compensation of the diffusion gradients in response to these corrections. Manual skull stripping was performed for the removal of non-brain tissue. Free-water and free-water-corrected fractional anisotropy (FA_T) maps were calculated from the preprocessed motion and eddy current corrected volumes using custom code written in MATLAB (version R2013a; MathWorks, Natick, MA). To create the free-water map, a

minimization procedure was used such that a two-compartment model was fit to each voxel to quantify free-water volume. The two-compartment model predicts the signal attenuation in the presence of free-water contamination. The free-water component is then eliminated from each voxel to generate the FA_T map. To standardize the data, the resultant free-water and FA_T maps were registered to a single mouse brain b0 image by an affine transformation matrix with limited degrees of freedom and trilinear interpolation using FSL FLIRT.

Statistical Analysis

For the rsfMRI data, a one-sample t-test was performed to determine significant clusters in each group following the back reconstruction to individual ICA components. This t-test identified significant ICA components in each group and provided confirmation that the technique was successful. Between-group comparisons were examined by submitting functional connectivity z-scores, FW, and FA_T values to voxel-wise, independent-samples t-tests (i.e., Dyt1 KI versus WT). Within- and between-group differences within a single voxel were thresholded at a voxel-level of $P < 0.005$. Functional and diffusion MRI data were corrected for multiple comparisons using a Monte Carlo simulation. The significance level of the contrasts of interest were set at minimum cluster size of 0.200 mm^3, the equivalent of $P < 0.05$ corrected using the family-wise error rate (FWER). Notably, one Dyt1 KI mouse was excluded from fMRI analyses due to incomplete volume acquisition during scanning and five mice (one Dyt1 KI and four WT) were removed from diffusion analyses due to motion-related signal distortions and issues with partial alignment during data preprocessing. For subjects included in both analyses (18 Dyt1 KI, 16 WT), the correlation between free-water values and functional connectivity z-scores was computed using Pearson's correlation

coefficients. Correlations were performed by combining free-water and functional connectivity values across Dyt1 KI and WT mice. P-values were adjusted for multiple comparisons using the Benjamini-Hochberg-Yekutieli false discovery rate [FDR ($P < 0.05$)].

A subsequent analysis sought to determine if functional connectivity differences alone could distinguish between groups (i.e., Dyt1 KI and WT). To accomplish that objective, the average z-score values from component clusters where significant between-group effects were detected were extracted from a training cohort of 24 (12 Dyt1 KI, 12 WT) randomly selected mice – and submitted to a linear kernel support vector machine classification algorithm with 10-fold cross-validation using the library for Support Vector Machines (LIBSVM) (Chang and Lin, 2011). Reliability of the algorithm was evaluated in a testing cohort of 15 mice (seven Dyt1 KI, eight WT).

Results

Resting-State fMRI: Identifying Components at 50-ICASSO

To delineate specific cortical, basal ganglia, and cerebellar components that displayed significant functional connectivity, a within-subjects t-tests on the rsfMRI data was performed separately for Dyt1 KI and WT groups. At 50-ICASSO, the results yielded reasonable anatomical decomposition of functional component clusters that were either localized to a specific brain region or region consisting of adjacent anatomical structures. In both groups, a high degree of functional connectivity was observed in several component clusters within each of the general cortical, basal ganglia, and cerebellar areas. In general, voxels expressing the highest degree of connectivity within each individual component were revealed across two to three slices. To elucidate, Fig. 2-1 provides an exemplar visual depiction of three separate

component clusters that overlap across multiple coronal slices within cortical, basal ganglia, and cerebellar brain structures. In line with previous ICA models in mice (Jonckers *et al*., 2011; Mechling *et al*., 2014), the results show unilateral functional connectivity patterns such that component clusters localized to one side of the brain were not revealed in homologous structures in the contralateral hemisphere.

Resting-State fMRI: Between-Group Differences in Functional Connectivity

Voxel-wise independent-samples t-tests were used to examine resting-state functional connectivity differences within the 50 identified ICA components (19 Dyt1 KI versus 20 WT). Dyt1 KI mice were associated with significantly increased functional connectivity compared to WT controls in the right striatum (Fig. 2-2A-B), primary somatosensory cortex (Fig. 2-2B), thalamus (Fig. 2-3A-B), and hippocampus (all corrected $P < 0.05$). In turn, compared to WT, Dyt1 KI mice showed decreased functional connectivity in the right primary motor cortex (Fig. 2-2C: PMC) and left cerebellar cortex (Fig. 2-4A–B) (all corrected $P < 0.05$). To further elucidate between-group functional connectivity differences, Fig. 2-5 shows subject-by-subject average z-score values for the aforementioned components.

Several aforementioned structures revealed multiple component clusters that were significantly different between groups. In terms of the right striatal component, Dyt1 KI mice showed significantly increased functional connectivity in two separate clusters localized to the right dorsal striatum (Fig. 2-2A: Dorsal-1, Fig. 2-2B: Dorsal-2). For the thalamic component, two separate component clusters in the ventral thalamic area (Fig. 2-3B: Vthal-1, Fig. 2-3A: Vthal-2) revealed significantly increased functional connectivity in Dyt1 KI mice. Similarly, Fig. 2-4 shows that Dyt1 KI mice were associated with significantly decreased functional connectivity in two separate clusters

within the cerebellar paramedian (Fig. 2-4A: PaL) and anisiform (Fig. 2-4B: AnL) lobules.

To determine if functional connectivity could accurately classify mouse genotype (Dyt1 KI, WT), the mean z-score values from clusters where significant between-group differences were detected were submitted to a linear kernel support vector machine algorithm with 10-fold cross validation. Mice were separated into a training dataset for the model using 24 mice (12 Dyt1 KI, 12 WT) and a testing dataset that included 15 mice (seven Dyt1 KI, eight WT). As shown in Table 2-1, the results of the analysis from the training cohort yielded an area under the curve (AUC) classification accuracy between 0.63 and 1.0. Importantly, three key regions that showed a strong AUC in the training dataset and prediction in the testing cohort were the primary motor cortex, dorsal striatum (Dorsal-1), and cerebellar cortex (AnL). As indicated in Table 2-1, other multi-region combinations also yielded high AUC and prediction values.

Diffusion MRI: Free-Water and Free-Water-Corrected FA

A two-compartment free-water model was used to examine free-water and FA_T differences in cortical, basal ganglia, and cerebellar regions between 19 Dyt1 KI and 16 WT mice. As shown in Fig. 2-6, Dyt1 KI mice exhibited increased free-water in the right dorsal striatum and lobule II/III of the cerebellum compared to WT controls (all corrected $P < 0.05$). No significant between-group differences in FA_T were detected.

Correlation Analysis

Pearson's correlation coefficients were computed to assess the relation between free-water values and functional connectivity in cortical, basal ganglia, and cerebellar regions. In the first analysis, correlations were computed between free-water in the striatum and functional connectivity z-scores where significant between-group

differences were detected, separately for each group. As shown in Fig. 2-7, the results of this analysis yielded a negative correlation between striatal free-water and functional connectivity in the PaL and AnL of the cerebellum, as well as the PMC. The second analysis assessed the relationship between functional connectivity and free-water in lobule II/III of the cerebellum. As shown in Fig. 2-7, cerebellar free-water was negatively correlated with functional connectivity in the PMC and AnL of the cerebellum. In turn, cerebellar free-water and functional connectivity showed a positive correlation in both thalamic regions, striatum (Dorsal-2), and hippocampus.

Discussion

The present study provides the first high-field *in vivo* fMRI- and diffusion MRI-based assays of functional connectivity and structural integrity of cortical, basal ganglia, and cerebellar regions in a mouse model of DYT1 dystonia. Dyt1 KI mice exhibited increased functional connectivity across the striatum, thalamus, and somatosensory cortex; and reduced functional connectivity in the motor and cerebellar cortices compared to WT mice. Further, Dyt1 KI mice demonstrated increased free-water in the striatum and cerebellum, which directly correlated with changes in functional connectivity.

Basal Ganglia Structure-Function Relationship in Dyt1 KI Mice

Previous work has shown that Dyt1 KI mice are associated with increased cortico-striatal excitation and LTD deficit (Dang *et al*., 2012; Yokoi *et al*., 2015). LTD is thought to underlie plasticity changes related to sensorimotor integration and associative learning of goal-directed movement as more functional synapses are formed between the cortex and striatum (Centonze *et al*., 2001; Wang *et al*., 2006). In particular, the level of cortico-striatal activation is modulated by the firing properties of

striatal cholinergic interneurons (SCIs) (Deffains and Bergman, 2015). SCIs exert their effects via the release of acetylcholine (ACh), which act on muscarinic receptors of striatal medium spiny neurons (MSNs). In control mice, HFS of the striatum inhibits the release of ACh from SCIs – promoting MSN calcium influx and a resultant inhibition of glutamate-mediated sensorimotor activation (Calabresi *et al*., 1992*a, b*; Pisani *et al*., 2006; Wang *et al*., 2006; Dang *et al*., 2012; see also Aosaki *et al*., 1994). *In vitro* studies, however, have shown that WT mice have a reduction in the autonomous pace-making tone of SCIs in response to striatal HFS, whereas the tonic firing patterns of SCIs in Dyt1 KI mice remain elevated (i.e., LTD deficit: Dang *et al*., 2012; Maltese *et al*., 2014; Yokoi *et al*., 2015). This finding has been attributed to the disrupted binding affinity of D2 dopamine receptors in the indirect basal ganglia pathway (Calabresi *et al*., 1992*a, b*; Balcioglu *et al*., 2007) and the resultant disinhibition of ACh release from SCIs (Pisani *et al*., 2006; Martella *et al*., 2009; Dang *et al*., 2012; Napolitano *et al*., 2010).

Given the above findings, the current study used ICA on the rsfMRI data to contrast functional connectivity within basal ganglia regions across Dyt1 KI and WT mice. The current findings demonstrate a significant increase in functional connectivity in the striatum and thalamus of Dyt1 KI mice, providing further evidence that impaired functional interaction among neurons within the basal ganglia circuit contributes to the pathophysiology underlying DYT1 dystonia. It is important to recognize, however, that Dyt1 KI mice are overtly asymptomatic and do not display apparent abnormal postures as observed in other Dyt1 conditional KO models (e.g., Liang *et al*., 2014; Pappas *et al*., 2015). Thus, the observations in this paper could be viewed as an endophenotype for the genetic underpinnings triggered by the ΔE mutation. An alternative viewpoint is that

the observations could be compensatory for the underlying pathophysiology. A number of studies have shown that LTD deficit and impaired motor function are restored in Dyt1 KI (Dang *et al*., 2012; Maltese *et al*., 2014; DeAndrade *et al*., 2016) and conditional KO (Liang *et al*., 2014; Pappas *et al*., 2015) mice following the administration of anticholinergic therapeutics. As such, future studies focused on elucidating restorative effects of anticholinergic medications on functional connectivity will prove to be important in supporting the position that impaired basal ganglia connectivity manifests as a function of disease-specific pathogenesis.

To examine striatal free-water and FA_T in Dyt1 KI and WT mice, diffusion MRI data was examined using a novel two-compartment diffusion analysis pipeline (Pasternak *et al*., 2009; Pasternak *et al*., 2012; see also Ofori *et al*., 2015*a, b*; Planetta *et al*., 2016). Using a two-compartment model can be important because conventional single-tensor diffusion models do not account for extracellular free-water within the voxel, which can bias diffusion measures such as fractional anisotropy (FA) (Metzler-Baddeley *et al*., 2012). Free-water values in the dorsal striatum were significantly increased in Dyt1 KI mice compared to their WT control counterparts. Further, the correlation analysis yielded a significant negative correlation between striatal free-water and functional connectivity in the PMC and the PaL and AnL of the cerebellum. This finding of altered striatal microstructure supports prior work by Uluğ *et al*. (2011) who reported a significant reduction in FA in the dorsal striatum of Dyt1 KI mice. In the current study, the two-compartment model corrected for free-water contamination within the voxel and did not yield between-group differences in FA_T. Thus, it appears that it is the free-water metric that is driving the FA changes in the striatum in Dyt1 KI mice

previously found using a single-tensor model (Uluğ *et al*., 2011). As well, Pappas *et al*. (2015) found that the conditional KO of torsinA within forebrain cholinergic and GABAergic progenitors caused a 40–50% reduction in the number of SCIs in the dorsal striatum of Dyt1 mice. This represents a salient finding as abnormal striatal pathology in Dyt1 KO mice produces a behavioral phenotype consistent with abnormal contractions commonly expressed in manifesting DYT1 gene carriers (see also Liang *et al*., 2014; Weisheit and Dauer, 2015). These results add to this work insomuch as it demonstrates that microstructural changes in the striatum relate to large-scale impairments in cortical and cerebellar functional connectivity.

Sensorimotor Cortical Connectivity in Dyt1 KI Mice

Dyt1 KI mice showed decreased functional connectivity in the PMC and increased functional connectivity in the somatosensory cortex compared to WT controls. These findings extend prior work employing $H_2{}^{15}O$-PET showing abnormal sensorimotor cortical activation in human DYT1 dystonia patients (Carbon *et al*., 2010). As well, previous human studies contend that increased EMG activation patterns and muscular co-contraction in dystonia (Berardelli *et al*., 1996; 1998) is attributed, in part, to impaired motor cortical surround inhibition [SI: Mink, 1996; Sohn and Hallett, 2004*a, b*; Beck and Hallett, 2011; Hallett, 2011)]. SI is characterized by a transient, top-down inhibition of motor cortical excitability, which serves to facilitate selection between different populations of motor neurons competing for a common movement threshold (Mink, 1996; Sohn and Hallett, 2004b). The most frequently examined SI paradigm involves using transcranial magnetic stimulation (TMS) and cortical motor evoked potentials (MEP) prior to – and during – the initiation of goal-directed movement. For example, Sohn and Hallett (2004a) delivered self-triggered motor cortical TMS at various intervals

following initial EMG activation in the flexor digitorum superficialis muscle during a self-paced finger flexion task. The authors reported that MEPs related to several finger flexion muscles were significantly increased in focal hand dystonia patients compared to normal healthy controls (see also Ridding *et al*., 1995).

In terms of the somatosensory-related increase in functional connectivity, the data suggest that the functional organization of somatosensory cortical neurons are enhanced in Dyt1 KI mice when integrating sensory feedback related to amplified cortical motor drive via the basal ganglia. As described above, previous work has reported that Dyt1 KI mice elicit impaired inhibitory modulation of cortical evoked potentials via striatal HFS *in vitro* (Dang *et al*., 2012). Moreover, abnormal sensorimotor evoked functional connectivity may account for recent evidence that the Dyt1 KI mouse model elicits sustained EMG activity and intermittent co-contractions of the biceps and rectus femori muscles (DeAndrade *et al*., 2016). These findings are in line with previous human studies that have reported increased volumetric grey-matter changes and amplified somatosensory activation in accounting for the overflow of conflicting cortical motor commands (i.e., SI) in patients with writer's cramp, orofacial dystonia, and focal hand dystonia (Garraux *et al*., 2004; Lerner *et al*., 2004; Dresel *et al*., 2006). Simonyan and Ludlow (2010) showed that symptomatic voice production in focal spasmodic dysphonia patients is associated with increased motor and somatosensory related activity; and similar changes in sensorimotor evoked activity have been reported in other task-specific focal dystonias (Pujol *et al*., 2000; Haslinger *et al*., 2010). In addition, Nelson *et al*. (2009) showed overlapping activation patterns in the somatotopic representation of the first three hand digits in patients with task-specific writer's cramp.

Cerebellar Structure-Function Relationship in Dyt1 KI Mice

Although dystonia is primarily considered a basal ganglia circuit disorder, recent literature has emphasized a clear role of the cerebellum in motor dysfunction. For example, previous work has shown that surgical removal of the cerebellum can eradicate the paroxysmal dystonic effects of toxic vectors (i.e., 6-hydroxydopamine, quinolinic acid) that induce widespread striatal degeneration (Neychev *et al*., 2008; see also Campbell *et al*., 1999; Chen *et al*., 2014). The results showed that Dyt1 KI mice were associated with decreased functional connectivity within two regions of the cerebellar cortex: the PaL and AnL. Notably, functional connectivity patterns in these regions yielded a strong AUC and moderate-to-high classification accuracy (0.8/66.7 and 0.93/80.0 for PaL and AnL, respectively). These findings are consistent with previous PET work showing changes in regional cerebellar metabolism in both manifesting and non-manifesting DYT1 gene carriers (Eidelberg *et al*., 1998; Carbon *et al*., 2004*a*; 2008*a*); and alteration of low-frequency amplitude fluctuations in the cerebellum in patients with benign essential blepharospasm (Zhou *et al*., 2013). Abnormal regional glucose metabolism has also been demonstrated in the cerebellar vermis of Dyt1 KI and KO mice (Uluğ *et al*., 2011; Vo *et al*., 2015*a*) and the Purkinje cell layer of the cerebellum in hMT mice (Zhao *et al*., 2011) using *in vivo* PET. These findings have been attributed to decreased inhibitory input to the vermis via cerebellar Purkinje cells (Vo *et al*., 2015*a*). Indeed, previous work has shown that Dyt1 KI and Purkinje-cell specific Dyt1 KO pathology is characterized by microstructural adaptations including reduced quantity of cerebellar Purkinje cell dendrites and spines (Zhang *et al*., 2011). It is possible that in the current study, morphological changes to Purkinje cell

dendrites in the PaL and AnL impair the functional connectivity of neurons within these regions.

Interestingly, in the same line of Dyt1 KI mice (Dang *et al*., 2005; Zhang *et al*., 2011), free-water values were increased compared to WT controls in lobule II/III of the cerebellum – which contains a high concentration of cerebellar Purkinje neurons (Ozol *et al*., 1999). These findings extend prior work that used single-tensor analyses of diffusion MRI data and reported significant FA reductions and microstructural changes within cerebellar regions in human DYT1 dystonia patients (Carbon *et al*., 2008*b*; Argyelan *et al*., 2009; Vo *et al*., 2015*b*). Only one previous study has examined brain microstructure in Dyt1 KI mice using diffusion MRI. In particular, Uluğ *et al*. (2011) employed a single-tensor tractography analysis to determine the microstructural integrity of the cerebello-thalamo-cortical tract and reported significant FA reductions within the cerebellum. After correcting for free-water contamination, the results from the current study did not reveal between-group differences in FA_T values. Thus, the results provide new evidence that extracellular free-water may serve as a sensitive measure of microstructural adaptations of cerebellar and basal ganglia regions in a mouse model of DYT1 dystonia. Further, the correlation analysis establishes a clear relationship between cerebellar microstructural integrity and functional connectivity patterns across the PMC, striatum, thalamus, and cerebellar cortex (AnL).

It remains unclear whether functional connectivity patterns exhibited in the cerebellar cortex are related to the respective increase and decrease in functional connectivity in the somatosensory-basal ganglia circuit and PMC. Indeed, anatomical tracing and electrophysiological studies have shown that the sensorimotor cortex, basal

ganglia and cerebellum comprise a major parallel multi-synaptic (i.e., afferent and efferent) pathway – and that cerebellar Purkinje cell output mediates the excitability of striatal neurons via di-synaptic cerebello-thalamo projections (Middleton and Strick, 2000; Hoshi *et al*., 2005; Bostan and Strick, 2010; Chen *et al*., 2014). For example, Chen *et al*. (2014) demonstrated that stimulation of cerebellar dentate nucleus and intralaminar thalamic nuclei in awake mice produced a proportional, short-latency increase in the firing rate of striatal MSNs. The current findings of adaptations in rsfMRI and diffusion MRI measures across the cortex, basal ganglia and cerebellum further contribute to the hypothesis that DYT1 dystonia likely results from a network-level change across structures within these regions.

Limitations and Conclusions

There are several limitations to note in this study. In particular, it remains to be determined whether the subtle motor impairments that exist in the Dyt1 KI mouse model (Dang *et al*., 2005; Yokoi *et al*., 2015) can be regarded as a reliable experimental representation of motor impairments in human DYT1 patients. The Dyt1 KI mouse model used in the current paradigm represents a genetically derived experimental corollary of both manifesting and non-manifesting human DYT1 gene carriers. Although Dyt1 KI mice demonstrate hyperactive behavior and subtle motor impairments, they remain resistant to the expression of an overt dystonia-like phenotype. Notably, however, recent intramuscular EMG evidence has shown that compared to WT mice, Dyt1 KI mice exhibit sustained contractions and intermittent co-contractile properties of the biceps and rectus femori muscles (DeAndrade *et al*., 2016). Furthermore, such antagonistic muscle activity is alleviated via acute administration of trihexiphenidyl (DeAndrade *et al*., 2016), suggesting both face and predictive validity. Second, in the

current study mice were induced to resting-state using isoflurane anesthesia at 2% concentration and maintained in an unconscious state for the duration of the imaging protocol at concentrations between 1 and 1.5%. Previous work has shown that isoflurane in rodents at high doses (i.e., > 1.8%) interferes with functional connectivity patterns and produces less defined network-level spatial segmentation (Liu *et al*., 2013), whereas isoflurane at lower doses (i.e., < 1.5%) preserves resting-state functional connectivity patterns and anatomical decomposition of resting-state networks (Ferron *et al*., 2009; Liu *et al*., 2013). Given these findings, it is not anticipated that any confounding effects of isoflurane anesthesia contributed to between-group differences in functional connectivity patterns across cortical and subcortical brain regions in the current study.

In summary, the current study provides the first *in vivo* MRI-based evidence that the removal of a single glutamic acid residue in the carboxyl terminus of the torsinA protein engenders large-scale changes in functional connectivity and microstructure across cortical and subcortical brain regions. The functional connectivity patterns were robust in machine learning algorithms for training and test datasets. Further, the microstructural elevation of free-water in the striatum and cerebellum correlated with the patterns of functional connectivity. Future studies that use these techniques in other animal models of dystonia that demonstrate an overt phenotype (Liang *et al*., 2014; Pappas *et al*., 2015) will prove important in furthering our understanding of connectivity adaptations and pathophysiology of dystonia.

Table 2-1. Summary of Support Vector Machine Classification Model in Dyt1 KI Mice. The results of the support vector machine cross-validation analysis based on mean functional connectivity z-score values in a training cohort of 12 Dyt1 KI and 12 WT mice. Algorithm prediction reliability was evaluated in a testing cohort of 15 mice (seven Dyt1 KI and eight WT). AUC = training cohort area under the curve; CBX = cerebellar cortex; HIP = hippocampus; PMC = primary motor cortex; prediction = testing cohort classification accuracy; PSC = primary somatosensory cortex; STR = striatum; THA = thalamus.

Summary of Support Vector Machine Classification Model		
Component Cluster(s)	**AUC**	**Prediction**
STR (Dorsal-1)	1	100
STR (Dorsal-2)	0.63	46.7
STR (Dorsal-1, Dorsal-2)	0.84	73.3
CBX (PaL)	0.8	66.7
CBX (AnL)	0.93	80
CBX (PaL, AnL)	0.96	80
STR (Dorsal-1); CBX (PaL)	0.95	86.7
STR (Dorsal-1, Dorsal-2); CBX (PaL, AnL)	0.86	66.7
PSC	0.86	73.3
PSC; STR (Dorsal-1)	0.96	80
PSC; STR (Dorsal-1, Dorsal-2)	0.95	86.7
PSC; CBX (PaL, AnL)	1	86.7
PSC; STR (Dorsal-1, Dorsal-2); CBX (PaL, AnL)	0.95	80
HIP	1	73.3
THA (Vthal-1)	0.89	73.3
THA (Vthal-2)	0.88	80
THA (Vthal-1, Vthal-2)	0.96	80
HIP; THA (Vthal-1, Vthal-2)	0.98	93.3
STR (Dorsal-1, Dorsal-2); CBX (PaL, AnL); THA (Vthal-1, Vthal-2)	0.98	93.3
PMC	0.95	93.3
PMC; STR (Dorsal-1, Dorsal-2)	1	93.3
PMC; CBX (PaL, AnL)	0.98	93.3
PMC; THA (Vthal-1, Vthal-2)	0.96	80
PMC; THA (Vthal-1, Vthal-2), HIP	0.98	80
STR (Dorsal-1); HIP; CBX (AnL); PSC; PMC; THA (Vthal-1)	1	93.3

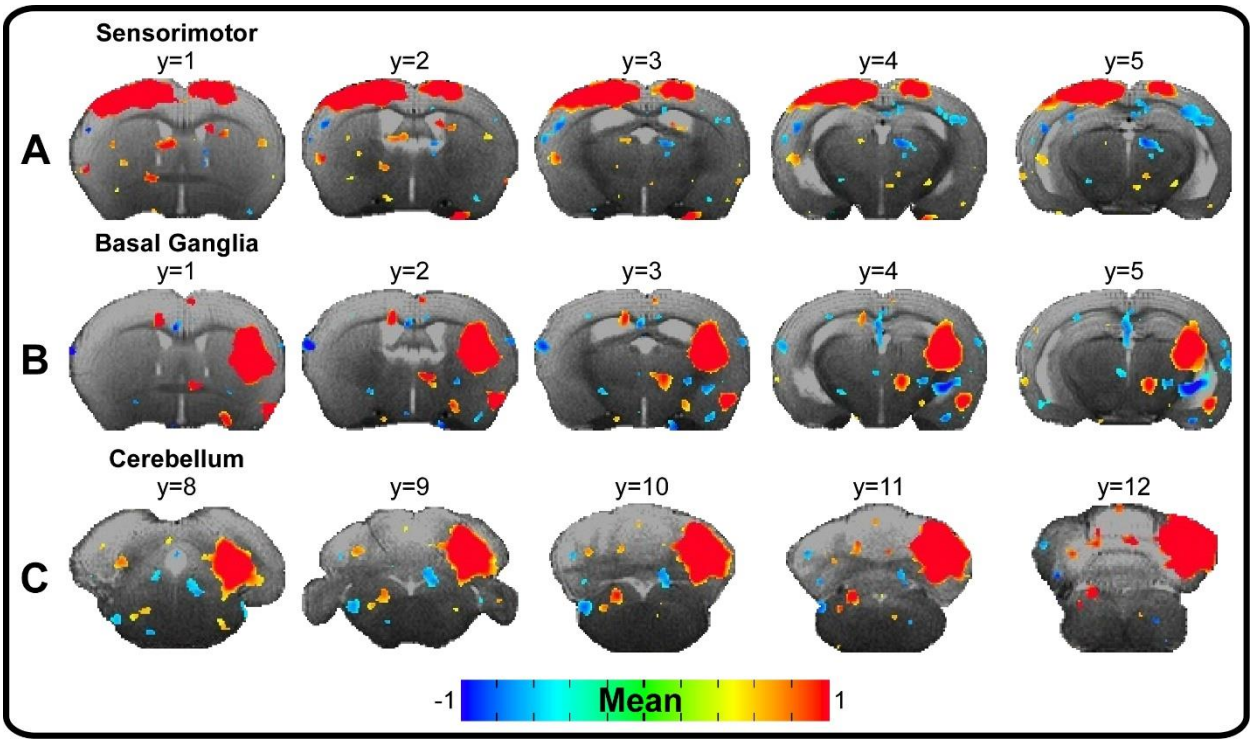

Figure 2-1. Exemplar Resting-State Functional Connectivity Color Maps. Spatial color-coded z-maps of three separate component clusters that overlap across multiple slices in Dyt1 KI mice. Colored voxels provide a measure of mean time-course dependence of resting-state hemodynamic signal fluctuations relative to the mean component time-course. Positive values, represented by warm (red) colors, denote a significant increase in the temporal correlation across voxels within the component, whereas negative values, represented by cold (blue) colors, represent a significant decrease in the temporal correlation across voxels. Results are thresholded at $P < 0.005$ at the voxel-level and FWER-corrected at $P < 0.05$. (A) Cortical component cluster wherein voxels expressing the highest degree of functional connectivity are localized to the sensorimotor cortex. (B) Basal ganglia component cluster depicting a high degree of functional connectivity localized to the right striatum. (C) Cerebellar component cluster depicting a high degree of functional connectivity within the right cerebellar cortex. Spatial color maps are superimposed over the T_2-weighted image of a single subject.

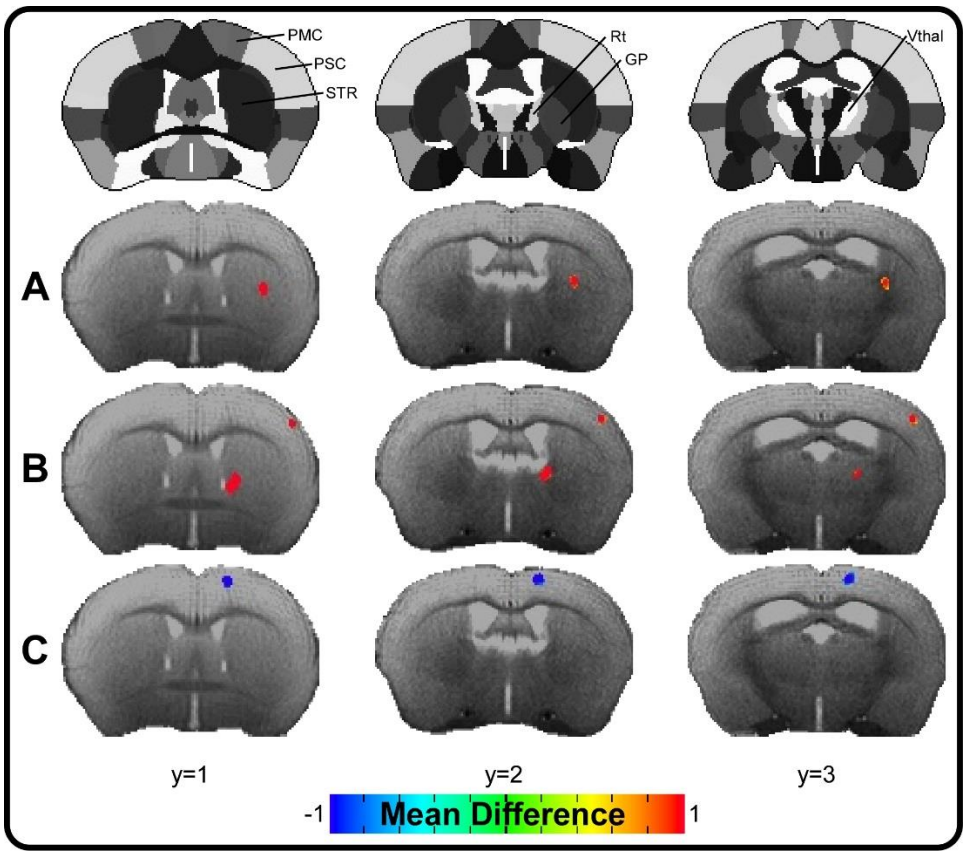

Figure 2-2. Between-Group Cortico-Striatal Functional Connectivity Color Maps. Color bars represent the mean difference in z-score values for between-group post-hoc comparisons (i.e., Dyt1 KI versus WT). Results are thresholded at $P < 0.005$ at the voxel-level and FWER-corrected at $P < 0.05$. Positive values, represented by warm (red) colors, denote a significant increase in functional connectivity in Dyt1 KI mice compared to WT mice in the (A-B) dorsal striatum and (B) primary somatosensory cortex, whereas negative values, represented by cold (blue) colors, denote a significant decrease in functional connectivity in Dyt1 KI versus WT mice in the (C) primary motor cortex. Spatial color maps are superimposed over the T_2-weighted image of a single subject. Stereotaxic template atlas provided by Ferris *et al*. (2014). GP = globus pallidus = PMC, primary motor cortex; PSC = primary somatosensory cortex; Rt = reticular thalamic area; STR = striatum; Vthal = ventral thalamic area.

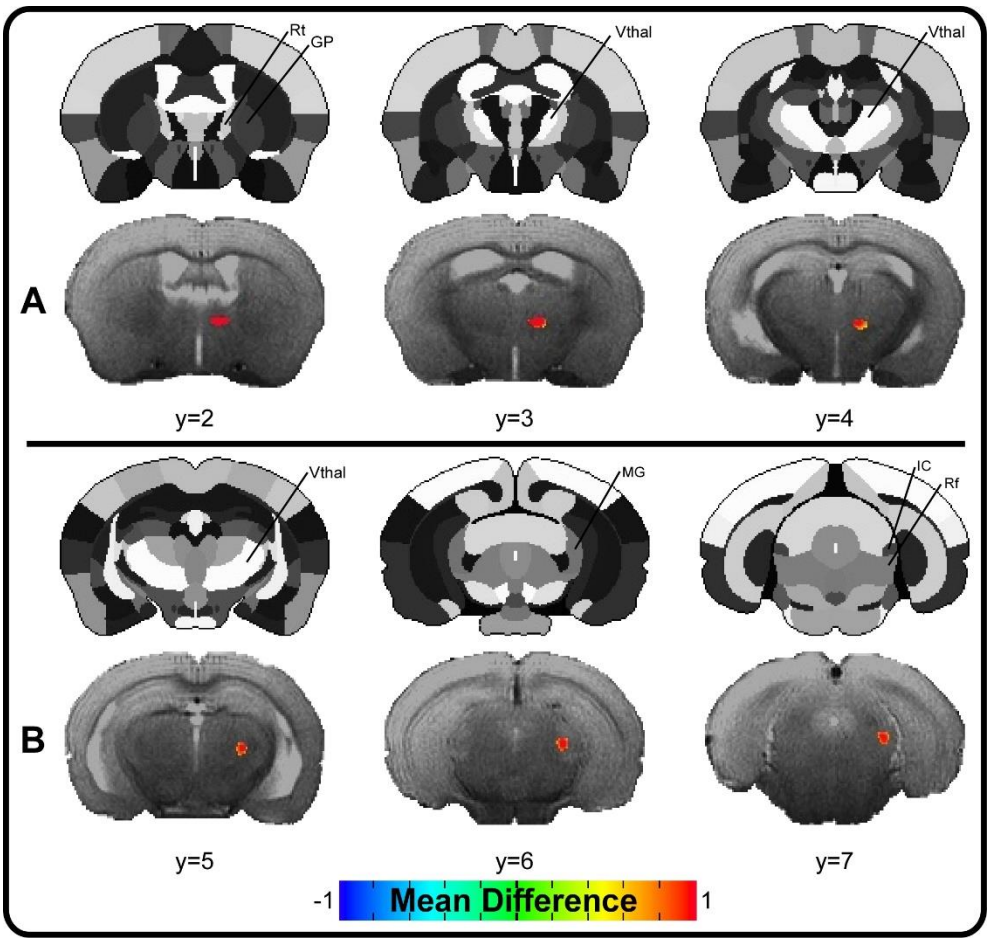

Figure 2-3. Between-Group Thalamic and Brainstem Functional Connectivity Color Maps. Color bars represent the mean difference in z-score values for between-group post-hoc comparisons (i.e., Dyt1 KI versus WT). Results are thresholded at $P < 0.005$ at the voxel-level and FWER-corrected at $P < 0.05$. Positive values, represented by warm (red) colors, denote a significant increase in functional connectivity in Dyt1 KI mice compared to WT mice. Dyt1 KI mice demonstrated increased functional connectivity within two thalamic component clusters. The majority of voxels expressing a high degree of connectivity in Dyt1 KI mice were localized to components within the (A–B) ventral thalamic area (A: Vthal-2; B: Vthal-1) and (B) brainstem. Spatial color maps are superimposed over the T_2-weighted image of a single subject. Stereotaxic template atlas provided by Ferris *et al*. (2014). IC = inferior colliculus; MG = medial geniculate nucleus; Rf = reticular formation; Rt = reticular thalamic area; Vthal = ventral thalamic area.

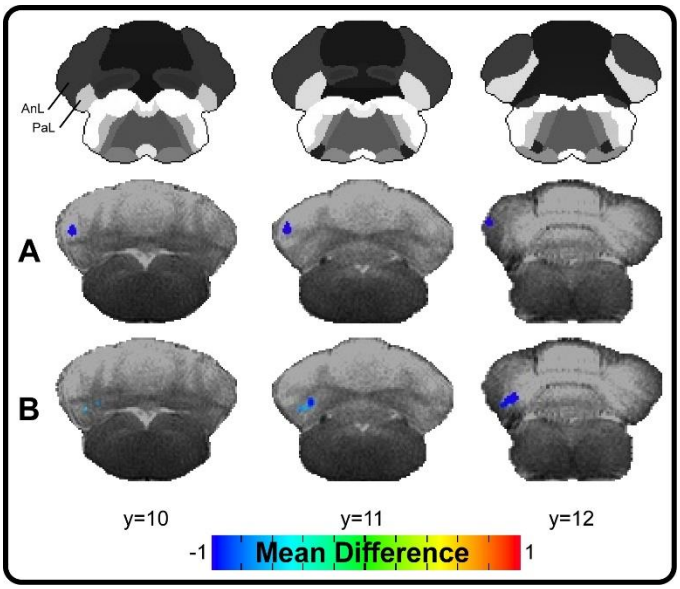

Figure 2-4. Between-Group Cerebellar Functional Connectivity Color Maps. Color bars represent mean difference in z-score values for between-group post-hoc comparisons (i.e., Dyt1 KI versus WT). Results are thresholded at $P < 0.005$ at the voxel-level and FWER-corrected at $P < 0.05$. Negative values, represented by cold (blue) colors, denote a significant decrease in functional connectivity in Dyt1 KI versus WT mice in the (A) paramedian (PaL) and (B) anisiform (AnL) lobules. Spatial color maps are superimposed over the T_2-weighted image of a single subject. Stereotaxic template atlas provided by Ferris *et al*. (2014).

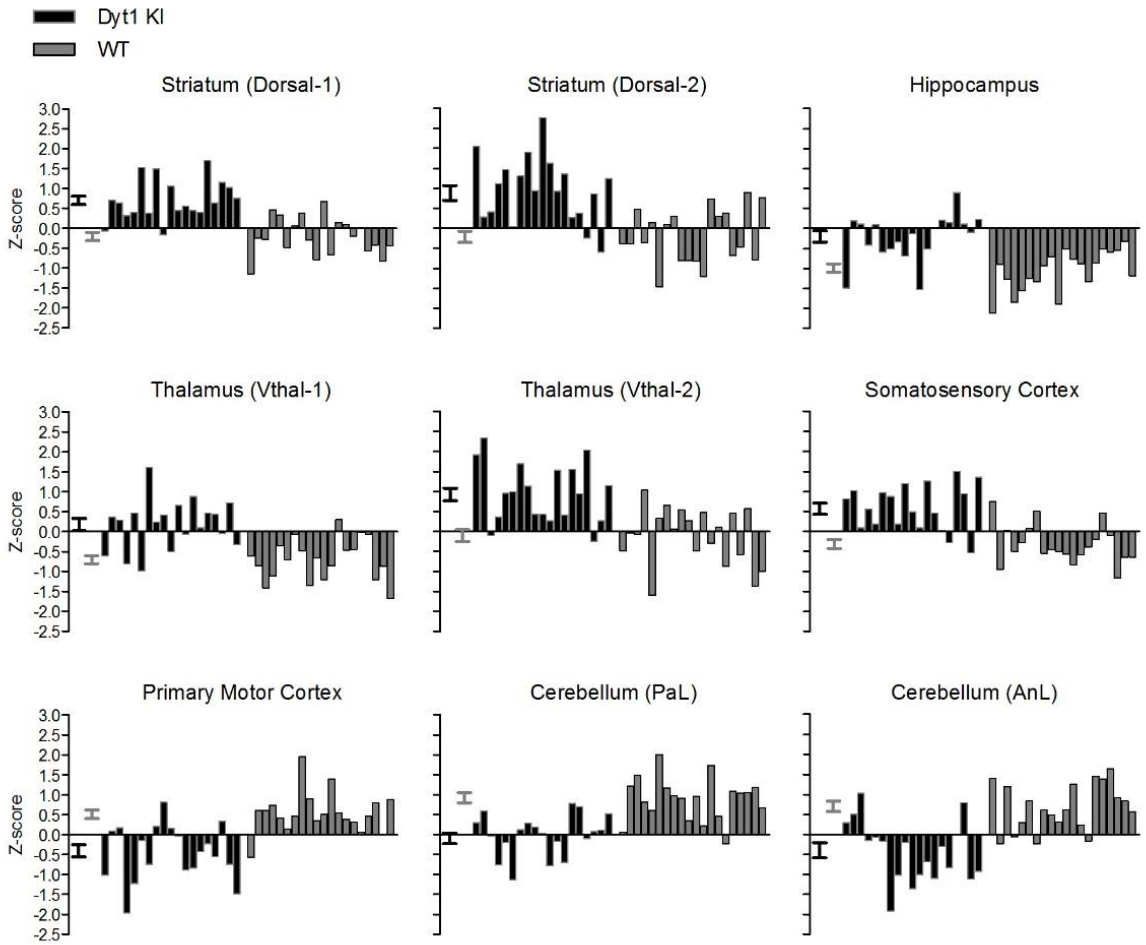

Figure 2-5. Between-Group Functional Connectivity Z-Score Plots. Comparison of subject-by-subject mean z-score values from components where significant between-group differences were detected across Dyt1 KI (black bars) and WT (grey bars) mice. Black and grey error bars represent ±1 SE centered on the mean z-score for Dyt1 KI and WT mice, respectively. Dorsal-1 = dorsal striatum component 1 (Fig. 2-2A); Dorsal-2 = dorsal striatum component 2 (Fig. 2-2B); Vthal-1 = ventral thalamic area component 1 (Fig. 2-3B); Vthal-2 = ventral thalamic area component 2 (Fig. 2-3A); PaL = paramedian lobule of cerebellum; AnL = anisiform lobule of cerebellum.

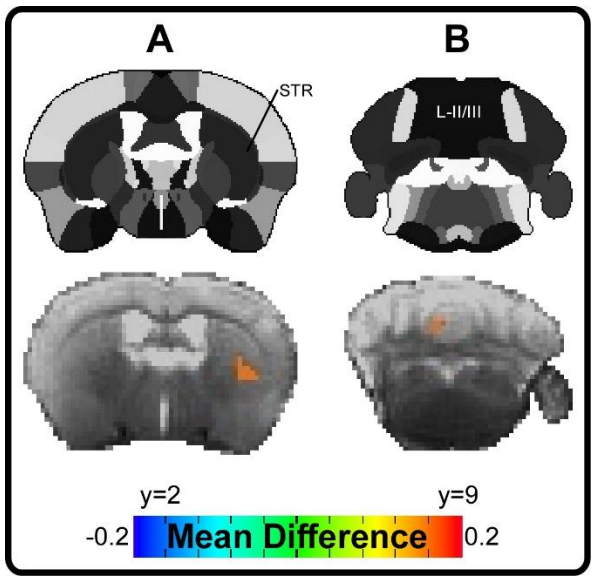

Figure 2-6. Between-Group Comparisons of Striatal and Cerebellar Free-Water. Color bars represent the mean difference in free-water values for between-group post-hoc comparisons (i.e., Dyt1 KI versus WT). Results are thresholded at $P < 0.005$ at the voxel-level and FWER-corrected at $P < 0.05$. Positive values, represented by warm (red) colors, denote a significant increase in free-water in Dyt1 KI mice compared to WT mice in (A) dorsal striatum (STR) and (B) lobule II/III of the cerebellum, L-II/III. Spatial color maps are superimposed over the b0 image of a single subject. Stereotaxic template atlas provided by Ferris *et al*. (2014).

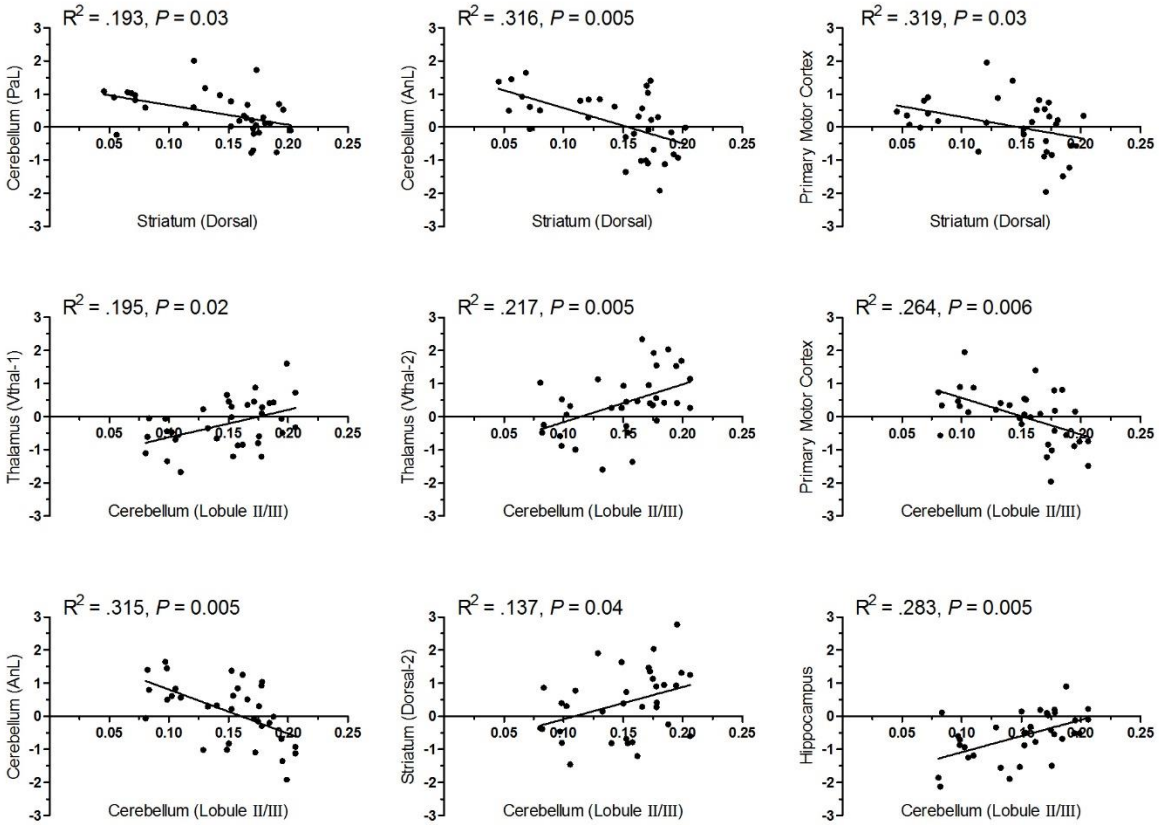

Figure 2-7. Correlations Between Free-Water and Functional Connectivity. Pearson's correlation coefficients relating mean free-water values in the striatum and cerebellum (x-axis) with mean functional connectivity z-scores (y-axis). Free-water in the striatum was negatively correlated with functional connectivity in the paramedian (PaL) and anisiform (AnL) lobules of the cerebellum, and the primary motor cortex. Free-water in the cerebellum was positively correlated with functional connectivity in the ventral thalamic areas (Vthal-1, Vthal-2), striatum (Dorsal-2), and hippocampus; and negatively correlated with functional connectivity in the primary motor cortex and AnL.

CHAPTER 3
FOREBRAIN KNOCKOUT OF TORSIN-A REDUCES STRIATAL FREE-WATER AND IMPAIRS WHOLE-BRAIN FUNCTIONAL CONNECITIVITY IN A SYMPTOMATIC MOUSE MODEL OF DYT1 DYSTONIA

Chapter Summary

Multiple lines of evidence implicate striatal dysfunction in the pathogenesis of dystonia, including in DYT1, a common inherited form of the disorder.* The impact of striatal dysfunction on connected motor circuits and their interaction with other brain regions is poorly understood. Conditional knockout of the protein torsinA from forebrain cholinergic and GABAergic neurons creates a symptomatic model that recapitulates many characteristics of DYT1 dystonia (Dlx-cKO mice), including the developmental onset of overt twisting movements that are responsive to antimuscarinic drugs. Diffusion MRI and resting-state functional MRI were performed on Dlx-cKO mice of either sex to define adaptations of diffusivity and functional connectivity in cortical, subcortical, and cerebellar regions. The striatum was the only region to exhibit diffusivity changes, indicating a selective microstructural adaptation in Dlx-cKO mice. The striatum of Dlx-cKO mice exhibited widespread increases in functional connectivity with somatosensory cortex, thalamus, vermis, cerebellar cortex and nuclei, and brainstem. The current study provides the first *in vivo* support that direct pathological insult to forebrain torsinA in a symptomatic mouse model of DYT1 dystonia can engage genetically normal hind brain regions into an aberrant connectivity network. These findings have important implications for the assignment of a causative region in CNS disease.

---

* A version of this chapter has been published as DeSimone JC, Pappas SS, Febo M, Burciu RG, Shukla P, Colon-Perez LM, Dauer WT, Vaillancourt DE. Forebrain knock-out of torsinA reduces striatal free-water and impairs whole-brain functional connectivity in a symptomatic mouse model of DYT1 dystonia. Neurobiol Dis 2017; 106: 124-132. Reprinted as per Elsevier Author's Rights.

Introduction

Dystonia musculorum deformans (“Oppenheim’s dystonia”) is an inherited neurodevelopmental movement disorder (DYT1 dystonia) characterized by sustained, involuntary twisting movements and disabling postures (Fahn, 1988; Ozelius and Lubarr, 1999; Breakefield *et al*., 2008). DYT1 dystonia is caused by a dominant three base-pair deletion (ΔGAG) in the TOR1A gene that eliminates a single glutamic acid residue (ΔE) in the C-terminus of the AAA+ protein torsinA (Ozelius *et al*., 1997).

Convergent evidence from human and animal studies establish the striatum as a key region in dystonia pathophysiology. Lesion studies point to an association between putaminal lesions and clinical symptoms in patients with secondary dystonia (Burton *et al*., 1984; Marsden *et al*., 1985; Fross *et al*., 1987; Bhatia and Marsden, 1994). Deep brain stimulation of major striatal output targets such as the globus pallidus internus and subthalamic nucleus is an effective therapy for DYT1 dystonia (Vidailhet *et al*., 2005; Kupsch *et al*., 2006; Ostrem *et al*., 2014). Moreover, studies in multiple mouse models of DYT1 dystonia have implicated dysfunction of striatal cholinergic interneurons (SCI), including disruption of cortico- and thalamo-striatal synaptic integration and plasticity (Pisani *et al*., 2006; Martella *et al*., 2009; Dang *et al*., 2012; Sciamanna *et al*., 2012*a, b*; Maltese *et al*., 2014). It remains unclear how striatal dysfunction affects network-level changes in functional connectivity (Biswal *et al*., 1995; Fox *et al*., 2005) across cortical, subcortical, and cerebellar networks. Understanding how striatal pathology affects functional connectivity in pre-clinical models is important for dissecting pathophysiology and providing readouts for disease-modifying interventions. Further, understanding network-level connectivity in a translational model of generalized dystonia is opportune

because motor impairments in human subjects with focal dystonia points to disturbances in functional connectivity (Battistella *et al*., 2016; 2017).

To explore these questions, *in vivo* diffusion MRI and resting-state functional MRI (rsfMRI) were acquired in a mouse model characterized by the conditional knockout of torsinA from forebrain (i.e., striatum, cortex, globus pallidus, basal forebrain, and reticular thalamic nucleus) cholinergic and GABAergic neurons [Dlx-cKO mice (Pappas *et al*., 2015)]. In contrast to human DYT1 dystonia brains, which do not exhibit overt structural lesions, the striatum of this mouse model exhibits selective neurodegeneration of SCIs. As well, surviving SCIs exhibit cell soma hypertrophy and dysfunctional electrophysiological properties, implicating striatal connectivity adaptations. In turn, the microstructural and functional integrity of forebrain GABAergic neurons is preserved despite the loss of torsinA. Two hypotheses were tested. First, diffusion MRI combined with a two-compartment free-water model was used to test the hypothesis that the loss of torsinA in Dlx-cKO mice causes adaptations in extracellular free-water and tissue compartment diffusivity (free-water-corrected mean diffusivity: MD_T) within the striatum. This computational approach fits a two-compartment model to diffusion MRI data, separating the diffusion properties of water in brain tissue from that of water in the extracellular space (Pasternak *et al*., 2009). Since prior work in the Dlx-cKO model demonstrated that surviving SCIs are associated with significant cell soma hypertrophy (Pappas *et al*., 2015), it was predicted that the extracellular free-water compartment of striatal regions would be reduced, whereas the MD_T would be increased. Second, rsfMRI was used to test the hypothesis that functional connectivity

is impaired between the pathologically abnormal striatum and other key cortical, subcortical, and cerebellar motor regions.

Methods

Animals and Housing

Mice originating from the Dauer Laboratory at the University of Michigan were housed and imaged at the University of Florida McKnight Brain Institute. Eighteen (10 male, eight female; age 6.9 $\pm$ 0.8 months) Dlx5/6-Cre^{+} Tor1a$^{flx/-}$ (Dlx-cKO) and 18 (seven male, 11 female; age 6.7 ± 1.3 months) Cre^{-} Tor1a$^{flx/+}$ littermate wild-type controls were used in this experiment. Mice were prepared and genotyped for Tor1a and Cre using the PCR protocol described by Liang *et al*. (2014). Dlx-cKO and control mice were bred as previously described (Pappas *et al*., 2015). Prior to animal transport, motor abnormalities (i.e., fore limb and hind limb clasping, abnormal posturing) were confirmed in all Dlx-cKO mice by days postnatal 49-56 via the tail suspension assessment (Pappas *et al*., 2015). Mice were housed in groups of one to three in a temperature and humidity-controlled environment, maintained on an alternating 12 h light-dark cycle (i.e., lights off at 19:00 h), and were provided *ad libitum* food and water access. All experimental protocols and procedures were approved and monitored by both the University of Michigan Committee on the Use and Care of Animals (UCUCA) and the University of Florida Institutional Animal Care and Use Committee (IACUC). Animals were acquired and cared for in accordance with the ethical standards set forth by the Guide for the Care and Use of Laboratory Animals (8th Edition, 2011) and the American Association for Laboratory Animal Science guidelines.

MRI Preparation and Data Acquisition

Experimenters involved in data collection had no advanced knowledge of the genotype of each animal during MRI acquisition and the blind was not broken until the final between-group statistics were performed. Mice were anesthetized for the duration of the experiment. Isoflurane anesthesia was delivered using compressed air through a Surgivet vaporizer (Dublin, OH, USA) connected to a charcoal trap. Mice were initially induced at 3-4% isoflurane for 1-2 minutes in an enclosed knock-in chamber. Anesthesia was reduced to 2% for animal setup and 1.0-1.5% for MRI acquisition. Notably, this level of anesthesia was considered appropriate based on previous reports that concentrations within this bandwidth preserve functional connectivity patterns in rodent models (Ferron *et al*., 2009; Liu *et al*., 2013). Animals were placed in a prone position on a custom design plastic mouse bed equipped with a bite bar that served to immobilize the head and deliver anesthesia during scanning. An in-house 2.5×3.5 cm quadrature surface transmit/receive coil (Advanced Magnetic Resonance Imaging and Spectroscopy Facility, University of Florida, Gainesville, FL, USA) was affixed to the top of the skull and tuned to 470.7 MHz (^{1}H resonance) for B^{1} excitation and signal detection. Respiratory vitals were monitored using a respiration pad (SA Instruments, Stony Brook, NY). Core body temperature (37-38°C) was maintained using a custom recirculating waterbed heating system.

MRI data were acquired using an 11.1 Tesla Magnex Scientific horizontal magnet (Agilent, Inc., Santa Clara, CA, USA, 205/120HD gradient set with 120 mm inner gradient bore size; maximum gradient strength 600 mT/m and rise time of 130 μs) at the University of Florida McKnight Brain Institute. MRI sequences were prepared and

acquired using VNMRJ software (Agilent Technologies, Version 3.1) and included acquisition of anatomical scout sequences for real-time visual depiction of brain positioning, as well as whole-brain voxel shimming for magnetic field homogeneity. The MRI acquisition sequences were ordered as follows: two rsfMRI scans, one diffusion MRI scan, and one T_2-weighted anatomical scan.

Diffusion weighted images were acquired using an 8-shot echo planar imaging (EPI) sequence with the following parameters: repetition time (TR) = 2,500 ms; echo time (TE) = 25.88 ms; flip angle = 90°; max b-value = 900s/mm^2; averages = 3; dummy scans = 2; directions = 42; slices = 12; coronal orientation; thickness = 0.75 mm; gap = 0 mm; field of view (FOV) = 19.2×19.2 mm; data acquisition matrix = 128×128 in-plane.

Resting-state fMRI was acquired using a 2-shot EPI sequence with the following parameters: TR = 1,000 ms; TE = 20 ms; repetitions = 210; flip angle = 90°; dummy scans = 4; slices = 12; coronal orientation; thickness = 0.75 mm; gap = 0 mm; FOV = 19.2×19.2 mm; data acquisition matrix = 64×64 in-plane.

Anatomical images were acquired using a fast-spin echo T_2-weighted imaging sequence with the following parameters: TR = 2,000 ms; effective TE = 31.6 ms; echo spacing = 8.04; echo train length = 8 ms; slices = 12; coronal orientation; thickness = 0.75 mm; gap = 0 mm; FOV = 19.2×19.2 mm; data acquisition matrix = 192×192 in-plane.

Diffusion MRI Data Preprocessing and Analysis

Diffusion MRI preprocessing and analysis was performed using previously described methods (DeSimone *et al*., 2016) and a rodent-modified two-compartment diffusion analysis pipeline (Pasternak *et al*., 2009). The FMRIB Software Library (FSL: Oxford, UK) and custom designed Unix shell scripts in Analysis of Functional

NeuroImages software [AFNI (Cox, 1996; Version 16.0.19)] were used to correct for eddy current and head motion artifacts, compensation of diffusion gradient rotations in response to these corrections, and manual skull stripping for the removal of non-brain tissue. Free-water and free-water-corrected diffusion tensor imaging (DTI) maps were calculated from the preprocessed motion and eddy current corrected volumes using custom code written in MATLAB (Version R2013a; MathWorks, Natick, MA). To create the free-water map, a minimization procedure was used such that a two-compartment model (Pasternak *et al*., 2009) was fit to each voxel in order to quantify free-water volume. The free-water component was then eliminated from each voxel to generate a free-water-corrected mean diffusivity (MD_T) map. To standardize the data, the b0 image from each mouse was registered to a single mouse b0 image using an affine transformation matrix and trilinear interpolation using the FSL Linear Image Registration Tool (FLIRT). The resultant transformation matrix was then applied to the free-water and MD_T maps. Between-group comparisons were examined by submitting free-water and MD_T values to voxel-wise independent-samples t-tests (i.e., Dlx-cKO minus control) at an alpha level threshold of $P < 0.005$ using the 3dttest++ function in AFNI. A Monte Carlo simulation using the 3dClustSim function in AFNI was employed to estimate the required adjustment for multiple comparisons using the family-wise error rate (FWER). Type I error adjustment was achieved by setting the significance level for the contrasts of interest to a voxel-level threshold of $P < 0.05$ FWER-corrected and minimum cluster size of 7 voxels.

Functional MRI Data Preprocessing and Analysis

Functional MRI data preprocessing was performed using FSL and custom designed Unix shell scripts in AFNI. To account for magnetization equilibrium, the first

five volumes of both EPI sequences were discarded. The remaining volumes were concatenated into a single sequence with 410 volumes. Data preprocessing additionally included manual skull stripping for the removal of non-brain tissue and motion correction. To standardize the data, the EPI image of each mouse brain was co-registered to their respective T_2-weighted image. The T_2-weighted image of each mouse was then registered to that of a single mouse brain and the resultant data matrix was applied to the EPI image via affine transformation with limited degrees of freedom and trilinear interpolation using FSL FLIRT. Additionally, spatial normalization and in-plane smoothing was performed on the EPI image using a Gaussian FWHM kernel of 0.2 mm^2 (x-y planes) and data was temporally filtered using a band-pass filter with a cut-off frequency between 0.01 and 0.1 Hz.

Functional MRI data were examined using a seed-based functional connectivity analysis in AFNI with four bilateral seed regions of interest in the striatum (i.e., eight total seed locations). Seed locations were selected *a priori* based on evidence of overlapping striatal free-water and diffusivity changes in Dlx-cKO mice (Fig. 3-1). Moreover, seed regions were consistent with established regions of cholinergic degeneration in Dlx-cKO mice (Pappas *et al*., 2015). After obtaining the residual time-series, Pearson's correlation coefficients were computed between the time-series of the seed region and all other brain voxels. The correlation coefficient was then transferred to a z-value, and the z-value extracted from each voxel provided a standardized measure of the degree of connectivity with each of the striatal seeds. Between-group comparisons were examined for each seed by submitting z-scores to voxel-wise independent-samples t-tests (i.e., Dlx-cKO minus control) at an alpha level threshold of

$P < 0.005$. A Monte Carlo simulation was used to estimate the required adjustment for multiple comparisons using the family-wise error rate (FWER). The voxel-level significance threshold for the contrasts of interest was set to $P < 0.05$ FWER-corrected and minimum cluster size of 31 voxels.

A subsequent analysis was used to determine if functional connectivity values were robust in classifying mouse genotype (i.e., Dlx-cKO, control). Functional connectivity z-score values from a training cohort of 11 Dlx-cKO and 11 control mice were submitted to a linear kernel support vector machine classification algorithm with 10-fold cross-validation using the Library for Support Vector Machines (LIBSVM: Chang and Lin, 2011). Classification reliability of the algorithm was evaluated in an independent testing cohort of seven Dlx-cKO and seven control mice.

Results

Diffusion MRI: Free-Water and Mean Diffusivity

A core feature of forebrain torsinA deletion in dystonic Dlx-cKO mice is the marked degeneration and morphological adaptation of SCIs (Pappas *et al*., 2015). It was hypothesized that free-water and MD_T may serve as a reflective marker of SCI adaptations. To explore this possibility, whole-brain free-water and MD_T values were computed for Dlx-cKO and control mice and values were submitted to voxel-wise independent-samples t-tests. Consistent with the original hypothesis, Dlx-cKO mice demonstrated a significant decrease in free-water relative to controls in the right and left striatum (all FWER-corrected $P < 0.05$). Conversely, MD_T was increased in the left and right striatum compared to that of controls (Fig. 3-1). Free-water and MD_T differences between Dlx-cKO and control mice were confined to the striatum, consistent with prior

work demonstrating that the conditional KO of torsinA from forebrain cholinergic and GABAergic precursors imparts a striatum-specific structural lesion.

Correlation Analysis: Free-Water and Mean Diffusivity

Compared to control mice, striatal MD_T and free-water values in dystonic Dlx-cKO mice were increased and decreased, respectively. Notably, voxels expressing increased MD_T rendered a high degree of spatial overlap (i.e., 75%) with voxels exhibiting reduced free-water. To examine the relationship between tissue and extracellular derived diffusion indices, Pearson's correlation coefficients were computed between free-water and MD_T values across common voxels in the striatum. Correlations between free-water and MD_T values were examined separately for Dlx-cKO and control groups. MD_T values yielded significant, moderate-to-strong inverse correlations with free-water values in the left, right, and bilateral (i.e., averaged across right and left) striatum of Dlx-cKO mice (Ps < 0.005) (Fig. 3-2). In contrast, correlation coefficients between MD_T and free-water values in control mice failed to reach statistical significance.

Functional MRI: Increased Whole-Brain Connectivity with Striatum

Having localized microstructural adaptations to the striatum, it was important to establish whether this abnormality influenced functional connectivity between the striatum and other brain regions. First, within-group t-tests were performed independently for Dlx-cKO and control mice for each of the eight striatal seed regions. In control mice, the striatum demonstrated a high degree of connectivity with brain regions ipsilateral to the seed, and significant negative correlation (i.e., anti-connectivity) with brain regions contralateral to the seed. Similarly, Dlx-cKO mice demonstrated significantly increased functional connectivity between the striatal seed location and

voxels within ipsilateral brain regions. However, unlike their control counterparts, the striatum in Dlx-cKO mice demonstrated absent or significantly less extensive contralateral anti-connectivity than controls (Fig. 3-3). This pattern of seed-based connectivity of the striatum with ipsilateral and contralateral brain regions across Dlx-cKO and control groups was observed for all seed locations.

Next, voxel-wise independent-samples t-tests (i.e., Dlx-cKO versus control) were performed to examine group differences in functional connectivity independently for each of the eight striatal seed locations. Functional connectivity differences between Dlx-cKO and controls were more extensive for seeds originating in the left striatum compared to that of the right. For left seed locations, abnormal functional connectivity clusters extended across cortical, subcortical, cerebellar, and brainstem regions in Dlx-cKO mice. Compared to controls, Dlx-cKO mice exhibited increased functional connectivity of the left striatum with the primary somatosensory cortex, thalamus, medial geniculate nucleus, superior colliculus, hippocampus, vermis, cerebellar nuclei (dentate and interposed), and anisiform and paramedian lobules (all FWER-corrected $P < 0.05$) (Fig. 3-4 – 3-5). Between-group functional connectivity effects were less extensive for seeds originating in the right striatum. Abnormal functional connectivity clusters in Dlx-cKO mice were restricted to cortical and subcortical regions. In particular, Fig. 3-6 shows that dystonic Dlx-cKO mice demonstrated increased functional connectivity with the striatum in the thalamus, hypothalamus, midbrain (precommissural nucleus), primary somatosensory cortex, posterior parietal association area, and hippocampus (all FWER-corrected $P < 0.05$).

A classification analysis was performed based on the extracted z-scores from functional connectivity clusters revealed by between-group post-hoc analyses using a 10-fold cross validation support vector machine algorithm in randomly selected training (11 Dlx-cKO, 11 control) and testing (seven Dlx-cKO, seven control) cohorts. Single- and multi-cluster combinations yielded an area under the curve (AUC) between 0.73 and 0.91 in the training cohort, and moderate-to-high independent classification accuracy (71 to 100%) in the testing cohort. The results of the support vector machine analysis are presented in Table 3-1. This analysis indicates that the functional connectivity findings are robust in discriminating between groups.

Discussion

Using multi-modal imaging assays in an overtly symptomatic model of DYT1 dystonia that exhibits construct, face and therapeutic validity, this study demonstrates a selective microstructural adaptation of the striatum and abnormal connectivity of this structure with cortical and subcortical brain regions. These observations establish a neuroimaging readout of direct and/or indirect neuronal adaptations to forebrain torsinA deficiency and provide a set of connectivity adaptations to be explored as pathophysiological substrates in DYT1 dystonia pathogenesis.

Reduced Striatal Free-Water in Dlx-cKO Mice

The first objective was to determine whether adaptations in extracellular and tissue derived diffusion indices may exist, reflecting striatal neurodegeneration or its consequences. Original work in the Dlx-cKO mouse model SCI-specific neurodegeneration, whereas the microstructural integrity of forebrain GABAergic neurons was unaffected (Pappas *et al*., 2015). Given that post-mortem cellular measures were not performed in Dlx-cKO mice in the current study, it was important to

employ a sensitive and alternative assay of microstructural adaptations to forebrain torsinA loss. A two-compartment diffusion pipeline (Pasternak *et al*., 2009; 2012) was used to disentangle the diffusivity of brain tissue (MD_T) from that of extracellular free-water. The two-compartment technique provides a sensitive and reproducible measure of neurodegeneration and disease progression (Pasternak *et al*., 2012; Ofori *et al*., 2015*a, b*; Planetta *et al*., 2016). This computational approach is important because it provides an *in vivo* interpretation of neuropathological adaptations to torsinA loss and affords a direct translational metric that can be used to monitor such adaptations in human studies. Further, metrics derived from this analysis serve as a foundation for future *in vivo* studies examining longitudinal progression of microstructural adaptations in animal models of DYT1 dystonia. Consistent with the original hypothesis, striatal free-water values in Dlx-cKO mice were reduced relative to controls, suggesting extracellular volumetric decline in response to SCI hypertrophy. This finding is consistent with work using a two-compartment model in acute concussion patients (Pasternak *et al*., 2014), which was interpreted to reflect regional trauma glial cell migration and swelling in injured areas. The reduced free-water in the striatum of Dlx-cKO mice is consistent with prior work demonstrating soma hypertrophy of surviving SCIs (Pappas *et al*., 2015), although it is possible that other mechanisms beyond SCI adaptations influence the free-water metric.

In order to evaluate tissue specific water translation in the striatum, MD_T was quantified after correcting for free-water contamination. MD_T provides an averaged multi-directional measure of diffusivity within grey and white matter and is inversely related to cellular integrity (i.e., cellularity, swelling) (Pierpaoli *et al*., 1996; Feldman *et*

al., 2010; Alexander *et al*., 2011; Basser and Pierpaoli, 2011). MD_T in Dlx-cKO mice was increased in the left and right striatum of Dlx-cKO mice relative to controls. This finding may reflect altered membrane depolarization resistance (i.e., increased cell capacitance) and cell soma hypertrophy in surviving SCIs of Dlx-cKO mice (Pappas *et al*., 2015). Indeed, cell capacitance (Fernández *et al*., 1982) is proportional to the insulator density of proteins that comprise the interstitial phospholipid bi-layer, and increased membrane density and inflammation can hinder directionally constrained cellular diffusion properties (Alexander *et al*., 2007; 2011).

Free-water and MD_T changes converged across a significant area of the striatum in Dlx-cKO mice. Given that SCIs occupy a relatively small proportion of striatal cell types in rodents (Oorschot, 2013), assays derived from diffusion MRI in the current study may reflect microstructural adaptations independent of SCI degeneration and cell soma hypertrophy. In accounting for this discrepancy, it is important to note that while forebrain regions exposed to torsinA eradication in Dlx-cKO mice demonstrate no evidence of gliosis during initial development, it is possible that degenerative insult influenced post-developmental glial cell migration, thereby influencing partial volume effects (e.g., Wang *et al*., 2011; Pasternak *et al*., 2014). Alternatively, dendritic arborization, which is not incorporated into cell soma hypertrophy measures, may represent a compensatory mechanism following neurodegeneration in the striatum. Future progression studies aimed at combining *in vivo* imaging and post-mortem histological assays will prove important in furthering the current understanding on the relation between diffusion MRI metrics and underlying changes in brain microstructure.

Increased Whole-Brain Connectivity with the Striatum in Dlx-cKO Mice

The results provide direct *in vivo* support that diffusion MRI can serve as a sensitive marker of striatal microstructural adaptations in response to forebrain torsinA loss. SCIs that do not degenerate in Dlx-cKO mice have increased membrane capacitance, increased spontaneous inhibitory post-synaptic currents, and hyperexcitation in response to depolarizing current pulses (Pappas *et al*., 2015). As such, this study sought to determine whether striatal dysfunction triggers adaptations in the temporal correlation between low-frequency fluctuations in resting-state blood-oxygenation-level dependent signal between the striatum and cortical, subcortical, cerebellar, and brainstem regions. In addressing whole-brain network connectivity adaptations in Dlx-cKO mice, this study employed a region-of-interest approach to functional connectivity using eight seed locations within the striatum.

Electrophysiological evidence of impaired bi-directional plasticity and synaptic integration within the cortico-striatal-thalamic pathway of overtly asymptomatic DYT1 mouse models has been related to a paradoxical increase in the activity of SCIs (Martella *et al*., 2009; Sciamanna *et al*., 2011; Dang *et al*., 2012; Martella *et al*., 2014; Sciamanna *et al*., 2012*a, b*; see also Eskow Jaunarajs *et al*., 2015). The current findings support cholinergic involvement in the compromised integrity of this major functional pathway in a symptomatic mouse model. In Dlx-cKO mice studied here, the loss of torsinA from forebrain cholinergic and GABAergic neurons resulted in significantly increased striatal functional connectivity with the primary somatosensory cortex and thalamus. This is compatible with previous work using an exploratory-based independent component analysis (ICA) (DeSimone *et al*., 2016) showing increased functional connectivity in the striatum, thalamus, and somatosensory cortex in overtly

asymptomatic Dyt1 KI mice, which emulate the human DYT1 genotype (Dang *et al*., 2005). Additionally, this finding is consistent with positron emission tomography (PET) studies reporting sensorimotor hyperexcitability in clinically affected DYT1 patients compared to non-manifesting DYT1 carriers (Carbon *et al*., 2010). Moreover, studies using DTI and probabilistic tractography have shown that thalamo-cortical microstructural differences dichotomize symptomatic from asymptomatic DYT1 carriers (Argyelan *et al*., 2009; Vo *et al*., 2015*b*).

In addition to traditional models of basal ganglia dysfunction in DYT1 dystonia (Vitek *et al*., 1999; Vitek, 2002; Zhuang *et al*., 2004), a growing body of literature has implicated the cerebellum as a focal region-of-interest. Previous imaging studies in animal models of DYT1 dystonia have focused on the axonal tract of the cerebello-thalamo-cortical pathway from a microstructural perspective; that is, imaging these tracts using DTI and probabilistic tractography *ex vivo* (e.g. Uluğ *et al*., 2011; Vo *et al*., 2015*a*). Tractography regions in these studies were selected on the basis of altered regional metabolic activity derived from changes in *ex vivo* FA and *in vivo* micro-PET and demonstrated reduced axonal fiber connectivity within cerebello-thalamo-cortical and ponto-cerebellar tracts (Uluğ *et al*., 2011; Vo *et al*., 2015*a*). Similarly, this study examined *in vivo* cerebellar and brainstem functional connectivity with the striatum based on striatal free-water and diffusivity adaptations. The striatum in Dlx-cKO mice demonstrated increased functional connectivity with the cerebellar cortex (anisiform and paramedian lobules), vermis, cerebellar (dentate) nuclei, and brainstem (pons, medulla).

These findings are consistent with prior studies in humans and animal models of DYT1 dystonia. Increased striatal functional connectivity with a distant, yet connected cerebellum is in agreement with studies showing amelioration of cerebellar-induced dystonia when di-synaptic interplay between the cerebellum and basal forebrain are interrupted (Neychev *et al*., 2008; Chen *et al*., 2014). The human DYT1 condition has been characterized by reduced FA in the dorsal pontine brainstem (Carbon *et al*. 2008*b*), which is thought to represent abnormalities of the cerebello-thalamic tract, and increased cerebellar regional blood flow and metabolic activity using PET (Eidelberg *et al*., 1998; Carbon *et al*., 2004*a*; 2008*a*; Carbon and Eidelberg, 2009; Carbon *et al*., 2010). Based on DTI findings in human subjects, Eidelberg and colleagues (Argyelan *et al*., 2009; Niethammer *et al*., 2011; Vo *et al*., 2015*b*) suggested that disease penetrance depends on the presence of an abnormality of thalamo-cortical connectivity, with manifesting patients and non-manifesting mutation carriers respectively *lacking* or *exhibiting* a distal tract lesion. They interpreted these findings to suggest that a “second hit” prevents the cerebello-thalamic defect from driving abnormal movements. A parallel set of studies in Dyt1 KI and KO mice, which do not mimic dystonic features (and may represent the non-manifesting carrier condition), exhibited abnormalities of both cerebello-thalamo-cortical and thalamo-cortical tracts (Uluğ *et al*., 2011; Vo *et al*., 2015*a*). Selective introduction of the heterozygous ΔE genotype in the hind brain, however, did not produce the dystonic movements predicted by this model (Weisheit and Dauer, 2015). Studies in models of other forms of dystonia have also emphasized dysfunction of the cerebellar nuclei and Purkinje cells to be involved in generalized dystonia (LeDoux *et al*., 1993; 1998; LeDoux and Lorden, 2002; Neychev *et al*., 2008;

Fremont *et al*., 2017). Moreover, altered functional connectivity was previously demonstrated in the anisiform and paramedian lobules of Dyt1 KI mice using exploratory ICA *in vivo* (DeSimone *et al*., 2016).

The major finding from this study is that forebrain torsinA deficiency triggers whole-brain connectivity changes across cortical, subcortical, and cerebellar functional networks *in vivo*. Unlike Dyt1 KI mice, which exhibit subtle motor abnormalities (Dang *et al*., 2005), Dlx-cKO mice spontaneously develop a dystonic-like twisting behavior, which responds to antimuscarinic therapies. Thus, forebrain eradication of torsinA in the Dlx-cKO model affords developmental, behavioral, and therapeutic effects which are akin to the manifesting carrier state in human DYT1 dystonia (Pappas *et al*., 2015). The current study provides a foundation for future work examining anticholinergic effects on functional connectivity in the Dlx-cKO mouse model, which will prove important in understanding whether whole-brain functional connectivity reflects the disease-state or manifests as an endophenotype underlying forebrain torsinA deficiency.

A final issue to address is whether striatal functional connectivity outcomes are explicitly dependent on altered microstructural and functional integrity of SCIs. Original work in the Dlx-cKO mouse model found neurodegenerative, morphological, and functional effects of forebrain torsinA deficiency to be specific to SCIs, whereas the integrity and functionality of GABAergic neurons were unaffected (Pappas *et al*., 2015). It is possible, however, that regions in Dlx-cKO mice unoccupied by cholinergic cell types (i.e., cortex) result in whole-brain functional connectivity changes. Such a finding would suggest that the suppression of GABAergic torsinA function could be partially responsible for whole-brain connectivity changes with regions containing both

cholinergic and GABAergic cell types (i.e., striatum). Future studies evaluating multi-modal imaging markers associated with the conditional knockout of torsinA specific to GABAergic or cholinergic neurons will prove important in understanding the exact nature of functional connectivity outcomes derived from such cell types.

Conclusions

This study demonstrates increased striatal functional connectivity with cortical, subcortical, cerebellar, and brainstem functional circuits in a model of DYT1 dystonia exhibiting construct, face, and predictive validity. Increased functional connectivity across multiple cerebellar and brainstem regions in Dlx-cKO mice in the absence of a cerebellar molecular lesion indicates the ability of forebrain-specific loss of torsinA to cause whole-brain changes in functional connectivity. Consistent with previous work (DeSimone *et al*., 2016), the free-water metric is again found to be a sensitive measure of microstructural integrity in mouse models of DYT1 dystonia.

Table 3-1. Summary of Support Vector Machine Classification Model in Dlx-cKO Mice. Results are based on single- and multi-cluster functional connectivity mean z-score values in a training cohort of 11 Dlx-cKO and 11 control mice and evaluated in an independent testing cohort of seven Dlx-cKO and seven control mice. AUC = receiver operating characteristic area under the curve representing sensitivity and specificity in the training cohort; Prediction = 10-fold cross validation classification accuracy in testing cohort. Common slashes denote the separation of multiple adjacent regions that comprise a common cluster of voxels with correlated time-series.

Summary of Support Vector Machine Classification Model		
Functional Connectivity Cluster(s)	**AUC**	**Prediction**
somatosensory cortex	0.86	71.4
sensory-motor thalamus	0.91	78.6
superior colliculus	0.91	71.4
pons	0.95	78.6
vermis/cerebellar nuclei	0.91	71.4
anisiform lobule	0.91	92.9
thalamus	0.91	85.7
somatosensory cortex + posterior parietal assoc.	0.83	64.3
somatosensory cortex + sensory-motor thalamus	0.82	78.6
somatosensory cortex + vermis/cerebellar nuclei	0.82	92.9
somatosensory cortex + sensory-motor thalamus + vermis + vermis/cerebellar nuclei + anisiform lobule	0.75	100
somatosensory cortex + thalamus + superior colliculus + anisiform lobule	0.75	100
somatosensory cortex + sensory-motor thalamus + superior colliculus + anisiform lobule + vermis	0.73	100
somatosensory cortex + hypothalamus/midbrain + geniculate group + anisiform lobule + vermis	0.74	100

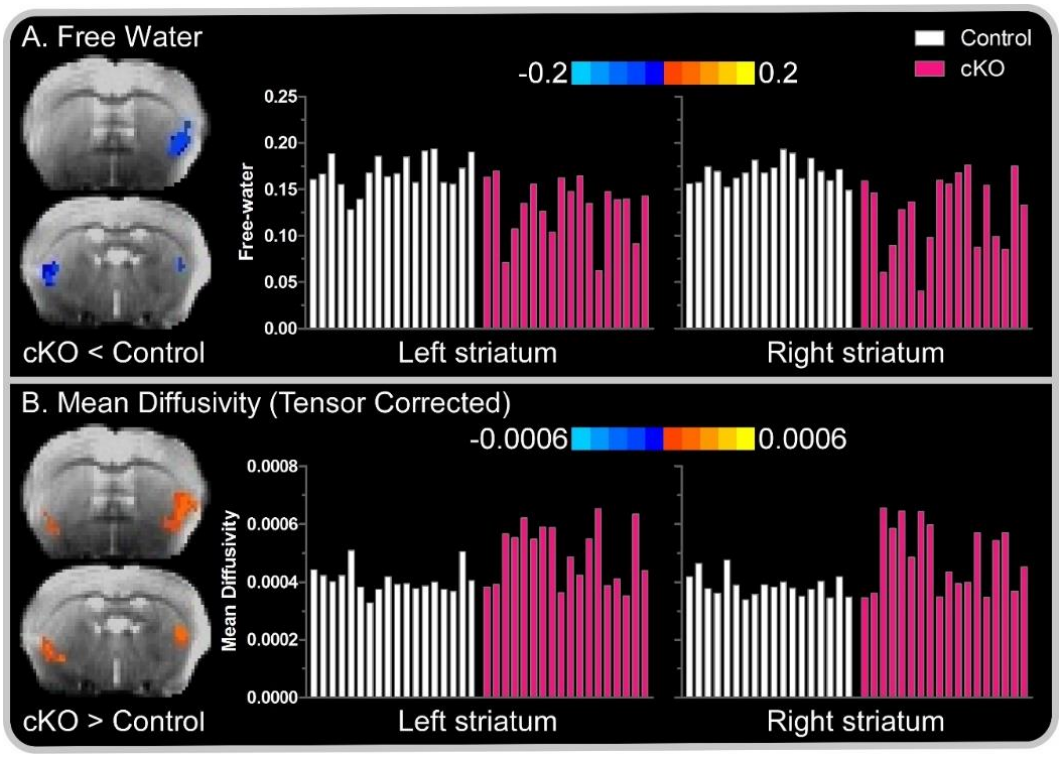

Figure 3-1. Between-Group Striatal Free-Water and Tensor-Corrected Mean Diffusivity. Color bars represent the mean difference in free-water and free-water-corrected mean diffusivity (MD_T) values for between-group post-hoc comparisons (i.e., Dlx-cKO versus control). (A) Negative values, represented by cold (blue) colors superimposed over the b0 image of a single subject, denote a significant decrease in free-water in Dlx-cKO mice compared to controls in the left and right striatum. (B) Positive values, represented by warm (red) colors, denote a significance increase in MD_T in Dlx-cKO mice compared to controls in the left and right striatum. In each panel, subject-by-subject mean free-water and MD_T values for the associated colored voxels are depicted by white and pink bars for control and Dlx-cKO mice, respectively. Results are thresholded at $P < 0.005$ at the voxel-level and FWER-corrected at $P < 0.05$.

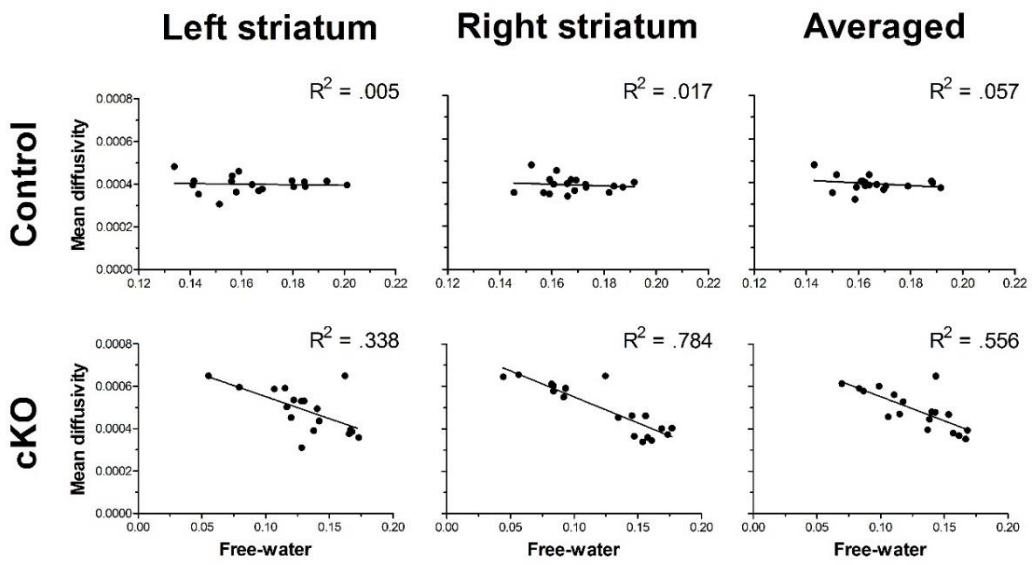

Figure 3-2. Free-Water and Tensor-Corrected Mean Diffusivity Correlations. Pearson correlations between mean free-water values (x-axis) and free-water-corrected mean diffusivity (MD_T: y-axis) in the striatum for control (top panel) and Dlx-cKO (bottom panel) mice. Values for free-water and MD_T were extracted from common voxels where between-group difference for each measure were detected. MD_T in the striatum yielded a significant moderate-to-high inverse correlation with free-water values for Dlx-cKO mice in the left and right striatum, as well as when averaged across both right and left striatum. Free-water and MD_T values in the striatum were not correlated in control mice.

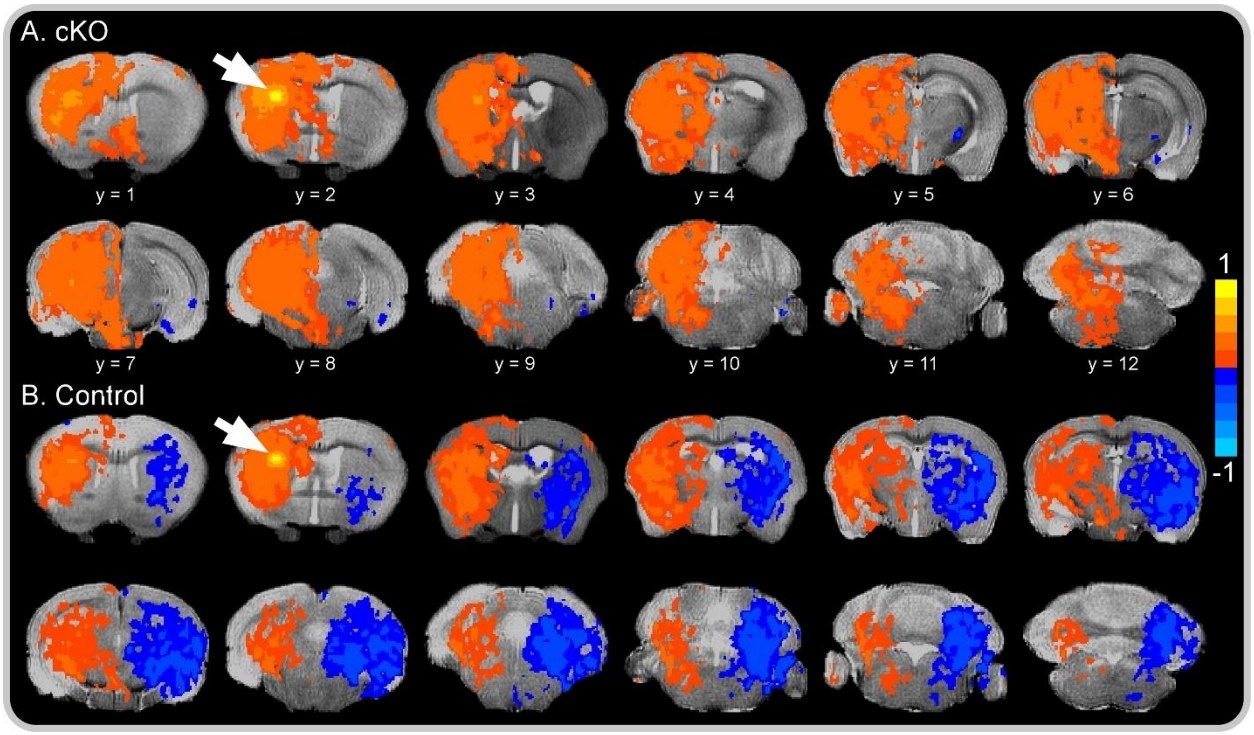

Figure 3-3. Resting-State Functional Connectivity Color Maps. Spatial color-coded z-maps for (A) Dlx-cKO and (B) control mice of functional connectivity networks across all 12 coronal brain slices originating from a single seed location in the left dorsolateral striatum (white arrow). Positive values, represented by warm (red) colors, denote a significant increase in functional connectivity with the seed location, whereas negative values, represented by cold (blue) colors, denote a significant decrease in functional connectivity with the seed location. Results are voxel-level thresholded at $P < 0.005$ and FWER-corrected at $P < 0.05$. Color maps are superimposed over the T_2-weighted image of a single subject.

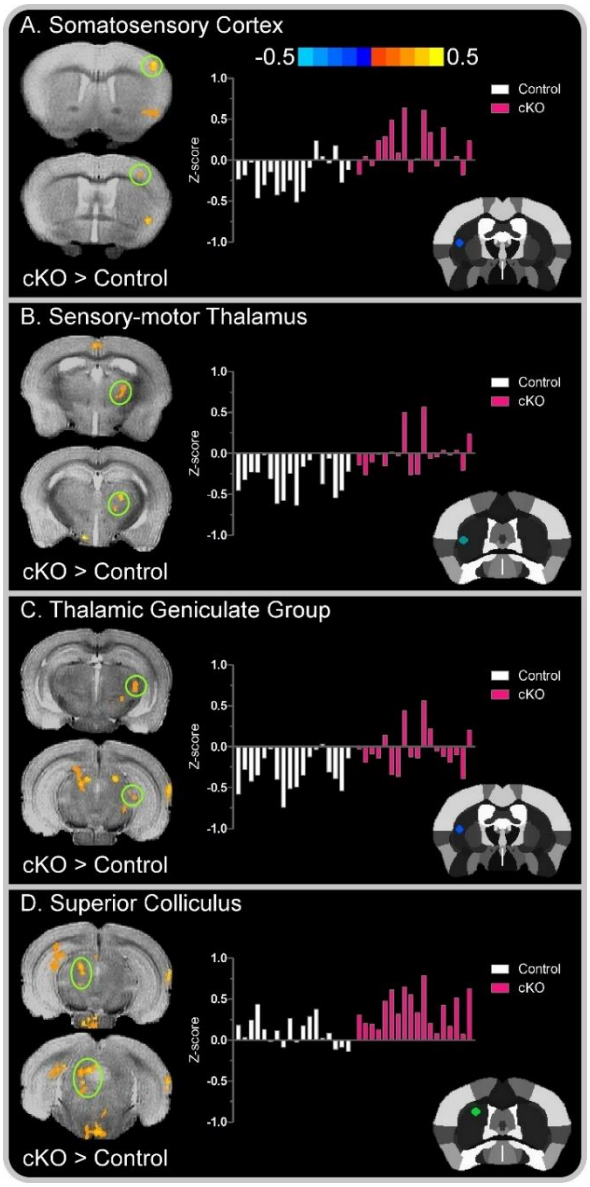

Figure 3-4. Left Seed Cortical and Subcortical Between-Group Functional Connectivity Color Maps. Color bar represents the mean difference in z-score values for Dlx-cKO versus control mice. Cluster results are voxel-level thresholded at $P < 0.005$ and FWER-corrected at $P < 0.05$. Positive values, represented by warm (red) colors, denote a significant increase in functional connectivity for Dlx-cKO mice in the (A) primary somatosensory cortex; (B) sensory-motor thalamus (C) thalamic geniculate group and (D) superior colliculus. Functional connectivity clusters are superimposed over the T_2-weighted image of a single subject. The offset right bar plot in each panel depicts the subject-by-subject mean z-score values for the associated cluster in controls (white bars) and Dlx-cKO mice (pink bars). The stereotaxic template atlas (Ferris *et al*. 2014) in each panel depicts the seed location within the left striatum wherein connectivity clusters originated.

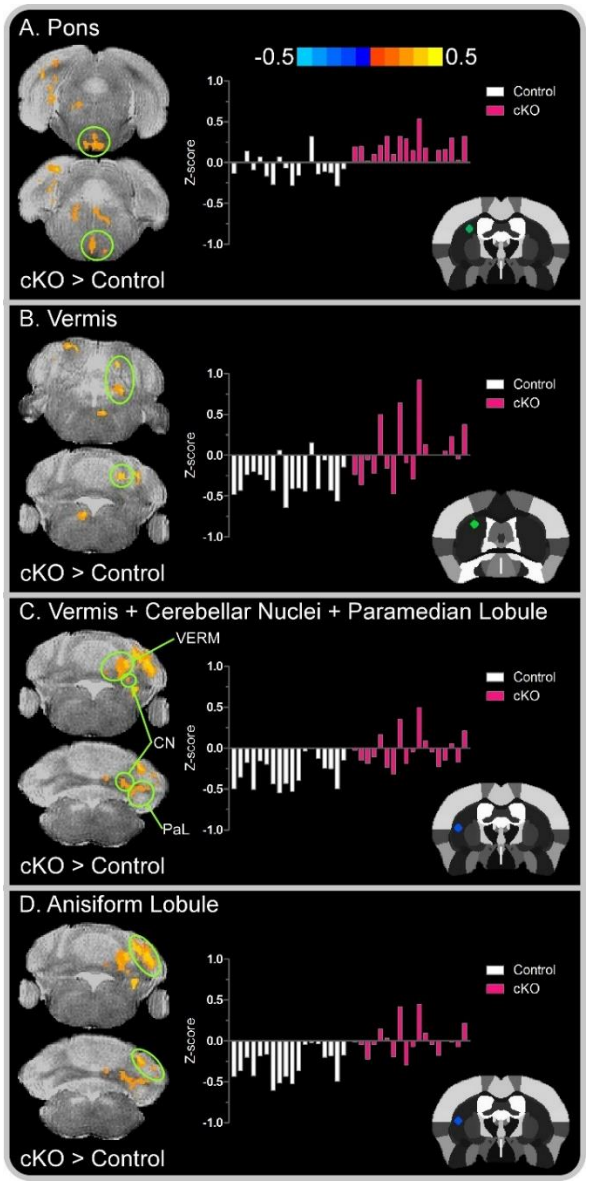

Figure 3-5. Left Seed Brainstem and Cerebellar Between-Group Functional Connectivity Color Maps. Color bar represents the mean difference in z-score values for Dlx-cKO versus control mice. Cluster results are voxel-level thresholded at $P < 0.005$ and FWER-corrected at $P < 0.05$. Positive values, represented by warm (red) colors, denote a significant increase in functional connectivity for Dlx-cKO mice in the (A) Pons; (B) vermis; (C) cluster comprised of the vermis, cerebellar nuclei, and paramedian lobule; and (D) anisiform lobule. The offset right bar plot in each panel depicts the subject-by-subject mean z-score values for the associated cluster in controls (white bars) and Dlx-cKO mice (pink bars). The stereotaxic template atlas (Ferris *et al*. 2014) in each panel depicts the seed location within the left striatum wherein connectivity clusters originated. Abbreviations: VERM = vermis; CN = cerebellar nuclei; PaL = paramedian lobule.

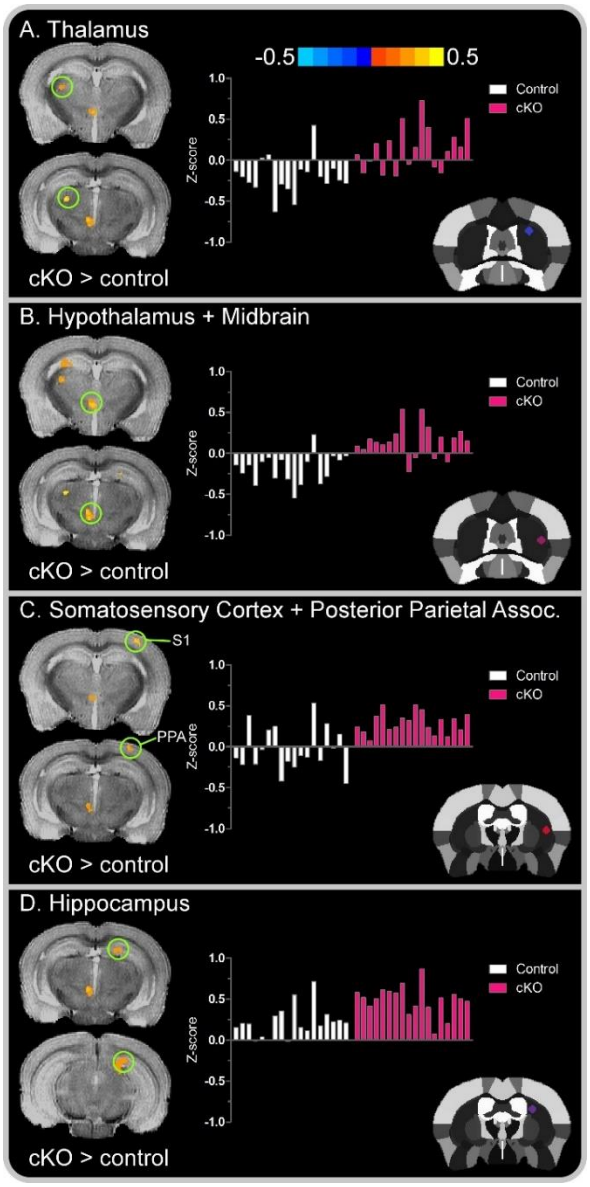

Figure 3-6. Right Seed Cortical and Subcortical Between-Group Functional Connectivity Color Maps. Color bar represents the mean difference in z-score values for Dlx-cKO versus control mice. Cluster results are voxel-level thresholded at $P < 0.005$ and FWER-corrected at $P < 0.05$. Positive values, represented by warm (red) colors, denote a significant increase in functional connectivity for Dlx-cKO mice in the (A) thalamus; (B) cluster comprised of the hypothalamus and midbrain; (C) cluster comprised of the primary somatosensory cortex and posterior parietal association area; and (D) hippocampus. The offset right bar plot in each panel depicts the subject-by-subject mean z-score values for the associated cluster in controls (white bars) and Dlx-cKO mice (pink bars). The stereotaxic template atlas (Ferris *et al*. 2014) in each panel depicts the seed location within the left striatum wherein

connectivity clusters originated. Abbreviations: S1= primary somatosensory cortex; PPA = posterior parietal association area.

CHAPTER 4
IMPAIRED SENSORY-EVOKED BRAIN ACTIVATION AND CONNECTIVITY RELATES TO MOTOR DEFICITS IN D2R-EXPRESSING STRIATUM-SPECIFIC DYT1 CONDITIONAL KNOCKOUT MICE

Chapter Summary

Early-onset generalized dystonia (DYT1 dystonia) is caused by a loss-of-function mutation in the protein torsinA, leading to involuntary muscle contractions, involuntary movements, and severe disabling postures. Dopamine type-2 receptor (D2R)-expressing medium spiny neurons and cholinergic interneurons of the striatum are centrally involved in the mediation of motor control. Dysfunction of these neurons has been extensively implicated in dystonia pathogenesis. Developing markers of network-level brain function related to the loss of D2R-expressing torsinA is fundamental to our understanding of dystonia pathophysiology and developing novel therapeutic strategies. The current study used *in vivo* functional and diffusion magnetic resonance imaging to examine brain function and microstructure in a mouse model of dystonia characterized by conditional knockout of torsinA from striatum-specific D2R-expressing cells (Dyt1 d2KO mice). Until now, neuroimaging studies in dystonia mouse models have used resting-state paradigms to understand the neural network-level signatures that may characterize the expression of dystonia. The loss of movement control in dystonia highlights a critical need for a brain imaging approach that can gain insight into the dysfunction of task-related sensorimotor pathways. To this end, a novel aspect of the current study is the use of sensory-evoked fMRI to understand how loss of torsinA in D2R-expressing striatal neurons influences blood-oxygen-level dependent (BOLD) activation and functional connectivity within sensorimotor brain regions. Here, d2KO mice exhibited impaired BOLD activation in the cortex, striatum, globus pallidus, and

thalamus compared to controls, and BOLD signal in d2KO mice correlated with motor performance deficits. Furthermore, d2KO mice exhibted anti-correlated BOLD signal during the sensory task. Resting-state fMRI in combination with striatal seed-based correlation revealed adaptations in cortical and brainstem connectivity. Neurite orientation dispersion and density imaging (NODDI), a technique sensitive to microstructural properties of neuronal tissue and free-water compartments, revealed no differences between d2KO mice and controls. This study provides fresh evidence that the loss of torsinA in striatal D2R-expressing neurons impairs the integration of exogenous sensory information, which may contribute to motor deficits in dystonia. Furthermore, this study establishes the utility of sensory-evoked fMRI to explore substrates of sensorimotor adaptations underlying dystonia pathophysiology, and this technique has high translational leverage for studies in human patients.

Introduction

Early-onset generalized dystonia (DYT1 dystonia) – the most common and clinically severe form of the disorder – is characterized by involuntary movements and disabling postures affecting axial and appendicular musculature (Albanese *et al*., 2013). DYT1 dystonia is linked to a dominantly inherited ΔGAG deletion within the DYT1/TOR1A gene encoding the protein torsinA (Ozelius *et al*., 1997). The exact pathogenic mechanism by which torsinA dysfunction causes dystonia is not yet clear. Convergent evidence from human and animal studies has implicated an imbalance in striatal dopaminergic and cholinergic neurotransmission as a core feature of dystonia pathophysiology (Eskow Jaunarajs *et al*., 2015). Reduced dopamine type-2 receptor (D2R) availability and binding has been reported in DYT1 mutation carriers (Asanuma *et al*., 2005; Carbon *et al*., 2009) and Dyt1 +/ΔGAG [Dyt1 knock-in (KI)] mice, which have

the 3-base pair mutation analogous to human patients (Dang *et al*., 2005). Defective D2R binding and a resultant hypercholinergic state has been posited to cause deficits in cortico-striatal plasticity in Dyt1 KI mice and transgenic mice overexpressing human mutant torsinA (Pisani *et* al., 2006; Martella *et al*., 2009; Dang *et al*., 2012; Martella *et al*., 2014; Scarduzio *et al*., 2017). In dystonia patients, muscarinic anticholinergic drugs can help alleviate symptoms (Jankovic, 2013), and similar therapeutic benefits to motor control (Dang *et al*., 2012; Pappas *et al*., 2015; DeAndrade *et al*., 2016) and cortico-striatal plasticity deficits (Martella *et al*., 2009; Dang *et al*., 2012; Maltese *et al*., 2014) can be achieved in various dystonia mouse models. Providing *in vivo* readouts of the systems-level changes in brain function and microstructure related to dysfunction of dopaminergic and cholinergic cell types is fundamental to our understanding of dystonia and developing improved therapeutic strategies.

Striatal cholinergic interneurons (SCI) play a critical role in the modulation of basal ganglia dopaminergic and cholinergic pathways (Eskow Jaunarajs *et al*., 2015). The maintenance and function of SCIs is selectively vulnerable to the loss of torsinA within a set of neuronal cell types. SCIs in heterozygous Dyt1 conditional cholinergic knockout (KO) mice exhibit paradoxical excitation in response to the D2R agonist quinpirole (Sciamanna *et al*., 2012*b*). Whole-brain KO of torsinA within a single allele combined with conditional heterozygous KO of torsinA in forebrain cholinergic and GABAergic neurons [Dlx-cKO mice (Pappas *et al*., 2015)], as well as cholinergic neurons throughout the neuraxis [ChAT-cKO mice (Pappas *et al*., 2018)] causes high-yield SCI-specific cell loss and overt twisting postures consistent with motor features of dystonia. The loss of torsinA specific to striatal D2R-expressing cells is sufficient to

recapitulate this cell autonomous effect. Mice with homozygous conditional KO of torsinA within striatum-specific D2R-expressing neurons (Dyt1 d2KO mice) similarly exhibited high-yield SCI-specific cell loss and striatal neurochemical changes (Yokoi *et al*., *in preparation*). Moreover, d2KO mice exhibited rotarod and beam-walking deficits despite the absence of an overt dystonia phenotype. How the loss of striatal D2R-expressing torsinA influences systems-level changes in brain pathophysiology is not yet clear. This represents an important research question because recent work has pointed to large-scale changes in functional connectivity in Dlx-cKO mice (DeSimone *et al*., 2017). Acquiring *in vivo* markers related to loss of striatal D2R-expressing torsinA is an important and logical step in understanding how specific dysfunction of dopaminergic and cholinergic cell types contributes to dystonia.

In accomplishing this objective, the current study used *in vivo* functional MRI (fMRI) and diffusion MRI at high-field (11.1 Tesla) in d2KO mice. Brain function was examined using two techniques. First, fMRI in combination with thermal stimulation of the hind limb [sensory-evoked fMRI (stimfMRI)] was used to test the hypothesis that blood-oxygen-level dependent (BOLD) activation and functional connectivity within sensorimotor regions of the cortex, basal ganglia, and cerebellum is impaired in d2KO mice. D2R-expressing cells, such as striatal medium spiny neurons (MSN) and SCIs, are centrally involved in the convergence of thalamo-striatal and cortico-striatal input and mediation of motor output (Apicella, 2007; Aosaki *et al*., 2010; Thorn and Graybiel, 2010; Calabresi *et al*., 2014; Eskow Jaunarajs *et al*., 2015). Adaptations in sensory-evoked brain function caused by loss of D2R-expressing torsinA may provide insight on the underlying mechanisms contributing to loss of movement control in dystonia.

Second, resting-state fMRI (rsfMRI) in combination seed-based correlation (e.g., Biswal *et al*., 1995; Fox *et al*., 2005) was used to test the hypothesis that striatal D2R-expressing torsinA dysfunction would cause changes in functional connectivity between the striatum and connected cortical and subcortical regions. In addition, multi-shell high-angular-resolution diffusion imaging (HARDI) combined with a three-compartment neurite orientation dispersion and density imaging model [NODDI (Zhang *et al*., 2012)] was used map microstructural adaptations in the striatum of d2KO mice.

Methods

Animals and Housing

Twenty-one adult male d2KO mice (age: 194.6 ± 28.0 days) and 21 adult male Dyt1 loxP +/- or Dyt1 loxP -/- control mice (age: 194.6 ± 26.6 days) were used in this experiment. Generation of d2KO mice has been previously described (Yokoi *et al*., *in preparation*). Drd2-Cre mice were purchased from MMRRC (Cat. No. 032108; B6.FVB(Cg)-Tg(Drd2 cre)ER44Gsat/Mmucd) (Gong *et al*., 2007). Dyt1 loxP mice, which had floxed exons 3-4, were prepared as previously described (Yokoi *et al*., 2008). Double heterozygote Drd2-Cre +/- Dyt1 loxP +/- mice were generated by crossing the Drd2-Cre +/- mice and either Dyt1 loxP +/- or Dyt1 loxP -/- mice. Dyt1 d2KO mice were generated by crossing the double heterozygote mice and either Dyt1 loxP +/- or Dyt1 loxP -/- mice. Mice were housed in groups of one to three under condition of an alternating 12 h light-dark cycle (i.e., lights off at 18:00 h) and were provided *ad libitum* food and water access. All experimental procedures were conducted in ethical accordance with the Guide for the Care and Use of Laboratory Animals and the Institutional Animal Care and Use Committee at the University of Florida.

Motor Behavior Assessment and Analysis

Balance and coordination ability of d2KO and control mice were evaluated using accelerated rotarod (Economex, Columbus Instruments) and beam-walking assessments. In order to eliminate potential confounding effects of behavioral testing stress on brain function, behavioral testing was performed 32.0 ± 13.9 days and 25.4 ± 13.6 days prior to brain imaging for rotarod and beam-walking assessments, respectively.

For the rotarod test, mice were placed on a rotating spindle with an initial speed of 4 rpm. The spindle rotation gradually accelerated at a rate of 0.2 rpm/s and latency-to-fall time was measured with a 3-minute cut-off time. Each mouse was tested on three trials each day for two consecutive days and a 1 h rest interval was afforded between trials.

For beam-walking, mice were trained to transverse a medium size (14 mm width) square beam on three trials each day for two consecutive days. Mice were then tested across two trials on the medium square beam and a medium round beam (17 mm diameter) on the third day, and a small square beam (7 mm width) and small round beam (10 mm diameter) on the fourth day. The length of each beam was 100 cm. Total beam slips for each beam were recorded.

Data were analyzed using logistic regression with negative binomial distribution using the GEE model in SAS/STAT (Version 9.1.3). Data were log-transformed to obtain normal distribution. Data from control mice were normalized to 0 and d2KO were normalized to that of control mice. Model variables for rotarod included latency-to-fall times for all six trials, age, and weight. Model variables for beam-walking included beam

slips for all four beams, slip side (left, right), repeat variable (trial), age, and weight. The response variable in both models was group (d2KO, control).

MRI Preparation

Mice were placed under general anesthesia for the duration of each experiment using isoflurane delivered using compressed air through Surgivet vaporizer (Dublin, OH) connected to charcoal trap. Initial knock-down was performed in an enclosed chamber using 3% isoflurane for approximately 1-minute. Mice were maintained under anesthesia using 1-1.5% isoflurane for the duration of setup and MRI acquisition sequences. As shown in Fig. 4-1A-B, mice were placed in a prone position on a custom designed plastic mouse bed equipped with a bite-bar that immobilized the head and delivered anesthesia. An in-house 2.5×3.5 cm quadrature surface transmit/receive coil was affixed to the top of the skull and tuned to 470.7 MHz (^{1}H resonance) for B^{1} excitation and signal detection (AMRIS, University of Florida, Gainesville, FL). Respiration rate was monitored using a respiration pad (SA Instruments, Stony Brook, NY) placed beneath the abdomen. Core body temperature was monitored via thermal rectal probe (SA Instruments, Stony Brook, NY) and maintained using a custom recirculating waterbed heating system. A 256 mm^2 MR compatible advanced thermal stimulator (ATS) thermode (PATHWAY System, Medoc Advanced Medical Systems, Chapel Hill, NC) was affixed to the bottom of the right hind paw (Fig. 4-1C), which delivered a heat stimulus during stimfMRI.

MRI Acquisition

MRI data was acquired using an 11.1 Tesla Magnex Scientific 40 cm horizontal magnet (Bruker BioSpin, Billerica, MA) with RRI BFG-240/120-S6: bore size 120mm, Gmax = 1000 mT/m @325A with 200 µs rise time. Acquisition sequences were

prepared and controlled using ParaVision (Version 6.0.1). T_2-weighted anatomical scans were acquired for spatial normalization using a turbo RARE sequence with the following parameters: TR = 5,500 ms; TE = 30 ms; excitation angle = 90°; refocusing angle = 180°; dummy scans = 1; averages = 7; slices = 13; orientation = coronal; thickness = 0.9 mm; gap = 0 mm; FOV = 15×15 mm; data matrix = 256×256 in-plane.

Two separate stimfMRI scans were acquired using spin echo EPI sequences with the following parameters: TR = 2,000 ms; TE = 15 ms; repetitions = 360; flip angle = 90°; dummy scans = 2; slices = 13; orientation = coronal; thickness = 0.9 mm; gap = 0 mm; FOV = 15×15 mm; data matrix = 64×64 in-plane. Two separate rsfMRI scans were acquired using the same sequence and parameters as stimfMRI with half the repetitions (180). Notably, during rsfMRI acquisition, the thermode remained affixed to the hind paw but the PATHWAY terminal was turned off.

During each stimfMRI run, thermal stimulation was applied to the bottom of the right hind paw via heating thermode attached to PATHWAY model terminal. The PATHWAY System was calibrated such that the thermode alternated between five 60 s blocks of no thermal stimulation (NO-STIM) and five 60 s blocks of thermal stimulation (STIM) (Fig. 4-1D). Each run began and ended with a 30 s and 60 s NO-STIM block, respectively. The thermode temperature was maintained at 30°C during NO-STIM blocks and 42°C during STIM blocks. The thermode heated and cooled at a rate of 8°C/s, permitting alteration between NO-STIM and STIM epochs within 2 s. Similar techniques using temperatures between 46 and 48°C have been used to define nociceptive processing pathways in rodents, including key sensory processing nodes

within the sensorimotor cortex, striatum, thalamus, cerebellum, and brainstem (Becerra *et al*., 2011; Bosshard *et al*., 2015).

A two-shell HARDI protocol was used to acquire diffusion MRI data. The acquisition consisted of the following parameters: TR = 4,000 ms; TE = 19 ms; averages = 4; flip angle = 90°; slices = 17; orientation = coronal; thickness = 0.7 mm; gap = 0 mm; FOV = 15×11 mm; data matrix = 128×96 in-plane. The following diffusion parameters were used: two non-diffusion weighted b0 images; small shell b-value = 600 s/mm^2; large shell b-value = 2000 s/mm^2; directions = 52 total (six at b-value = 600 s/mm^2; 46 at b-value = 2000 s/mm^2).

stimfMRI: Preprocessing and Analysis

Functional MRI data preprocessing was performed using custom-designed UNIX shell scripts in FMRIB Software Library (FSL: Oxford, UK) and Analysis of Functional NeuroImages (AFNI: Cox, 1996). Preprocessing for each stimfMRI run included removal of the first five volumes for magnetization equilibrium, rigid-body volume registration, spatial co-registration of the fMRI scan to the anatomical scan, spatial normalization of each fMRI scan to an anatomical template image, and in-plane spatial smoothing with a Gaussian full width at half-maximum (FWHM) kernel of 0.5 mm^2. Six head motion parameters were calculated using the 1d_tool.py function and consecutive TRs exceeding a 0.45 mm motion criterion in the x-, y-, and z- directions were censored. Mice were excluded from the analysis if the number of censored TRs exceeded 25% of total TRs. Six control and six d2KO mice were removed from stimfMRI analyses due to high motion volumes exceeding this threshold. Two types of statistical analyses were performed on stimfMRI data including (1) examination of BOLD β-coefficients in the

framework of the general linear model to examine sensory-evoked brain activation and (2) seed-based correlation (e.g., Fox *et al*., 2005) to examine functional connectivity between the striatum and all other brain voxels.

In the BOLD analysis, for each subject the instantaneous BOLD signal at each voxel and each time-point was scaled by the average BOLD signal across its respective time-series. The BOLD signals obtained from the NO-STIM and STIM blocks were modeled using a boxcar regressor convolved with a canonical hemodynamic response function. Using 3dDeconvolve in AFNI, the regression was performed across NO-STIM and STIM blocks to estimate the β-coefficient and its associated t-statistic for the BOLD contrast, separately for each run. Non-specific sources of nuisance from the head motion parameters calculated during data preprocessing were regressed. β-coefficients were analyzed using a 2 (group: d2KO, control) by 2 (run: 1, 2) voxel-wise ANOVA model (3dANOVA2). The cluster-extent required to control false positive rate and achieve a voxel-wise significance threshold of $P < 0.005$ ($P < 0.05$ FWER-corrected) was determined by submitting the β-coefficient values to an independent-samples t-test (3dttest++) with 3dClustSim bootstrapping option, separately for each stimfMRI run. The average cluster extent threshold across both runs (0.936 mm^3) was used to determine group-level ANOVA effects.

Sensory-evoked functional connectivity was analyzed by examining the entire stimfMRI time-series across NO-STIM and STIM blocks using a seed-based correlation approach, separately for each run. For each subject, a mask was manually drawn within the ventricles to calculate CSF-related noise signal. Non-specific sources of nuisance from the six head motion parameters and CSF signal were regressed using

3dDeconvolve. Sixteen *a priori* selected seed regions-of-interest in the striatum were used in this analysis. In both the right and left striatum, a seed was manually drawn in each of the four striatal quadrants (dorsolateral, dorsomedial, ventrolateral, ventromedial), on both rostral and caudal coronal slices of the striatum. Notably, the selection of striatal seeds was based on the hypothesis that torsinA deficiency within striatal D2R-expressing cells would engage connected regions of the cortex, basal ganglia, and cerebellum into an aberrant connectivity network. Furthermore, these regions-of-interest correspond to regions containing loss of SCIs and neurochemical abnormalities as previously described in original work of this model (Yokoi *et al*., *in preparation*), suggesting impaired function of this region. After obtaining the residual time-series, Pearson's correlation coefficients were computed (3dTcorr1D) between the time-series of the seed and that of all other brain voxels, separately for each stimfMRI run. Correlation coefficients were converted to z-scores using Fisher r-to-z transformations. For the group-level analysis, z-scores were analyzed using a 2 (group: d2KO, control) by 2 (run: 1, 2) voxel-wise ANOVA, separately for each seed. The cluster-extent required to control false positive rate and achieve a voxel-wise significance threshold of $P < 0.005$ ($P < 0.05$ FWER-corrected) was determined using an independent-samples t-test with 3dClustSim bootstrapping option for a single seed, separately for each rsfMRI run. The average cluster-extent threshold across both runs (0.985 mm^3) was used to determine group-level effects in the ANOVA for each seed.

rsfMRI: Preprocessing and Analysis

Preprocessing for each rsfMRI run included removal of the first five volumes, rigid-body volume registration, de-spiking of time-series signal outliers, spatial co-registration of the fMRI scan to the anatomical scan, spatial normalization of each fMRI

to an anatomical template image, and in-plane spatial smoothing with a Gaussian FWHM kernel of 0.5 mm^2. Six head motion parameters were calculated and consecutive TRs exceeding a 0.45 mm motion criterion in the x-, y-, and z- directions were censored. Three control and three d2KO mice were removed from this analysis due to high motion volumes exceeding 25% of total TRs. For each subject, a mask was manually drawn within the ventricles to calculate CSF-related noise signal. Nuisance variance from the six motion parameters and CSF signal were regressed and the residual signal was temporally filtered using band-pass filter (3dbandpass) with cut-off frequency between 0.01-0.1 Hz.

The striatal seed locations, computation of z-scores, and group-level analyses were performed as described for stimfMRI functional connectivity. The cluster-extent required to control false positive rate and achieve a voxel-wise significance threshold of $P < 0.005$ ($P < 0.05$ FWER-corrected) was determined using the same procedure as described for the stimfMRI functional connectivity analysis applied to both rsfMRI runs. The average cluster-extent threshold across both runs (0.690 mm^3) was used to determine group-level effects in the ANOVA for each seed.

Correlation Analysis

Spearman rank correlations were performed to determine the relation between motor performance and brain function. Correlation analyses were performed independently for the d2KO and control groups. For each mouse, the average β-coefficient across voxels revealing significant between-group effects in the ANOVA was computed and averaged across stimfMRI runs. For stimfMRI and rsfMRI functional connectivity, the average z-score within clustered voxels revealing significant between-group effects in the ANOVA was computed and averaged across runs. Average β-

coefficient and z-score values were tested against average latency-to-fall times across the six trials in the rotarod assessment and average number of beam slips across the two beam-walking trials for the small round beam. Notably, the analysis was performed using the small round beam because the medium sized beams and small square beam yielded few slips in both the d2KO and control groups.

NODDI: Preprocessing and Analysis

Diffusion MRI preprocessing was performed using custom designed Unix shell scripts in FSL and AFNI. The preprocessing pipeline included eddy-current and head motion correction, compensation of diffusion gradient rotations in response to these corrections, and skull stripping of non-brain tissue. NODDI parameters were computed using the NODDI toolbox extension (Version 1.0.1) in MATLAB (Version R2014a). From the eddy-current and motion-corrected volumes, NODDI (Zhang *et al*., 2012) partitions each voxel into three separate compartments including (1) an intra-neurite (intracellular) compartment containing axons and dendrites and modeled as anisotropic restricted diffusion, (2) an extra-neurite (extracellular) compartment containing cell soma and glia and modeled as hindered Gaussian anisotropic diffusion, and (3) a free-water (CSF) compartment modeled as isotropic Gaussian diffusion. The full normalized signal A within the NODDI framework can be written as:

$$A = (1 - V_{iso})(V_{ic}A_{ic} + 1 - V_{ic})A_{ec}) + V_{iso}A_{iso}$$

where *iso*, *ic*, and *ec* respectively represent free-water, intracellular, and extracellular compartments, V represents the compartmentalized partial volume, and A represents the normalized diffusion signal. V_{iso} and V_{ic} were the primary metrics obtained from the above equation and both range in values from 0.0 to 1.0. NODDI also uses Watson distribution (Mardia and Jupp, 1990) to compute orientation dispersion index (ODI) from

the normalized signal A_{ic}, which represents the degree of spread among non-parallel neurites about some central orientation. ODI values range from 0, representing low dispersion and perfect parallel orientation of neurites, to 1, representing maximal dispersion of neurites. To standardize the data, the DTIFIT function in FSL was used to fit a diffusion tensor to each voxel, and the resultant fractional anisotropy (FA) map from each mouse was non-linearly warped to a standard FA template using the ANTs toolbox (Release 1.5: Avants *et al*., 2011). The FA image was selected for the normalization procedure due to its superior contrast between grey matter, white matter, and CSF. The resultant FA data warp was applied to V_{iso}, V_{ic}, and ODI maps. Independent-samples t-tests in AFNI were used to examine between-group effects in V_{iso}, V_{ic}, and ODI. Two d2KO and four control mice were removed from this analysis due to high motion-related image distortion in the diffusion weighted images. The cluster-extent (1.35 mm^3) required to control false positive rate and achieve a voxel-wise significance threshold of $P < 0.005$ ($P < 0.05$ FWER-corrected) was determined using 3dClustSim.

Results

d2KO Mice Exhibit Motor Deficits Without Overt Dystonia

Although d2KO mice appear normal and do not exhibit overt dystonic-like movements and postures, they have been shown to exhibit deficits in fine motor coordination and balance (Yokoi *et al*., *in* preparation). To determine whether these behavioral features were present in the current cohort, d2KO and control mice were evaluated using the accelerated rotarod and beam-walking assessments. Mice in the d2KO group had significantly faster rotarod latency-to-fall times [normalized log latency-to-fall: control: 0.0 ± 0.0 s; d2KO: -0.2 ± 0.1 s, $P < 0.05$ (Fig. 4-2A)] and significantly

increased beam-walking slips compared to controls [log relative slips: control: 0.0 ± 0.0; d2KO: 0.62 ± 0.31, $P < 0.05$ (Fig. 4-2B)].

stimfMRI: Impaired BOLD Activation in d2KO Mice

Thermal stimulation of the hind limb was used to probe BOLD activation of sensorimotor regions in the brain. A first step included examination of the within-group effects on the β-coefficients, separately for d2KO and control groups. In both groups, BOLD activation was significantly increased within the sensorimotor cortex, cingulate, retrosplenial area, parietal cortex, striatum, globus pallidus, thalamus, cerebellar cortex, and brainstem. In general, the effects were stronger and more widespread in control compared to d2KO mice. BOLD activation with these regions is in line with prior studies using thermal stimulation to examine function of nociceptive processing pathways in rodents (Becerra *et al*., 2011; Bosshard *et al*., 2015) and provided confirmation that the thermal stimulation technique was successful in activating key sensorimotor processing nodes. In terms of between-group effects, d2KO mice showed an extensive pattern of reduced BOLD activation compared to control mice bilaterally in the striatum, globus pallidus, sensory cortex, associative cortex, and left thalamus (Fig. 4-3). These findings suggest that the loss of D2R-expressing striatal torsinA caused deficits in the integration of thermal sensory information.

stimfMRI: Impaired Sensory-Evoked Functional Connectivity in d2KO Mice

A seed-based correlation approach was used to examine functional connectivity with the striatum during sensory-evoked fMRI. Compared to control mice, d2KO mice exhibited reduced functional connectivity in the right striatum and associative cortex with a seed in the left rostral ventromedial striatum, as well as reduced functional

connectivity of the left striatum and associative cortex with a seed in the right rostral dorsolateral striatum (Fig. 4-4).

rsfMRI: Abnormal Cortical and Brainstem Connectivity in d2KO Mice

The same striatal seed-based correlation approach employed for stimfMRI was used to examine functional connectivity on the rsfMRI data. Compared to control mice, d2KO mice exhibited increased functional connectivity of the brainstem with a seed in the right rostral ventromedial striatum, as well as reduced functional connectivity of the right sensory cortex with a seed in the left rostral ventromedial striatum (Fig. 4-5).

Impaired BOLD Activation and Connectivity Relates to Motor Deficits in d2KO Mice

Average β-coefficient values within voxels where d2KO mice showed reduced BOLD activation compared to control mice (Fig. 4-3) yielded a significant positive correlation with rotarod latency-to-fall times ($r = 0.529$, $P = 0.043$) and significant negative correlation with beam slips ($r = -0.65$, $P = 0.009$). That is, reduced BOLD activation in d2KO mice was associated with faster latency-to-fall times and increased beam slips, suggesting that motor deficits in d2KO mice may relate, in part, to dysfunctional sensory integration. To determine if one or more region(s) revealing impaired BOLD activation in the d2KO group correlated more strongly with motor performance, average β-coefficient values were anatomically decomposed into six separate clusters including: (1) left sensory cortex, (2) left associative cortex, and (3) left striatum, globus pallidus, and thalamus, (4) right sensory cortex, (5) right associative cortex, and (6) right striatum and globus pallidus. Cluster 3 yielded a significant positive correlation with rotarod latency-to-fall times in d2KO mice ($r = 0.564$, $P = 0.028$), whereas clusters 3 and 6 yielded significant negative correlations with small round

beam slips in d2KO mice (cluster 3: r = -0.589, *P* = 0.02; cluster 6: r = -0.835, *P* = 0.001). Thus, it is clear that the striatum, globus pallidus, and thalamus were primarily driving the correlation between reduced BOLD activation and motor performance deficits in d2KO mice. In addition, sensory-evoked z-score values from the cluster in the right striatum and associative cortex (left ventromedial seed: Fig. 4-4) revealed a significant negative correlation with small round beam slips (r = -0.523, *P* = 0.045). Average resting-state z-score values from clusters in the right sensory cortex and brainstem (Fig. 4-5) did not correlate with motor performance in d2KO mice. Average sensory-evoked β-coefficient values, and z-scores for sensory-evoked and resting-state functional connectivity did not correlate with rotarod or beam-walking performance in control mice.

NODDI: No Volumetric or Diffusivity Changes in d2KO Mice

An objective of this study was to provide an *in vivo* interpretation of changes in brain microstructure using diffusion MRI (NODDI), reflecting the loss of SCIs or potential cellular consequences in d2KO mice (Yokoi *et al*., *in preparation*). Specifically, the loss of SCIs was hypothesized to cause an increase and decrease in the partial volumes of the extracellular free-water (V_{iso}) and intracellular (V_{ic}) compartments, respectively. However, NODDI did not reveal volumetric or diffusivity differences between d2KO and control groups.

Discussion

The present study examined how loss of the dystonia protein torsinA within striatal D2R-expressing cells influenced functional brain activation and connectivity. Sensorimotor deficits in dystonia highlight a critical need for a brain imaging approach that can dissect the effects of cell-specific torsinA deficiency on the functional integrity

of task-related sensorimotor networks. A novel component of the present study is the implementation of sensory-evoked fMRI to examine BOLD activation and functional connectivity using thermal stimulation of the hind limb. The loss of torsinA from striatal D2R-expressing cells caused widespread deficits in BOLD activation within the sensory cortex, striatum, globus pallidus, and thalamus, as well as loss of functional connectivity strength between the left and right striatum. A salient finding was that reduced sensory-evoked BOLD activation and connectivity significantly correlated with rotarod and beam-walking deficits, suggesting that sensory dysfunction may contribute to the loss of motor control in d2KO mice. This study establishes the utility of sensory-evoked fMRI in evaluating task-related brain function in animal models of dystonia.

Impaired Sensory-Evoked Brain Activation and Connectivity in d2KO Mice

A standard neuroimaging approach in mouse models of dystonia is the implementation of resting-state paradigms, including rsfMRI functional connectivity (DeSimone *et al*., 2016; 2017) and [^{18}F]-FDG micro-PET gluco-metabolism (Uluğ *et al*., 2011; Zhao *et al*., 2011; Vo *et al*., 2015*a*). Indeed, these techniques are opportune for *in vivo* studies because they do not require advanced training of mouse models to execute a motor task and anesthesia limits motion-related distortions of MR signals. A drawback of resting-state paradigms, however, is that they do not provide consideration for task-positive network properties. Identifying brain regions functionally modulated by sensory- and/or motor-related task conditions may provide better insight into the neural network-level signatures underlying clinical features of dystonia. A novel aspect of the current study is the use of sensory-evoked fMRI to understand how torsinA deficiency of striatal D2R-expressing neurons influences BOLD activation and functional connectivity within sensorimotor brain regions. This technique is advantageous because a sensory task

does not require advanced training of mice and can be implemented under the same experimental conditions as rsfMRI.

To this end, *in vivo* brain activation and functional connectivity were examined using sensory-evoked fMRI involving thermal stimulation applied to the hind limb. The d2KO group exhibited significantly reduced BOLD activation in the sensory cortex, associative cortex, striatum, globus pallidus, and thalamus, as well as decreased coactivation of the left and right striatum relative to controls. Reduced β-coefficient values within these regions yielded moderate-to-strong correlations with faster rotarod latency-to-fall times and increased beam-walking slips in d2KO mice but not controls. Notably, after decomposing the BOLD activation effects into six anatomically defined clusters, it became clear that the striatum, globus pallidus, and thalamus were primarily driving the relation between sensory-evoked brain activation and motor performance. This set of findings suggests that motor control deficits in d2KO mice could be related, in part, to impaired integration of sensory information required for action selection and control. Assays of task-related impairments in the motor domain using $H_2{}^{15}O$-PET were revealed in sensorimotor cortex, supplementary motor area, pre-motor cortex, and inferior parietal lobule in clinically manifesting DYT1 patients during a kinematic limb control task (Carbon *et al*., 2010). Clinically unaffected DYT1 mutation carriers exhibited abnormalities of pre-frontal, auxiliary motor, associative parietal and occipital, and cerebellar regions during a motor sequence learning task (Ghilardi *et al*., 2003; Carbon *et al*., 2008*a*). These studies do not provide consideration of deficits in the sensory domain. This represents an important research question because in addition to motor symptoms, studies in focal dystonia have reported abnormalities in sensory function and

sensorimotor integration, including spatial and temporal discrimination, muscle proprioception, and sensory-gating (for reviews see Conte *et al*., 2019; Desrochers *et al*., 2019). Furthermore, a recent study reported that Dyt1 KI mice had longer response times in touching and removing an adhesive sticker placed on the nose and were less successful in transversing a beam after unexpected beam rotation was introduced (Richter *et al*., 2017). These findings were interpreted to reflect impaired ability to use proprioceptive input in guiding motor actions.

While the exact cause of sensory dysfunction in dystonia is not yet clear, the findings from the present study implicate reduced sensory-evoked activation and loss of connectivity strength as one possible substrate. Abnormal sensory processing of the cortex, basal ganglia, and thalamus are in line with imaging studies in focal dystonia. For example, patients with blepharospasm exhibited reduced activation of the somatosensory cortex in response to tactile stimulation of affected and unaffected body regions (Dresel *et al*., 2011). Somatosensory cortex activation was attenuated in response to median nerve stimulation in cervical dystonia patients (Opavský *et al*., 2012). Vibration of the mouth in blepharospasm patients (Feiwell *et al*., 1999) and hand in writer's cramp patients (Tempel and Perlmutter, 1993) was associated with reduced sensorimotor cortical activation using $H_2{}^{15}O$-PET. Peller *et al*. (2006) reported enhanced activation of the sensory cortex, basal ganglia, and thalamus in response to tactile input of the affected hand of patients with writer's cramp. Moreover, studies in focal task-specific dystonias using somatosensory evoked potentials implicate adaptive somatosensory reorganization (Bara-Jimenez *et al*., 1998; Meunier *et al*., 2001).

A putative role of the striatum is the sensory gating of thalamo-striatal and cortico-striatal inputs into fine-tuned motor actions (Thorn and Graybiel, 2010; Huerta-Ocampo *et al*., 2014; Eskow Jaunarajs *et al*., 2015). D2R-expressing MSNs and SCIs are target projections of signals arising from the caudal intralaminar thalamic nuclei (Matsumoto *et al*., 2001; Van der Werf *et al*., 2002; Smith *et al*., 2004). SCIs represent tonically active neurons and conditioned pauses in their activity in response to salient events are thought to modulate the preparatory-set guiding appropriate action-selection and motor responses (Blazquez *et al*., 2002; Cragg, 2006; Lee *et al*., 2006; Apicella, 2007; Aosaki *et al*., 2010; Ding *et al*., 2010). Reduced activation of the striatum and connected nodes of the globus pallidus, cortex, and thalamus – which correlated with motor deficits in d2KO mice – may manifest within dysfunction at the level of the basal ganglia-thalamic loop. Indeed, *in vitro* electrophysiological studies have reported a significant functional alteration of D2R-mediated cholinergic signaling in the striatum and maladaptive cortico-striatal plasticity in Dyt1 KI mice (Dang *et al*., 2012; Martella *et al*., 2014). In Dyt1 KI mice and transgenic mice overexpressing human mutant torsinA, repetitive stimulation of thalamo-striatal axons produced a shortened pause response in SCIs and altered pre- and post-synaptic activation of MSNs through involvement of muscarinic M1 and M2 receptors (Martella *et al*., 2009; Grundmann *et al*., 2012; Sciamanna *et al*., 2012*a*). Taken together, one possible interpretation for the current findings is that the loss of torsinA in d2KO mice triggers maladaptive response of SCIs to sensory information required for effective motor control.

Abnormal Resting-State Functional Connectivity in d2KO Mice

In the resting-state analysis, the striatum in d2KO mice exhibited reduced functional connectivity with the sensory cortex and increased functional connectivity with

the brainstem compared to controls. Abnormal resting-state functional connectivity is in line with previous work in both Dyt1 KI and Dlx-cKO mice (DeSimone *et al*., 2016; 2017). For example, Dlx-cKO mice exhibited widespread hyper-connectivity between the striatum and multiple regions within the cortex, basal ganglia, midbrain, and cerebellum (DeSimone *et al*., 2017). The severity of connectivity adaptations in Dlx-cKO mice may be due to more widespread loss of torsinA. In Dlx-cKO mice, torsinA is conditionally deleted within a single allele of cholinergic and GABAergic cells of the forebrain (cortex, striatum, globus pallidus, basal forebrain, reticular thalamus) and unconditionally deleted from the other allele. This molecular insult of torsinA produces overt dystonic postures and causes a cell autonomous effect on the maintenance and function of SCIs, including high-yeild cell loss, somatic swelling of surviving cells, dysfunctional electrophysiological properties, and reduced acetylcholine (ACh) production (Pappas *et al*., 2015). The d2KO mice studied here, however, were characterized by conditional homozygous loss of torsinA within striatum-specific D2R-expressing cells. Similar to the Dlx-cKO model, original work in d2KO mice reported a significant loss of SCIs (~30%) and resultant decrease in the production of striatal ACh (Yokoi *et al*., *in preparation*). Despite the presence of microstructural and functional adaptations specific to cholinergic cell types in both models, the loss of torsinA in the forebrain (including the striatum) causes more widespread changes in functional connectivity strength and severity of behavioral phenotype. Collectively, the above findings demonstrate that cell autonomous cholinergic dysfunction can engage distant, yet connected regions of the hindbrain into an aberrant connectivity network, which is

consistent with the view that the connections between the basal ganglia and cerebellum contribute to dystonia pathphysiology (e.g., Argyelan *et al*., 2009; Uluğ *et al*., 2011).

Changes in Brain Microstructure Not Detected in d2KO Mice

Primary dystonias, such as DYT1 dystonia, are typically associated with disturbances in brain function in the absence of identifiable changes in gross brain structure. However, convergent evidence from studies in patients and animal models has pointed to evidence of microstructural adaptations. Enlargement of dopaminergic neurons and midbrain containing ubiquitin-inclusions have been reported in post-mortem DYT1 brains (Rostasy *et al*., 2003; McNaught *et al*., 2004; Paudel *et al*., 2014). Studies in Dyt1 KI mice have revealed morphological adaptations of SCIs and MSNs (Song *et al*., 2013), shorter primary dendrites and reduced spines of Purkinje cells (Zhang *et al*., 2011; Song *et al*., 2014), and brainstem ubiquitin- and torsinA-positive aggregation (Dang *et al*., 2005). Furthermore, neuroimaging has revealed changes in fractional anisotropy (FA) of white matter pathways and free-water (Argyelan *et al*., 2009; Uluğ *et al*., 2011; Vo *et al*., 2015*a, b*; DeSimone *et al*., 2016; 2017).

An objective of the current study was to test the utility of NODDI in providing an *in vivo* readout of microstructural adaptations within the striatum of d2KO mice. The basis for this objective is that original work in d2KO mice demonstrated a marked reduction in SCI cell count within the striatum using ChAT and VAChT labelling (Yokoi *et al*., *in preparation*). Unlike conventional diffusion tensor imaging (Basser *et al*., 1994), the NODDI computational approach allows for microstructural quantification of intracellular and extracellular environments (Zhang *et al*., 2012). Interestingly, d2KO mice did not reveal differences in NODDI derived volumetric (V_{ic}, V_{iso}) and diffusion (ODI) indices compared to control mice. Prior work using a two-compartment free-water

model (Pasternak *et al*., 2009), which similarly accounts for CSF contamination (Metzler-Baddeley *et al*., 2012) by separating tissue and non-tissue compartments, revealed overlapping changes in free-water and free-water-corrected mean diffusivity in the striatum of Dlx-cKO mice (DeSimone *et al*., 2017). These findings were interpreted to reflect high-yield loss of SCIs and swelling of the cell soma in surviving SCIs (Pappas *et al*., 2015). One possible interpretation for the null volumetric and diffusivity effects here is that the magnitude of SCI loss in the current cohort of d2KO mice is substantially less than that of the original publication cohort. Of course, this cannot be confirmed given that ChAT-positive neuronal density was not calculated here. Furthermore, it is possible that even with substantial loss of SCIs in the current mouse cohort, NODDI was not sensitive to a significant decrease in such a small sub-population of all striatal neurons in rodents [1-2% (Oorschot, 2013)]. Future studies combining diffusion MRI and fluorescence immunohistochemistry and/or western blot is a critical next step in determining the *in vivo* sensitivity of NODDI and other advanced diffusion indexes to brain microstructural adaptations.

Conclusions

The current study provides the first *in vivo* interpretation of sensory-evoked brain activation and functional connectivity in a mouse model of DYT1 dystonia. A key finding was that d2KO mice were associated with impaired activation of the sensory cortex, striatum, globus pallidus, and thalamus, which correlated with motor performance deficits. This study provides fresh evidence that the loss of striatal D2R-expressing torsinA causes impaired integration of sensory signals, and these impairments may contribute to motor control deficits. Importantly, this study establishes the utility of sensory-evoked fMRI to explore substrates of sensorimotor adaptations underlying

dystonia pathophysiology and this technique has high translational potential for studies in human patients.

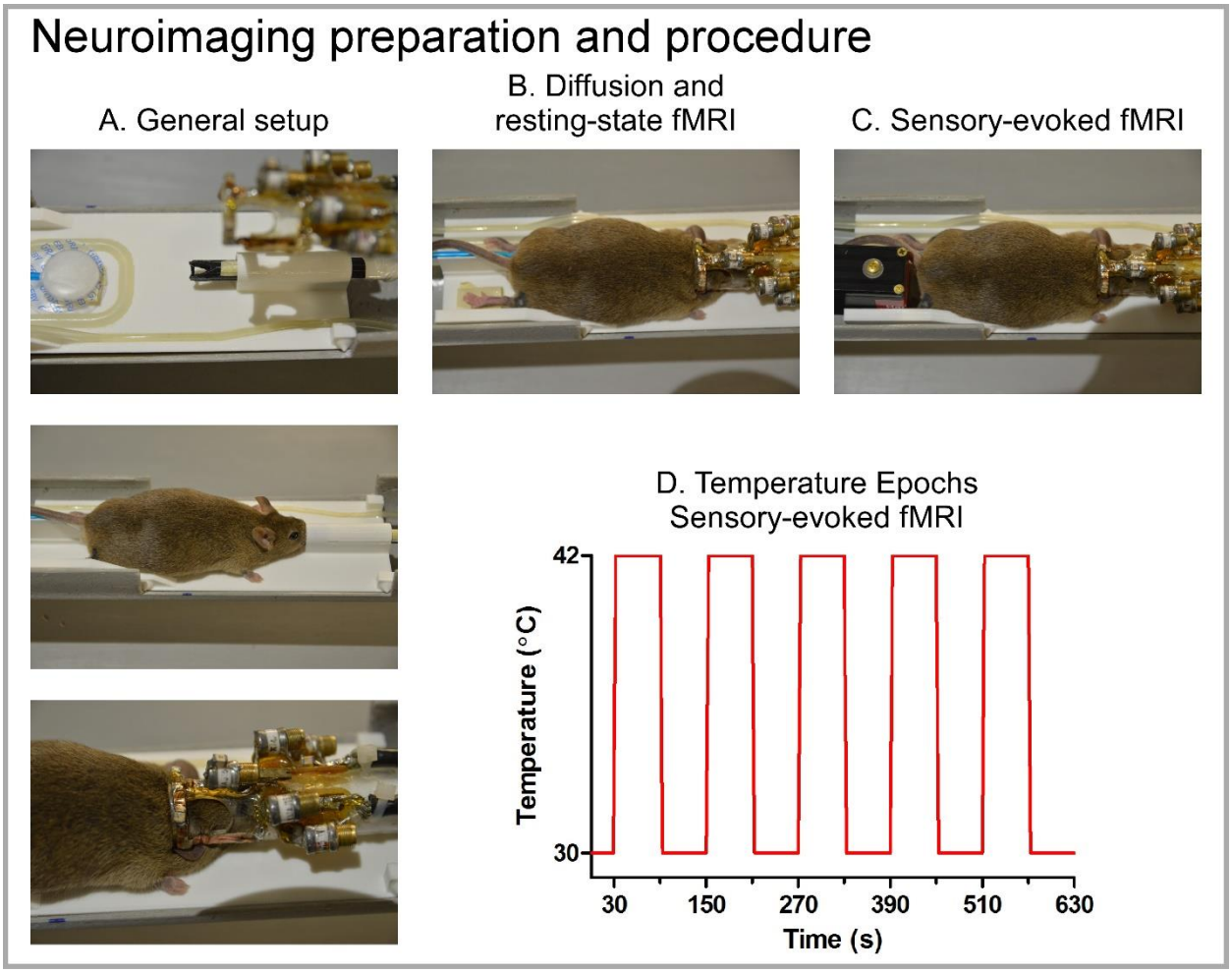

Figure 4-1. Animal Preparation and Procedure for Neuroimaging. (A) General imaging setup: The mouse cradle was equipped with respiration pad to monitor breathing, a heating tube to maintain core body temperature, which was monitored via rectal probe (not shown), and a bite-bar to deliver anesthesia during imaging (top panel). The mouse was secured by the bite bar to immobilize the head (middle panel) and a radiofrequency coil was affixed to the top of the head for MR signal acquisition (bottom panel). (B) The general imaging setup was used for the acquisition of diffusion MRI and resting-state fMRI. (C) For sensory-evoked fMRI, a thermode was affixed to the hind limb, which delivered the heat stimulus. (D) The heating thermode alternated between blocks of no thermal stimulation with a baseline temperature of 30˚C and temperature epochs of 42˚C.

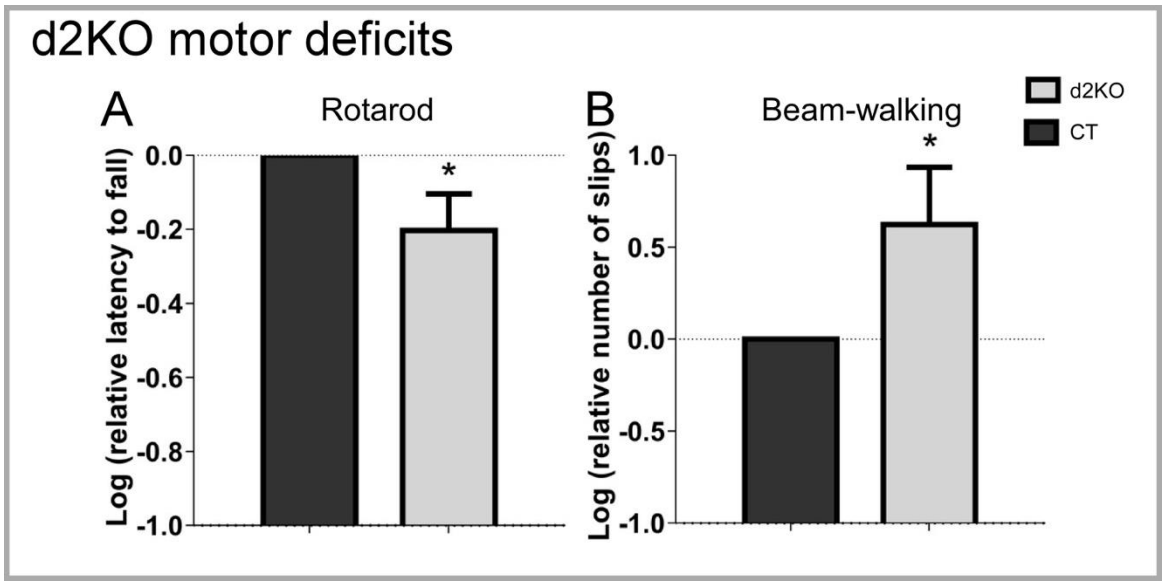

Figure 4-2. Motor Deficits in Dyt1 d2KO Mice. (A) d2KO mice exhibited faster latency-to-fall times in the rotarod assessment and (B) increased number of slips in the beam-walking assessment compared to control (CT) mice (*P*s < 0.05). Data were log-transformed to obtain normal distribution. Data from CT mice were normalized to 0 and d2KO were normalized to that of CT mice. Figure courtesy of Yuqing Li Lab.

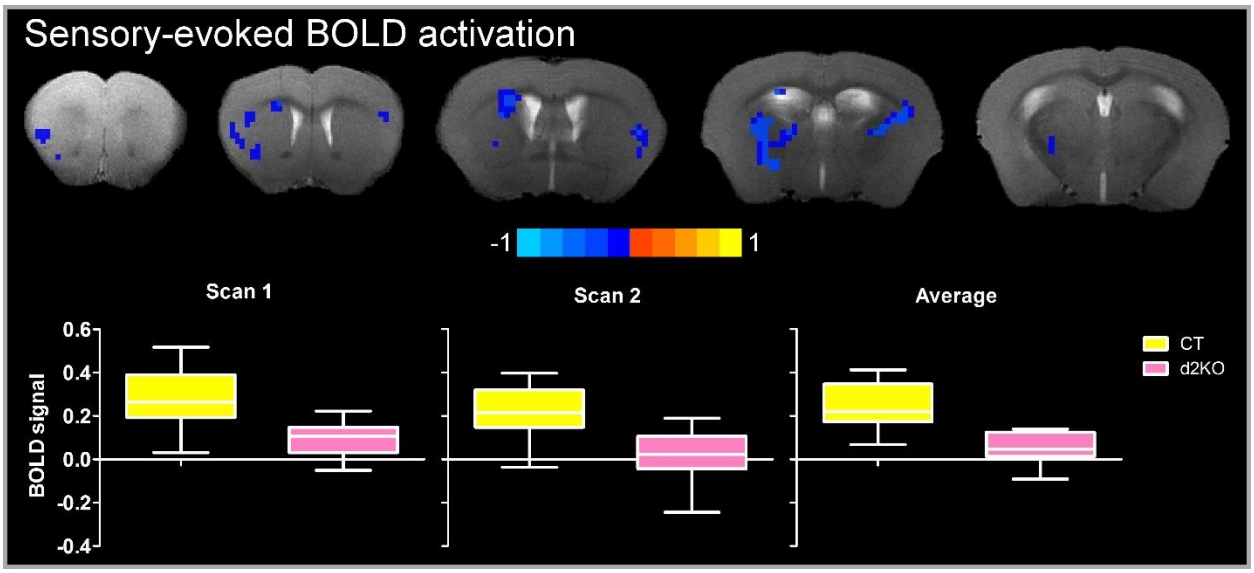

Figure 4-3. Impaired Sensory-Evoked BOLD Activation in Dyt1 d2KO Mice. Coronal slice representation of reduced BOLD signal amplitude in the cortex, striatum, globus pallidus, and thalamus in d2KO mice compared to control (CT) mice. The bottom panel shows box-and-whisker plots corresponding to the average BOLD signal across significant voxels shown in the coronal slices for CT (yellow) and d2KO (blue) mice. The average BOLD signal for both stimfMRI scans, as well the average BOLD signal across both scans are shown.

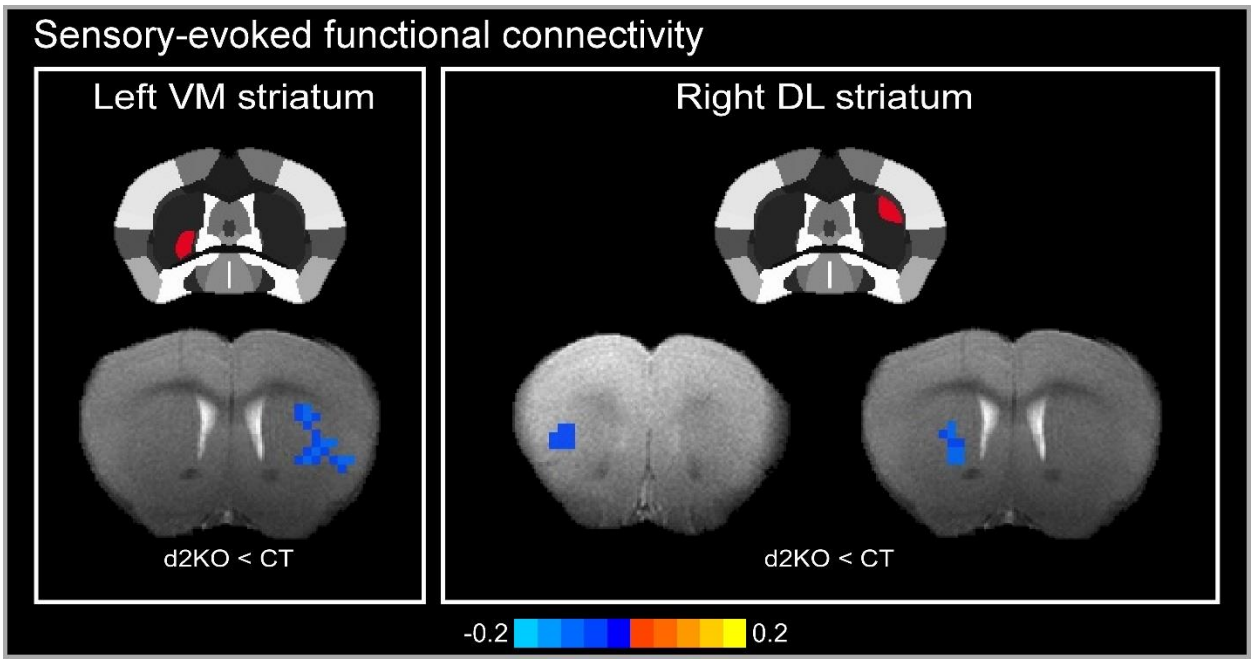

Figure 4-4. Reduced Sensory-Evoked Striatal Functional Connectivity in Dyt1 d2KO Mice. Compared to control (CT) mice, d2KO mice exhibited reduced functional connectivity in the right striatum and associative cortex with a seed location in the left rostral ventromedial striatum (left panel) and reduced functional connectivity in the left striatum and associative cortex with a seed location in the right rostral dorsolateral striatum (right panel). The seed location in both panels is depicted in red within the striatum of a template atlas (Ferris *et al*., 2014).

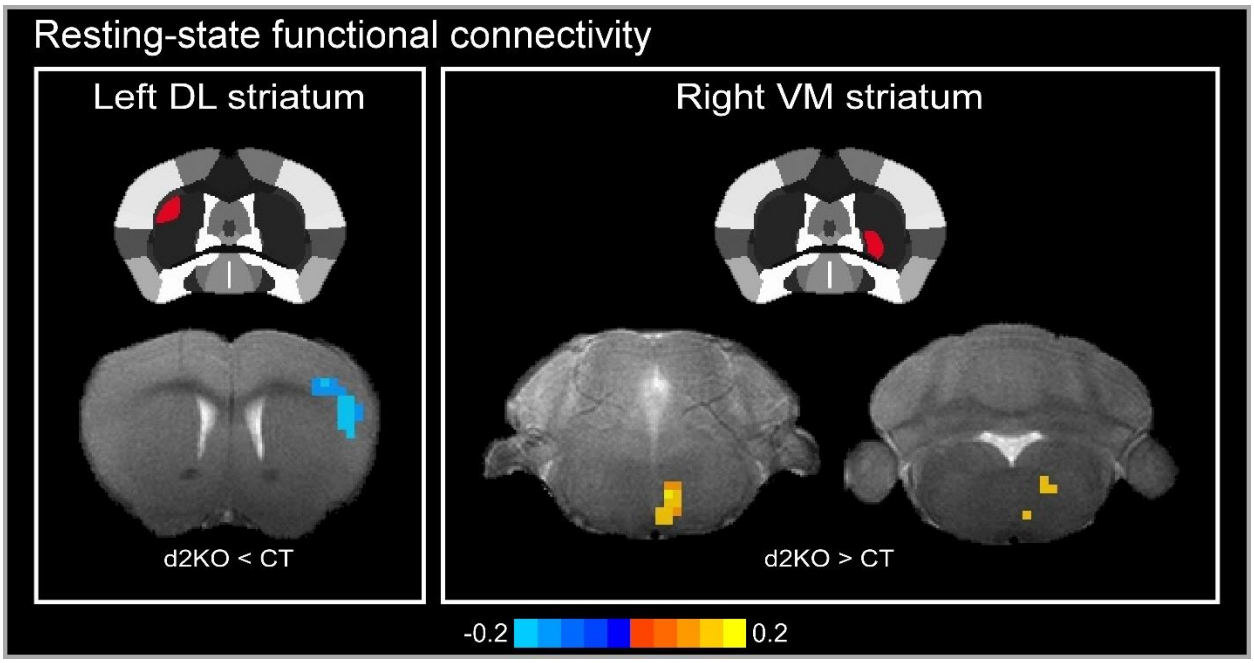

Figure 4-5. Abnormal Resting-State Functional Connectivity in Dyt1 d2KO Mice. Compared to control (CT) mice, d2KO mice exhibited reduced functional connectivity in the sensory cortex with a seed location in the left rostral dorsolateral striatum (left panel) and increased functional connectivity in the brainstem with a seed location in the right rostral ventromedial striatum (right panel). The seed location in both panels is depicted in red within the striatum of a template atlas (Ferris *et al*., 2014).

CHAPTER 5
GENERAL DISCUSSION

Functional MRI in Mouse Models of Dystonia

A core component of the described work was to determine how deficiency of torsinA within specific cell types influenced brain function and connectivity *in vivo*. ICA was used to examine functional connectivity in a mouse model characterized by the ΔGAG-Dyt1 mutation (Dyt1 KI mice). Dyt1 KI mice exhibited widespread functional connectivity adaptations across the cortex, basal ganglia, thalamus, and cerebellum compared to controls, and functional connectivity correlated with striatal and cerebellar free-water elevation. A striatal seed-based correlation approach was used to examine functional connectivity in mice with conditional Dyt1 KO of forebrain cholinergic and GABAergic neurons (Dlx-cKO). An extensive pattern of hyper-connectivity was revealed between the striatum and cortical, basal ganglia, midbrain, and cerebellar/brainstem regions in Dlx-cKO mice. In turn, the striatal seed-based correlation method revealed functional connectivity adaptations in only the sensory cortex and brainstem of D2R-expressing-cell-specific Dyt1 conditional KO mice (d2KO). Thus, it is clear that the loss of torsinA function beyond the striatum alone is a strong predictor of more widespread adaptations in functional connectivity strength.

Identifying brain regions functionally modulated by task conditions may provide better insight into the functional topology underlying the loss of movement control in dystonia. A novel component of the present work was the examination sensory-evoked fMRI to understand how loss of torsinA in D2R-expressing neurons of the striatum influenced BOLD activation and functional connectivity within sensorimotor brain regions of d2KO mice. The d2KO mice exhibited significantly reduced BOLD activation

in the sensory cortex, associative cortex, striatum, globus pallidus, and thalamus, as well as anti-connectivity of the left and right striatum relative to control mice. Furthermore, β-coefficient values within these regions were positively correlated with rotarod latency-to-fall times and negatively correlated with beam-walking slips in d2KO mice but not controls. This finding suggests that motor control deficits may be caused, in part, by impaired integration of sensory information required for appropriate action selection and control. Chapter 4 establishes the utility of sensory-evoked fMRI to explore substrates of sensorimotor adaptations underlying dystonia pathophysiology in mouse models and this technique has high translational potential for studies in human patients.

Diffusion MRI in Mouse Models of Dystonia

Diffusion MRI in combination with advanced multi-compartment modelling was used to provide an *in vivo* interpretation of brain microstructural adaptations in mouse models of dystonia. The two-compartment free-water model was used to examine microstructural adaptations in Dyt1 KI mice, which revealed increased free-water in the striatum and cerebellum compared to controls. The two-compartment free-water model was used in Dlx-cKO mice, which revealed overlapping changes in free-water and MD_T in the striatum. The three-compartment NODDI model (Zhang *et al*., 2012) was used to examine brain microstructure in d2KO mice but did not reveal volumetric or diffusivity changes compared to controls.

The preclusion of post-mortem cell-specific assays in these studies limits the interpretation of the diffusion MRI findings. This highlights the importance of combining *in vivo* diffusion MRI with post-mortem cell-specific assays in future studies. It is,

however, important to note that the regions exhibiting partial volume and diffusivity changes correspond to regions previously shown to exhibit microstructural adaptations in these mouse models. Studies in Dyt1 KI mice have reported morphological adaptations of striatal SCIs and MSNs (Song *et al*., 2013) and cerebellar Purkinje cells (Zhang *et al*., 2011; Song *et al*., 2013; 2014). Ubiquitin- and torsinA-positive perinuclear aggregates in the pedunculopontine nucleus have been reported in Dyt1 KI and hMT mice (Dang *et al*., 2005; Shashidharan *et al*., 2005; Grundmann *et al*., 2007). Original work in the Dlx-cKO mouse reported high-yield loss of SCIs and somatic hypertrophy in surviving SCIs (Pappas *et al*., 2015). The findings from the present work suggest that the two-compartment free-water model may be sensitive to these aforementioned microstructural adaptations *in vivo*. The utility of NODDI is not yet clear and will be better determined in future work. Original work in the d2KO mouse reported the loss of a significant proportion of striatal SCIs (Yokoi *et al*., *in preparation*). It remains unclear whether the absence of group-level effects between d2KO and control mice reflects limited sensitivity of NODDI to a decrease in a small sub-population of total striatal neurons or differences in the magnitude of SCI degeneration between the original and current experimental cohorts.

Conclusions

The studies in the present work have provided improved understanding of the large-scale effects in brain function and connectivity caused by the ΔGAG-Dyt1 mutation, as well as the loss of torsinA within specific cell types of the forebrain and striatum. Diffusion MRI findings have helped provide an *in vivo* readout of changes in brain microstructure characterizing these mouse models. A critical next step is to

address the relationship between the loss of torsinA function in other cell types and associated systems-level changes in brain pathophysiology. Combined assays from current and future work will shape a perspective of the cell-specific functional hierarchy driving the expression of dystonia. This work will be important in developing and testing more effective symptomatic and disease-modifying therapies that target certain cell types, ranging from pharmacological, surgical, and CRISPR/Cas9 genomic editing.

LIST OF REFERENCES

Albanese A, Lalli S. Update on dystonia [Review]. Curr Opin Neurol 2012; 25(4): 483-90.

Albanese A, Bhatia K, Bressman SB, Delong MR, Fahn S, Fung VS, et al. Phenomenology and classification of dystonia: a consensus update. Mov Disord 2013; 28(7): 863-73.

Alexander AL, Lee JE, Lazar M, Field AS. Diffusion tensor imaging of the brain [Review]. Neurotherapeutics 2007; 4(3): 316-29.

Alexander AL, Hurley SA, Samsonov AA, Adluru N, Hosseinbor AP, Mossahebi P, et al. Characterization of cerebral white matter properties using quantitative magnetic resonance imaging stains. Brain Connect 2011; 1(6): 23-46.

Aosaki T, Tsubokawa H, Ishida A, Watanabe K, Graybiel AM, Kimura M. Responses of tonically active neurons in the primate's striatum undergo systematic changes during behavioral sensorimotor conditioning. J Neurosci 1994; 14(6): 3969-84.

Aosaki T, Miura M, Suzuki T, Nishimura K, Masuda M. Acetylcholine-dopamine balance hypothesis in the striatum: an update [Review]. Geriatr Gerontol Int 2010; 10 Suppl 1: S148-57.

Apicella P. Leading tonically active neurons of the striatum from reward detection to context recognition [Review]. Trends Neurosci 2007; 30(6): 299-306.

Argyelan M, Carbon M, Niethammer M, Uluğ AM, Voss HU, Bressman SB, et al. Cerebellothalamocortical connectivity regulates penetrance in dystonia. J Neurosci 2009; 29(31): 9740-7.

Asanuma K, Ma Y, Okulski J, Dhawan V, Chaly T, Carbon M, et al. Decreased striatal D2 receptor binding in non-manifesting carriers of the DYT1 dystonia mutation. Neurology 2005; 64(2): 347-9.

Augood SJ, Hollingsworth Z, Albers DS, Yang L, Leung JC, Muller B, et al. Dopamine transmission in DYT1 dystonia: a biochemical and autoradiographical study. Neurology 2002; 59(3): 445-8.

Avants BB, Tustison NJ, Song G, Cook PA, Klein A, Gee JC. A reproducible evaluation of ANTs similarity metric performance in brain image registration. Neuroimage 2011; **54**(3): 2033-2044.

Balcioglu A, Kim MO, Sharma N, Cha JH, Breakefield XO, Standaert DG. Dopamine release is impaired in a mouse model of DYT1 dystonia. J Neurochem 2007; 102(3): 783-8.

Bara-Jimenez W, Catalan MJ, Hallett M, Gerloff C. Abnormal somatosensory homunculus in dystonia of the hand. Ann Neurol 1998; 44(5): 828-31.

Basser PJ, Mattiello J, LeBihan D. MR diffusion tensor spectroscopy and imaging. Biophys J 1994; 66(1): 259-67.

Basser PJ, Pierpaoli C. Microstructural and physiological features of tissues elucidated by quantitative-diffusion-tensor MRI. J Magn Reson 2011; 213(2): 560-70.

Battistella G, Fuertinger S, Fleysher L, Ozelius LJ, Simonyan K. Cortical sensorimotor alterations classify clinical phenotype and putative genotype of spasmodic dysphonia. Eur J Neurol 2016; 23(10): 1517-27.

Battistella G, Termsarasab P, Ramdhani RA, Fuertinger S, Simonyan K. Isolated Focal Dystonia as a Disorder of Large-Scale Functional Networks. Cereb Cortex 2017; 27(2): 1203-1215.

Battistella G, Simonyan K. Top-down alteration of functional connectivity within the sensorimotor network in focal dystonia. Neurology 2019; 92(16): e1843-e1851.

Becerra L, Chang PC, Bishop J, Borsook D. CNS activation maps in awake rats exposed to thermal stimuli to the dorsum of the hindpaw. Neuroimage 2011; 54(2): 1355-66.

Beck S, Hallett M. Surround inhibition in the motor system. Exp Brain Res 2011; 210(2): 165-72.

Berardelli A, Hallett M, Rothwell JC, Agostino R, Manfredi M, Thompson PD, et al. Single-joint rapid arm movements in normal subjects and in patients with motor disorders [Review]. Brain 1996; 119(Pt 2): 661-74.

Berardelli A, Rothwell JC, Hallett M, Thompson PD, Manfredi M, Marsden CD. The pathophysiology of primary dystonia [Review]. Brain 1998; 121(Pt 7): 1195-212.

Bhatia KP, Marsden CD. The behavioural and motor consequences of focal lesions of the basal ganglia in man. Brain 1994; 117 (Pt 4):859-76.

Biswal B, Yetkin FZ, Haughton VM, Hyde JS. Functional connectivity in the motor cortex of resting human brain using echo-planar MRI. Magn Reson Med 1995; 34(4): 537-41.

Blazquez PM, Fujii N, Kojima J, Graybiel AM. A network representation of response probability in the striatum. Neuron 2002; 33(6): 973-82.

Bosshard SC, Stuker F, von Deuster C, Schroeter A, Rudin M. BOLD fMRI of C-Fiber Mediated Nociceptive Processing in Mouse Brain in Response to Thermal Stimulation of the Forepaws. PLoS One 2015; 10(5): e0126513.

Bostan AC, Strick PL. The cerebellum and basal ganglia are interconnected. Neuropsychol Rev 2010; 20(3): 261-70.

Bostan AC, Dum RP, Strick PL. Cerebellar networks with the cerebral cortex and basal ganglia [Review]. Trends Cogn Sci 2013; 17(5): 241-54.

Bostan AC, Dum RP, Strick PL. Functional Anatomy of Basal Ganglia Circuits with the Cerebral Cortex and the Cerebellum. Prog Neurol Surg 2018; 33: 50-61.

Bostan AC, Strick PL. The basal ganglia and the cerebellum: nodes in an integrated network [Review]. Nat Rev Neurosci 2018; 19(6): 338-350.

Bragg DC, Camp SM, Kaufman CA, Wilbur JD, Boston H, Schuback DE, et al. Perinuclear biogenesis of mutant torsin-A inclusions in cultured cells infected with tetracycline-regulated herpes simplex virus type 1 amplicon vectors. Neuroscience 2004;125(3): 651-61.

Breakefield XO, Blood AJ, Li Y, Hallett M, Hanson PI, Standaert DG. The pathophysiological basis of dystonias [Review]. Nat Rev Neurosci 2008; 9(3): 222-34.

Bressman SB. Dystonia update [Review]. Clin Neuropharmacol 2000; 23(5): 239-51.

Burciu RG, Hess CW, Coombes SA, Ofori E, Shukla P, Chung JW, et al. Functional activity of the sensorimotor cortex and cerebellum relates to cervical dystonia symptoms. Hum Brain Mapp 2017; 38(9): 4563-4573.

Burton K, Farrell K, Li D, Calne DB. Lesions of the putamen and dystonia: CT and magnetic resonance imaging. Neurology 1984; 34(7): 962-5.

Calabresi P, Maj R, Mercuri NB, Bernardi G. Coactivation of D1 and D2 dopamine receptors is required for long-term synaptic depression in the striatum. Neurosci Lett 1992a; 142(1): 95-9.

Calabresi P, Maj R, Pisani A, Mercuri NB, Bernardi G. Long-term synaptic depression in the striatum: physiological and pharmacological characterization. J Neurosci 1992b; 12(11): 4224-33.

Calabresi P, Picconi B, Tozzi A, Ghiglieri V, Di Filippo M. Direct and indirect pathways of basal ganglia: a critical reappraisal. Nat Neurosci 2014;17(8): 1022-30.

Calderon DP, Fremont R, Kraenzlin F, Khodakhah K. The neural substrates of rapid-onset Dystonia-Parkinsonism. Nat Neurosci 2011; 14(3): 357-65.

Calhoun VD, Adali T, Pearlson GD, Pekar JJ. Spatial and temporal independent component analysis of functional MRI data containing a pair of task-related waveforms. Hum Brain Mapp 2001a; 13(1): 43-53.

Calhoun VD, Adali T, Pearlson GD, Pekar JJ. A method for making group inferences from functional MRI data using independent component analysis. Hum Brain Mapp 2001b; 14(3): 140-51. Erratum in: Hum Brain Mapp 2002; 16(2): 131.

Calhoun VD, Adalı T. Multisubject independent component analysis of fMRI: a decade of intrinsic networks, default mode, and neurodiagnostic discovery [Review]. IEEE Rev Biomed Eng 2012; 5: 60-73.

Campbell DB, North JB, Hess EJ. Tottering mouse motor dysfunction is abolished on the Purkinje cell degeneration (pcd) mutant background. Exp Neurol 1999; 160(1): 268-78.

Carbon M, Su S, Dhawan V, Raymond D, Bressman S, Eidelberg D. Regional metabolism in primary torsion dystonia: effects of penetrance and genotype. Neurology 2004a; 62(8): 1384-90.

Carbon M, Kingsley PB, Su S, Smith GS, Spetsieris P, Bressman S, et al. Microstructural white matter changes in carriers of the DYT1 gene mutation. Ann Neurol 2004b; 56(2): 283-6.

Carbon M, Ghilardi MF, Argyelan M, Dhawan V, Bressman SB, Eidelberg D. Increased cerebellar activation during sequence learning in DYT1 carriers: an equiperformance study. Brain 2008a; 131(Pt 1): 146-54.

Carbon M, Kingsley PB, Tang C, Bressman S, Eidelberg D. Microstructural white matter changes in primary torsion dystonia. Mov Disord 2008b; 23(2): 234-9.

Carbon M, Eidelberg D. Abnormal structure-function relationships in hereditary dystonia [Review]. Neuroscience 2009; 164(1): 220-9.

Carbon M, Niethammer M, Peng S, Raymond D, Dhawan V, Chaly T, et al. Abnormal striatal and thalamic dopamine neurotransmission: Genotype-related features of dystonia. Neurology 2009; 72(24): 2097-103.

Carbon M, Argyelan M, Habeck C, Ghilardi MF, Fitzpatrick T, Dhawan V, et al. Increased sensorimotor network activity in DYT1 dystonia: a functional imaging study. Brain 2010; 133(Pt 3): 690-700.

Centonze D, Picconi B, Gubellini P, Bernardi G, Calabresi P. Dopaminergic control of synaptic plasticity in the dorsal striatum [Review]. Eur J Neurosci 2001; 13(6): 1071-7.

Chang, C.-C., Lin, C.-J. LIBSVM: a library for support vector machines. ACM Trans Intell Syst Technol 2011; 2: 27.

Chen CH, Fremont R, Arteaga-Bracho EE, Khodakhah K. Short latency cerebellar modulation of the basal ganglia. Nat Neurosci 2014; 17(12): 1767-75.

Chen G, Popa LS, Wang X, Gao W, Barnes J, Hendrix CM, et al. Low-frequency oscillations in the cerebellar cortex of the tottering mouse. J Neurophysiol 2009; 101(1): 234-45.

Cif L, Vasques X, Gonzalez V, Ravel P, Biolsi B, Collod-Beroud G, et al. Long-term follow-up of DYT1 dystonia patients treated by deep brain stimulation: an open-label study. Mov Disord 2010; 25(3): 289-99.

Conte A, Defazio G, Hallett M, Fabbrini G, Berardelli A. The role of sensory information in the pathophysiology of focal dystonias [Review]. Nat Rev Neurol 2019; 15(4): 224-233.

Cox, R.W. AFNI: software for analysis and visualization of functional magnetic resonance neuroimages. Comput Biomed Res 1996; 29: 162–173.

Cragg SJ. Meaningful silences: how dopamine listens to the ACh pause. Trends Neurosci 2006; 29(3): 125-31.

Dang MT, Yokoi F, McNaught KS, Jengelley TA, Jackson T, Li J, et al. Generation and characterization of Dyt1 DeltaGAG knock-in mouse as a model for early-onset dystonia. Exp Neurol 2005; 196(2): 452-63.

Dang MT, Yokoi F, Pence MA, Li Y. Motor deficits and hyperactivity in Dyt1 knockdown mice. Neurosci Res 2006; 56(4): 470-4.

Dang MT, Yokoi F, Cheetham CC, Lu J, Vo V, Lovinger DM, et al. An anticholinergic reverses motor control and corticostriatal LTD deficits in Dyt1 ΔGAG knock-in mice. Behav Brain Res 2012; 226(2): 465-72.

Dauer W. Inherited isolated dystonia: clinical genetics and gene function [Review]. Neurotherapeutics 2014; 11(4): 807-16.

DeAndrade MP, Trongnetrpunya A, Yokoi F, Cheetham CC, Peng N, Wyss JM, et al. Electromyographic evidence in support of a knock-in mouse model of DYT1 Dystonia. Mov Disord 2016; 31(11): 1633-1639.

Defazio G, Abbruzzese G, Livera P, Berardelli A. Epidemiology of primary dystonia. Lancet Neurol 2004; 3: 673-678.

Deffains M, Bergman H. Striatal cholinergic interneurons and cortico-striatal synaptic plasticity in health and disease. Mov Disord 2015; 30(8): 1014-25.

Delnooz CC, Pasman JW, Beckmann CF, van de Warrenburg BP. Task-free functional MRI in cervical dystonia reveals multi-network changes that partially normalize with botulinum toxin. PLoS One 2013; 8(5): e62877.

Delnooz CC, Pasman JW, Beckmann CF, van de Warrenburg BP. Altered striatal and pallidal connectivity in cervical dystonia. Brain Struct Funct 2015; 220(1): 513-23.

DeSimone JC, Febo M, Shukla P, Ofori E, Colon-Perez LM, Li Y, et al. In vivo imaging reveals impaired connectivity across cortical and subcortical networks in a mouse model of DYT1 dystonia. Neurobiol Dis 2016; 95: 35-45.

DeSimone JC, Pappas SS, Febo M, Burciu RG, Shukla P, Colon-Perez LM, et al. Forebrain knock-out of torsinA reduces striatal free-water and impairs whole-brain functional connectivity in a symptomatic mouse model of DYT1 dystonia. Neurobiol Dis 2017; 106: 124-132.

Desrochers P, Brunfeldt A, Sidiropoulos C, Kagerer F. Sensorimotor Control in Dystonia [Review]. Brain Sci 2019; 9(4) pii: E79.

Ding JB, Guzman JN, Peterson JD, Goldberg JA, Surmeier DJ. Thalamic gating of corticostriatal signaling by cholinergic interneurons. Neuron 2010; 67(2): 294-307.

Doyle J, Ren X, Lennon G, Stubbs L. Mutations in the Cacnl1a4 calcium channel gene are associated with seizures, cerebellar degeneration, and ataxia in tottering and leaner mutant mice. Mamm Genome 1997; 8(2): 113-20.

Dresel C, Haslinger B, Castrop F, Wohlschlaeger AM, Ceballos-Baumann AO. Silent event-related fMRI reveals deficient motor and enhanced somatosensory activation in orofacial dystonia. Brain 2006; 129(Pt 1): 36-46.

Dresel C, Bayer F, Castrop F, Rimpau C, Zimmer C, Haslinger B. Botulinum toxin modulates basal ganglia but not deficient somatosensory activation in orofacial dystonia. Mov Disord 2011; 26(8): 1496-502.

Eidelberg D, Moeller JR, Antonini A, Kazumata K, Nakamura T, Dhawan V, et al. Functional brain networks in DYT1 dystonia. Ann Neurol 1998; 44(3): 303-12.

Eskow Jaunarajs KL, Bonsi P, Chesselet MF, Standaert DG, Pisani A. Striatal cholinergic dysfunction as a unifying theme in the pathophysiology of dystonia. Prog Neurobiol 2015; 127-128: 91-107.

Fahn S. Concept and classification of dystonia [Review]. Adv Neurol 1988; 50: 1-8.

Fan X, Hughes KE, Jinnah HA, Hess EJ. Selective and sustained α-amino-3-hydroxy-5-methyl-4-isoxazolepropionic acid receptor activation in cerebellum induces dystonia in mice. J Pharmacol Exp Ther 2012; 340(3): 733-41.

Feiwell RJ, Black KJ, McGee-Minnich LA, Snyder AZ, MacLeod AM, Perlmutter JS. Diminished regional cerebral blood flow response to vibration in patients with blepharospasm. Neurology 1999; 52(2): 291-7.

Feldman HM, Yeatman JD, Lee ES, Barde LH, Gaman-Bean S. Diffusion tensor imaging: a review for pediatric researchers and clinicians [Review]. J Dev Behav Pediatr 2010; 31(4): 346-56.

Fernández JM, Bezanilla F, Taylor RE. Distribution and kinetics of membrane dielectric polarization. II. Frequency domain studies of gating currents. J Gen Physiol 1982; 79(1): 41-67.

Ferron JF, Kroeger D, Chever O, Amzica F. Cortical inhibition during burst suppression induced with isoflurane anesthesia. J Neurosci 2009; 29(31): 9850-60.

Filip P, Gallea C, Lehéricy S, Bertasi E, Popa T, Mareček R, et al. Disruption in cerebellar and basal ganglia networks during a visuospatial task in cervical dystonia. Mov Disord 2017; 32(5): 757-768.

Fletcher CF, Lutz CM, O'Sullivan TN, Shaughnessy JD Jr, Hawkes R, Frankel WN, et al. Absence epilepsy in tottering mutant mice is associated with calcium channel defects. Cell 1996; 87(4): 607-17.

Fox MD, Snyder AZ, Vincent JL, Corbetta M, Van Essen DC, Raichle ME. The human brain is intrinsically organized into dynamic, anticorrelated functional networks. Proc Natl Acad Sci U S A 2005; 102(27): 9673-8.

Fremont R, Calderon DP, Maleki S, Khodakhah K. Abnormal high-frequency burst firing of cerebellar neurons in rapid-onset dystonia-parkinsonism. J Neurosci 2014; 34(35): 11723-32.

Fremont R, Tewari A, Khodakhah K. Aberrant Purkinje cell activity is the cause of dystonia in a shRNA-based mouse model of Rapid Onset Dystonia-Parkinsonism. Neurobiol Dis 2015; 82: 200-212.

Fremont R, Tewari A, Angueyra C, Khodakhah K. A role for cerebellum in the hereditary dystonia DYT1. Elife 2017; 6.

Fross RD, Martin WR, Li D, Stoessl AJ, Adam MJ, Ruth TJ, et al. Lesions of the putamen: their relevance to dystonia. Neurology 1987; 37(7): 1125-9.

Furukawa Y, Hornykiewicz O, Fahn S, Kish SJ. Striatal dopamine in early-onset primary torsion dystonia with the DYT1 mutation. Neurology 2000; 54(5):1193-5.

Garraux G, Bauer A, Hanakawa T, Wu T, Kansaku K, Hallett M. Changes in brain anatomy in focal hand dystonia. Ann Neurol 2004; 55(5): 736-9.

Ghilardi MF, Carbon M, Silvestri G, Dhawan V, Tagliati M, Bressman S, et al. Impaired sequence learning in carriers of the DYT1 dystonia mutation. Ann Neurol 2003; 54(1): 102-9.

Gong S, Doughty M, Harbaugh CR, Cummins A, Hatten ME, Heintz N, et al. Targeting Cre recombinase to specific neuron populations with bacterial artificial chromosome constructs. J Neurosci 2007; 27(37): 9817-23.

Gonzalez-Alegre P, Paulson HL. Aberrant cellular behavior of mutant torsinA implicates nuclear envelope dysfunction in DYT1 dystonia. J Neurosci 2004; 24(11): 2593-601.

Goodchild RE, Dauer WT. Mislocalization to the nuclear envelope: an effect of the dystonia-causing torsinA mutation. Proc Natl Acad Sci U S A 2004; 101(3): 847-52.

Goodchild RE, Dauer WT. The AAA+ protein torsinA interacts with a conserved domain present in LAP1 and a novel ER protein. J Cell Biol 2005; 168(6): 855-62.

Goodchild RE, Kim CE, Dauer WT. Loss of the dystonia-associated protein torsinA selectively disrupts the neuronal nuclear envelope. Neuron 2005; 48(6): 923-32.

Goodchild RE, Buchwalter AL, Naismith TV, Holbrook K, Billion K, Dauer WT, et al. Access of torsinA to the inner nuclear membrane is activity dependent and regulated in the endoplasmic reticulum. J Cell Sci 2015; 128(15): 2854-65.

Granata A, Warner TT. The role of torsinA in dystonia [Review]. Eur J Neurol 2010; 17 Suppl 1: 81-7.

Graybiel AM, Aosaki T, Flaherty AW, Kimura M. The basal ganglia and adaptive motor control [Review]. Science 1994; 265(5180): 1826-31.

Greene P, Kang UJ, Fahn S. Spread of symptoms in idiopathic torsion dystonia. Mov Disord 1995; 10(2): 143-52.

Grundmann K, Reischmann B, Vanhoutte G, Hübener J, Teismann P, Hauser TK, et al. Overexpression of human wildtype torsinA and human DeltaGAG torsinA in a transgenic mouse model causes phenotypic abnormalities. Neurobiol Dis 2007; 27(2): 190-206.

Grundmann K, Glöckle N, Martella G, Sciamanna G, Hauser TK, Yu L, et al. Generation of a novel rodent model for DYT1 dystonia. Neurobiol Dis 2012; 47(1): 61-74.

Haslinger B, Altenmüller E, Castrop F, Zimmer C, Dresel C. Sensorimotor overactivity as a pathophysiologic trait of embouchure dystonia. Neurology 2010; 74(22): 1790-7.

Hallett M. Neurophysiology of dystonia: The role of inhibition [Review]. Neurobiol Dis 2011; 42(2): 177-84.

Hewett J, Gonzalez-Agosti C, Slater D, Ziefer P, Li S, Bergeron D, et al. Mutant torsinA, responsible for early-onset torsion dystonia, forms membrane inclusions in cultured neural cells. Hum Mol Genet 2000; 9(9): 1403-13.

Hewett JW, Tannous B, Niland BP, Nery FC, Zeng J, Li Y, et al. Mutant torsinA interferes with protein processing through the secretory pathway in DYT1 dystonia cells. Proc Natl Acad Sci U S A 2007; 104(17): 7271-6.

Hisatsune C, Miyamoto H, Hirono M, Yamaguchi N, Sugawara T, Ogawa N, et al. IP3R1 deficiency in the cerebellum/brainstem causes basal ganglia-independent dystonia by triggering tonic Purkinje cell firings in mice. Front Neural Circuits 2013; 7: 156.

Hoshi E, Tremblay L, Féger J, Carras PL, Strick PL. The cerebellum communicates with the basal ganglia. Nat Neurosci 2005; 8(11): 1491-3.

Huerta-Ocampo I, Mena-Segovia J, Bolam JP. Convergence of cortical and thalamic input to direct and indirect pathway medium spiny neurons in the striatum. Brain Struct Funct 2014; 219(5): 1787-800.

Jankovic J. Medical treatment of dystonia [Review]. Mov Disord 2013; 28(7): 1001-12.

Jinnah HA, Neychev V, Hess EJ. The Anatomical Basis for Dystonia: The Motor Network Model [Review]. Tremor Other Hyperkinet Mov (N Y) 2017; 7: 506.

Jonckers E, Van Audekerke J, De Visscher G, Van der Linden A, Verhoye M. Functional connectivity fMRI of the rodent brain: comparison of functional connectivity networks in rat and mouse. PLoS One 2011; 6(4): e18876.

Jones DK, Knösche TR, Turner R. White matter integrity, fiber count, and other fallacies: the do's and don'ts of diffusion MRI. Neuroimage 2013; 73: 239-54.

Jungwirth MT, Kumar D, Jeong DY, Goodchild RE. The nuclear envelope localization of DYT1 dystonia torsinA-ΔE requires the SUN1 LINC complex component. BMC Cell Biol 2011; 12: 24.

Kupsch A, Benecke R, Müller J, Trottenberg T, Schneider GH, Poewe W, et al. Pallidal deep-brain stimulation in primary generalized or segmental dystonia. N Engl J Med 2006; 355(19): 1978-90.

Kustedjo K, Bracey MH, Cravatt BF. Torsin A and its torsion dystonia-associated mutant forms are lumenal glycoproteins that exhibit distinct subcellular localizations. J Biol Chem 2000; 275(36): 27933-9.

Kustedjo K, Deechongkit S, Kelly JW, Cravatt BF. Recombinant expression, purification, and comparative characterization of torsinA and its torsion dystonia-associated variant Delta E-torsinA. Biochemistry 2003; 42(51): 15333-41.

LeDoux MS, Lorden JF, Ervin JM. Cerebellectomy eliminates the motor syndrome of the genetically dystonic rat. Exp Neurol 1993; 120(2): 302-10.

LeDoux MS, Hurst DC, Lorden JF. Single-unit activity of cerebellar nuclear cells in the awake genetically dystonic rat. Neuroscience 1998; 86(2):533-45.

LeDoux MS, Lorden JF. Abnormal spontaneous and harmaline-stimulated Purkinje cell activity in the awake genetically dystonic rat. Exp Brain Res 2002; 145(4): 457-67.

Lee IH, Seitz AR, Assad JA. Activity of tonically active neurons in the monkey putamen during initiation and withholding of movement. J Neurophysiol 2006; 95(4): 2391-403.

Lerner A, Shill H, Hanakawa T, Bushara K, Goldfine A, Hallett M. Regional cerebral blood flow correlates of the severity of writer's cramp symptoms. Neuroimage 2004; 21(3): 904-13.

Li Z, Prudente CN, Stilla R, Sathian K, Jinnah HA, Hu X. Alterations of resting-state fMRI measurements in individuals with cervical dystonia. Hum Brain Mapp 2017; 38(8): 4098-4108.

Liang CC, Tanabe LM, Jou S, Chi F, Dauer WT. TorsinA hypofunction causes abnormal twisting movements and sensorimotor circuit neurodegeneration. J Clin Invest 2014; 124(7): 3080-92.

Lim SA, Kang UJ, McGehee DS. Striatal cholinergic interneuron regulation and circuit effects [Review]. Front Synaptic Neurosci 2014; 6: 22.

Liu X, Zhu XH, Zhang Y, Chen W. The change of functional connectivity specificity in rats under various anesthesia levels and its neural origin. Brain Topogr 2013; 26(3): 363-77.

Liu Z, Zolkiewska A, Zolkiewski M. Characterization of human torsinA and its dystonia-associated mutant form. Biochem J 2003; 374(Pt 1): 117-22.

Luc QN, Querubin J. Clinical Management of Dystonia in Childhood [Review]. Paediatr Drugs 2017; 19(5): 447-461.

Maltese M, Martella G, Madeo G, Fagiolo I, Tassone A, Ponterio G, et al. Anticholinergic drugs rescue synaptic plasticity in DYT1 dystonia: role of M1 muscarinic receptors. Mov Disord 2014; 29(13): 1655-65.

Matsumoto N, Minamimoto T, Graybiel AM, Kimura M. Neurons in the thalamic CM-Pf complex supply striatal neurons with information about behaviorally significant sensory events. J Neurophysiol 2001; 85(2): 960-76.

Mardia KV, Jupp PE, editors. Directional statistics. London: Wiley; 1990.

Martella G, Tassone A, Sciamanna G, Platania P, Cuomo D, Viscomi MT, et al. Impairment of bidirectional synaptic plasticity in the striatum of a mouse model of DYT1 dystonia: role of endogenous acetylcholine. Brain 2009; 132(Pt 9): 2336-49.

Martella G, Maltese M, Nisticò R, Schirinzi T, Madeo G, Sciamanna G, et al. Regional specificity of synaptic plasticity deficits in a knock-in mouse model of DYT1 dystonia. Neurobiol Dis 2014; 65: 124-32.

Marsden CD, Obeso JA, Zarranz JJ, Lang AE. The anatomical basis of symptomatic hemidystonia. Brain 1985; 108(Pt 2): 463-83.

Maurice N, Mercer J, Chan CS, Hernandez-Lopez S, Held J, Tkatch T, et al. D2 dopamine receptor-mediated modulation of voltage-dependent Na+ channels reduces autonomous activity in striatal cholinergic interneurons. J Neurosci 2004; 24(46): 10289-301.

McKeown MJ, Makeig S, Brown GG, Jung TP, Kindermann SS, Bell AJ, et al. Analysis of fMRI data by blind separation into independent spatial components. Hum Brain Mapp 1998a; 6(3): 160-88.

McKeown MJ, Jung TP, Makeig S, Brown G, Kindermann SS, Lee TW, et al. Spatially independent activity patterns in functional MRI data during the stroop color-naming task. Proc Natl Acad Sci U S A 1998b; 95(3): 803-10.

McNaught KS, Kapustin A, Jackson T, Jengelley TA, Jnobaptiste R, Shashidharan P, et al. Brainstem pathology in DYT1 primary torsion dystonia. Ann Neurol 2004; 56(4): 540-7.

Mechling AE, Hübner NS, Lee HL, Hennig J, von Elverfeldt D, Harsan LA. Fine-grained mapping of mouse brain functional connectivity with resting-state fMRI. Neuroimage 2014; 96: 203-15.

Metzler-Baddeley C, O'Sullivan MJ, Bells S, Pasternak O, Jones DK. How and how not to correct for CSF-contamination in diffusion MRI. Neuroimage 2012; 59(2): 1394-403.

Meunier S, Garnero L, Ducorps A, Mazières L, Lehéricy S, du Montcel ST, et al. Human brain mapping in dystonia reveals both endophenotypic traits and adaptive reorganization. Ann Neurol 2001; 50(4): 521-7.

Middleton FA, Strick PL. Basal ganglia and cerebellar loops: motor and cognitive circuits [Review]. Brain Res Brain Res Rev 2000; 31(2-3): 236-50.

Mink JW. The basal ganglia: focused selection and inhibition of competing motor programs [Review]. Prog Neurobiol 1996; 50(4): 381-425.

Naismith TV, Heuser JE, Breakefield XO, Hanson PI. TorsinA in the nuclear envelope. Proc Natl Acad Sci U S A 2004; 101(20): 7612-7.

Naismith TV, Dalal S, Hanson PI. Interaction of torsinA with its major binding partners is impaired by the dystonia-associated DeltaGAG deletion. J Biol Chem 2009; 284(41): 27866-74.

Napolitano F, Pasqualetti M, Usiello A, Santini E, Pacini G, Sciamanna G, et al. Dopamine D2 receptor dysfunction is rescued by adenosine A2A receptor antagonism in a model of DYT1 dystonia. Neurobiol Dis 2010; 38(3): 434-45.

Nelson AJ, Blake DT, Chen R. Digit-specific aberrations in the primary somatosensory cortex in Writer's cramp. Ann Neurol 2009; 66(2): 146-54.

Nery FC, Zeng J, Niland BP, Hewett J, Farley J, Irimia D, et al. TorsinA binds the KASH domain of nesprins and participates in linkage between nuclear envelope and cytoskeleton. J Cell Sci 2008; 121(Pt 20): 3476-86.

Neychev VK, Fan X, Mitev VI, Hess EJ, Jinnah HA. The basal ganglia and cerebellum interact in the expression of dystonic movement. Brain 2008; 131(Pt 9): 2499-509.

Neychev VK, Gross RE, Lehéricy S, Hess EJ, Jinnah HA. The functional neuroanatomy of dystonia [Review]. Neurobiol Dis 2011; 42(2): 185-201.

Niethammer M, Carbon M, Argyelan M, Eidelberg D. Hereditary dystonia as a neurodevelopmental circuit disorder: Evidence from neuroimaging. Neurobiol Dis 2011; 42(2): 202-9.

O'Riordan S, Raymond D, Lynch T, Saunders-Pullman R, Bressman SB, Hutchinson M. Age at onset as a factor in determining the phenotype of primary torsion dystonia. Neurology 2004; 63(8): 1423-6.

Ofori E, Pasternak O, Planetta PJ, Burciu R, Snyder A, Febo M, et al. Increased free water in the substantia nigra of Parkinson's disease: a single-site and multi-site study. Neurobiol Aging 2015a; 36(2): 1097-104.

Ofori E, Pasternak O, Planetta PJ, Li H, Burciu RG, Snyder AF, et al. Longitudinal changes in free-water within the substantia nigra of Parkinson's disease. Brain 2015b; 138(Pt 8): 2322-31.

Oorschot DE. The percentage of interneurons in the dorsal striatum of the rat, cat, monkey, and human: a critique of the evidence. Basal Ganglia 2013; 3: 19–24.

Opavský R, Hluštík P, Otruba P, Kaňovský P. Somatosensory cortical activation in cervical dystonia and its modulation with botulinum toxin: an fMRI study. Int J Neurosci 2012; 122(1): 45-52.

Ostrem JL, Markun LC, Glass GA, Racine CA, Volz MM, Heath SL, et al. Effect of frequency on subthalamic nucleus deep brain stimulation in primary dystonia. Parkinsonism Relat Disord 2014; 20(4): 432-8.

Ozelius LJ, Hewett JW, Page CE, Bressman SB, Kramer PL, Shalish C, et al. The early-onset torsion dystonia gene (DYT1) encodes an ATP-binding protein. Nat Genet 1997; 17(1): 40-8.

Ozelius L, Lubarr N. DYT1 Early-onset isolated dystonia. In: Adam MP, Ardinger HH, Pagon RA, Wallace SE, Bean LJH, Stephens K, Amemiya A, editors. GeneReviews®. Seattle (WA): University of Washington, Seattle; 1999.

Ozelius LJ, Bressman SB. Genetic and clinical features of primary torsion dystonia [Review]. Neurobiol Dis 2011; 42(2): 127-35.

Ozol K, Hayden JM, Oberdick J, Hawkes R. Transverse zones in the vermis of the mouse cerebellum. J Comp Neurol 1999; 412(1): 95-111.

Panov F, Gologorsky Y, Connors G, Tagliati M, Miravite J, Alterman RL. Deep brain stimulation in DYT1 dystonia: a 10-year experience. Neurosurgery 2013; 73(1): 86-93.

Pappas SS, Darr K, Holley SM, Cepeda C, Mabrouk OS, Wong JM, et al. Forebrain deletion of the dystonia protein torsinA causes dystonic-like movements and loss of striatal cholinergic neurons. Elife 2015; 4: e08352.

Pappas SS, Li J, LeWitt TM, Kim JK, Monani UR, Dauer WT. A cell autonomous torsinA requirement for cholinergic neuron survival and motor control. Elife 2018; 7: e36691.

Pasternak O, Sochen N, Gur Y, Intrator N, Assaf Y. Free water elimination and mapping from diffusion MRI. Magn Reson Med 2009; 62(3): 717-30. doi: 10.1002/mrm.22055.

Pasternak O, Westin CF, Bouix S, Seidman LJ, Goldstein JM, Woo TU, et al. Excessive extracellular volume reveals a neurodegenerative pattern in schizophrenia onset. J Neurosci 2012; 32(48): 17365-72.

Pasternak O, Koerte IK, Bouix S, Fredman E, Sasaki T, Mayinger M, et al. Hockey Concussion Education Project, Part 2. Microstructural white matter alterations in acutely concussed ice hockey players: a longitudinal free-water MRI study. J Neurosurg 2014; 120(4): 873-81.

Paudel R, Kiely A, Li A, Lashley T, Bandopadhyay R, Hardy J, et al. Neuropathological features of genetically confirmed DYT1 dystonia: investigating disease-specific inclusions. Acta Neuropathol Commun 2014; 2: 159.

Peller M, Zeuner KE, Munchau A, Quartarone A, Weiss M, Knutzen A, et al. The basal ganglia are hyperactive during the discrimination of tactile stimuli in writer's cramp. Brain 2006;1 29(Pt 10): 2697-708.

Perlmutter JS, Mink JW. Dysfunction of dopaminergic pathways in dystonia [Review]. Adv Neurol 2004; 94: 163-70.

Pierpaoli C, Jezzard P, Basser PJ, Barnett A, Di Chiro G. Diffusion tensor MR imaging of the human brain. Radiology 1996; 201(3): 637-48.

Pisani A, Martella G, Tscherter A, Bonsi P, Sharma N, Bernardi G, et al. Altered responses to dopaminergic D2 receptor activation and N-type calcium currents in striatal cholinergic interneurons in a mouse model of DYT1 dystonia. Neurobiol Dis 2006; 24(2): 318-25.

Pizoli CE, Jinnah HA, Billingsley ML, Hess EJ. Abnormal cerebellar signaling induces dystonia in mice. J Neurosci 2002; 22(17): 7825-33.

Planetta PJ, Ofori E, Pasternak O, Burciu RG, Shukla P, DeSimone JC, et al. Free-water imaging in Parkinson's disease and atypical parkinsonism. Brain 2016; 139(Pt 2): 495-508.

Prudente CN, Hess EJ, Jinnah HA. Dystonia as a network disorder: what is the role of the cerebellum? [Review]. Neuroscience 2014; 260: 23-35.

Pujol J, Roset-Llobet J, Rosinés-Cubells D, Deus J, Narberhaus B, Valls-Solé J, et al. Brain cortical activation during guitar-induced hand dystonia studied by functional MRI. Neuroimage 2000; 12(3): 257-67.

Raike RS, Pizoli CE, Weisz C, van den Maagdenberg AM, Jinnah HA, Hess EJ. Limited regional cerebellar dysfunction induces focal dystonia in mice. Neurobiol Dis 2013; 49: 200-10.

Richter F, Gerstenberger J, Bauer A, Liang CC, Richter A. Sensorimotor tests unmask a phenotype in the DYT1 knock-in mouse model of dystonia. Behav Brain Res 2017; 317: 536-541.

Ridding MC, Sheean G, Rothwell JC, Inzelberg R, Kujirai T. Changes in the balance between motor cortical excitation and inhibition in focal, task specific dystonia. J Neurol Neurosurg Psychiatry 1995; 59(5): 493-8.

Risch NJ, Bressman SB, deLeon D, Brin MF, Burke RE, Greene PE, et al. Segregation analysis of idiopathic torsion dystonia in Ashkenazi Jews suggests autosomal dominant inheritance. Am J Hum Genet 1990; 46(3): 533-8.

Risch NJ, de Leom D, Ozelius L, Kramer P, Almasy L, Singer B, et al. Genetic analysis of idiopathic torsion dystonia in Ashkenazi Jews and their recent descent from a small founder population. Nat Genet 1995; 9(2): 152-9.

Rostasy K, Augood SJ, Hewett JW, Leung JC, Sasaki H, Ozelius LJ, et al. TorsinA protein and neuropathology in early onset generalized dystonia with GAG deletion. Neurobiol Dis 2003; 12(1): 11-24.

Scarduzio M, Zimmerman CN, Jaunarajs KL, Wang Q, Standaert DG, McMahon LL. Strength of cholinergic tone dictates the polarity of dopamine D2 receptor modulation of striatal cholinergic interneuron excitability in DYT1 dystonia. Exp Neurol 2017; 295: 162-175.

Sciamanna G, Tassone A, Martella G, Mandolesi G, Puglisi F, Cuomo D, et al. Developmental profile of the aberrant dopamine D2 receptor response in striatal cholinergic interneurons in DYT1 dystonia. PLoS One 2011; 6(9): e24261.

Sciamanna G, Tassone A, Mandolesi G, Puglisi F, Ponterio G, Martella G, et al. Cholinergic dysfunction alters synaptic integration between thalamostriatal and corticostriatal inputs in DYT1 dystonia. J Neurosci 2012a; 32(35): 11991-2004.

Sciamanna G, Hollis R, Ball C, Martella G, Tassone A, Marshall A, et al. Cholinergic dysregulation produced by selective inactivation of the dystonia-associated protein torsinA. Neurobiol Dis 2012b; 47(3): 416-27.

Shakkottai VG, Batla A, Bhatia K, Dauer WT, Dresel C, Niethammer M, et al. Current Opinions and Areas of Consensus on the Role of the Cerebellum in Dystonia. Cerebellum 2017; 16(2): 577-594.

Shashidharan P, Sandu D, Potla U, Armata IA, Walker RH, McNaught KS, et al. Transgenic mouse model of early-onset DYT1 dystonia. Hum Mol Genet 2005; 14(1): 125-33.

Simonyan K, Ludlow CL. Abnormal activation of the primary somatosensory cortex in spasmodic dysphonia: an fMRI study. Cereb Cortex 2010; 20(11): 2749-59.

Simonyan K, Ludlow CL. Abnormal structure-function relationship in spasmodic dysphonia. Cereb Cortex 2012; 22(2): 417-25.

Smith Y, Raju DV, Pare JF, Sidibe M. The thalamostriatal system: a highly specific network of the basal ganglia circuitry [Review]. Trends Neurosci 2004; 27(9): 520-7.

Sohn YH, Hallett M. Surround inhibition in human motor system. Exp Brain Res 2004a; 158(4): 397-404.

Sohn YH, Hallett M. Disturbed surround inhibition in focal hand dystonia. Ann Neurol 2004b; 56(4): 595-9.

Song CH, Bernhard D, Bolarinwa C, Hess EJ, Smith Y, Jinnah HA. Subtle microstructural changes of the striatum in a DYT1 knock-in mouse model of dystonia. Neurobiol Dis 2013; 54: 362-71.

Song CH, Bernhard D, Hess EJ, Jinnah HA. Subtle microstructural changes of the cerebellum in a knock-in mouse model of DYT1 dystonia. Neurobiol Dis 2014; 62: 372-80.

Svetel M, Pekmezović T, Jović J, Ivanović N, Dragasević N, Marić J, et al. Spread of primary dystonia in relation to initially affected region. J Neurol 2007; 254(7): 879-83.

Tanabe LM, Kim CE, Alagem N, Dauer WT. Primary dystonia: molecules and mechanisms [Review]. Nat Rev Neurol 2009; 5(11): 598-609.

Tempel LW, Perlmutter JS. Abnormal cortical responses in patients with writer's cramp. Neurology 1993; 43(11):2252-7. Erratum in: Neurology 1994; 44(12): 2411.

Termsarasab P, Thammongkolchai T, Frucht SJ. Medical treatment of dystonia [Review]. J Clin Mov Disord 2016; 3: 19. Erratum in: J Clin Mov Disord 2018; 5: 8.

Thorn CA, Graybiel AM. Differential entrainment and learning-related dynamics of spike and local field potential activity in the sensorimotor and associative striatum. J Neurosci 2014; 34(8): 2845-59.

Torres GE, Sweeney AL, Beaulieu JM, Shashidharan P, Caron MG. Effect of torsinA on membrane proteins reveals a loss of function and a dominant-negative phenotype of the dystonia-associated DeltaE-torsinA mutant. Proc Natl Acad Sci U S A 2004; 101(44): 15650-5.

Trošt M, Carbon M, Edwards C, Ma Y, Raymond D, Mentis MJ, et al. Primary dystonia: is abnormal functional brain architecture linked to genotype?.Ann Neurol 2002; 52(6): 853-6.

Uluğ AM, Vo A, Argyelan M, Tanabe L, Schiffer WK, Dewey S, et al. Cerebellothalamocortical pathway abnormalities in torsinA DYT1 knock-in mice. Proc Natl Acad Sci U S A 2011; 108(16): 6638-43.

van der Kamp W, Berardelli A, Rothwell JC, Thompson PD, Day BL, Marsden CD. Rapid elbow movements in patients with torsion dystonia. J Neurol Neurosurg Psychiatry 1989; 52(9): 1043-9.

Van der Werf YD, Witter MP, Groenewegen HJ. The intralaminar and midline nuclei of the thalamus. Anatomical and functional evidence for participation in processes of arousal and awareness [Review]. Brain Res Brain Res Rev 2002; 39(2-3): 107-40.

Vander Heyden AB, Naismith TV, Snapp EL, Hodzic D, Hanson PI. LULL1 retargets TorsinA to the nuclear envelope revealing an activity that is impaired by the DYT1 dystonia mutation. Mol Biol Cell 2009; 20(11): 2661-72.

Vidailhet M, Vercueil L, Houeto JL, Krystkowiak P, Benabid AL, Cornu P, et al. Bilateral deep-brain stimulation of the globus pallidus in primary generalized dystonia. N Engl J Med 2005; 352(5): 459-67.

Vidailhet M, Jutras MF, Grabli D, Roze E. Deep brain stimulation for dystonia [Review]. J Neurol Neurosurg Psychiatry 2013; 84(9): 1029-42.

Vitek JL, Chockkan V, Zhang JY, Kaneoke Y, Evatt M, DeLong MR, et al. Neuronal activity in the basal ganglia in patients with generalized dystonia and hemiballismus. Ann Neurol 1999; 46(1): 22-35.

Vitek JL. Pathophysiology of dystonia: a neuronal model [Review]. Mov Disord 2002; 17 Suppl 3: S49-62.

Vo A, Sako W, Dewey SL, Eidelberg D, Uluğ AM. 18FDG-microPET and MR DTI findings in Tor1a+/- heterozygous knock-out mice. Neurobiol Dis 2015a; 73: 399-406.

Vo A, Sako W, Niethammer M, Carbon M, Bressman SB, Uluğ AM, et al. Thalamocortical Connectivity Correlates with Phenotypic Variability in Dystonia. Cereb Cortex 2015b; 25(9): 3086-94.

Walter JT, Alviña K, Womack MD, Chevez C, Khodakhah K. Decreases in the precision of Purkinje cell pacemaking cause cerebellar dysfunction and ataxia. Nat Neurosci 2006; 9(3): 389-97.

Wang Y, Wang Q, Haldar JP, Yeh FC, Xie M, Sun P, et al. Quantification of increased cellularity during inflammatory demyelination. Brain 2011; 134(Pt 12): 3590-601.

Wang Z, Kai L, Day M, Ronesi J, Yin HH, Ding J, et al. Dopaminergic control of corticostriatal long-term synaptic depression in medium spiny neurons is mediated by cholinergic interneurons. Neuron 2006; 50(3): 443-52.

Weisheit CE, Dauer WT. A novel conditional knock-in approach defines molecular and circuit effects of the DYT1 dystonia mutation. Hum Mol Genet 2015; 24(22): 6459-72.

Wichmann T. Commentary: Dopaminergic dysfunction in DYT1 dystonia [Review]. Exp Neurol 2008; 212(2): 242-6.

Xiao J, LeDoux MS. Caytaxin deficiency causes generalized dystonia in rats. Brain Res Mol Brain Res 2005; 141(2): 181-92.

Xiao J, Gong S, LeDoux MS. Caytaxin deficiency disrupts signaling pathways in cerebellar cortex. Neuroscience 2007; 144(2): 439-61.

Yokoi F, Dang MT, Mitsui S, Li J, Li Y. Motor deficits and hyperactivity in cerebral cortex-specific Dyt1 conditional knockout mice. J Biochem 2008; 143(1): 39-47.

Yokoi F, Dang MT, Li J, Standaert DG, Li Y. Motor deficits and decreased striatal dopamine receptor 2 binding activity in the striatum-specific Dyt1 conditional knockout mice. PLoS One 2011; 6(9): e24539.

Yokoi F, Dang MT, Li Y. Improved motor performance in Dyt1 ΔGAG heterozygous knock-in mice by cerebellar Purkinje-cell specific Dyt1 conditional knocking-out. Behav Brain Res 2012; 230(2): 389-98.

Yokoi F, Dang MT, Liu J, Gandre JR, Kwon K, Yuen R, et al. Decreased dopamine receptor 1 activity and impaired motor-skill transfer in Dyt1 ΔGAG heterozygous knock-in mice. Behav Brain Res 2015; 279: 202-10.

Zhang H, Schneider T, Wheeler-Kingshott CA, Alexander DC. NODDI: practical in vivo neurite orientation dispersion and density imaging of the human brain. Neuroimage 2012; 61(4): 1000-16.

Zhang L, Yokoi F, Jin YH, DeAndrade MP, Hashimoto K, Standaert DG, et al. Altered dendritic morphology of Purkinje cells in Dyt1 ΔGAG knock-in and purkinje cell-specific Dyt1 conditional knockout mice. PLoS One 2011; 6(3): e18357.

Zhao C, Brown RS, Chase AR, Eisele MR, Schlieker C. Regulation of Torsin ATPases by LAP1 and LULL1. Proc Natl Acad Sci U S A 2013; 110(17): E1545-54.

Zhao Y, Sharma N, LeDoux MS. The DYT1 carrier state increases energy demand in the olivocerebellar network. Neuroscience 2011; 177: 183-94.

Zhou B, Wang J, Huang Y, Yang Y, Gong Q, Zhou D. A resting state functional magnetic resonance imaging study of patients with benign essential blepharospasm. J Neuroophthalmol 2013; 33(3): 235-40.

Zhuang P, Li Y, Hallett M. Neuronal activity in the basal ganglia and thalamus in patients with dystonia. Clin Neurophysiol 2004; 115(11): 2542-57.

Zilber N, Inzelberg R, Kahana E, Korczyn AD. Natural course of idiopathic torsion dystonia among Jews. Neuroepidemiology 1994; 13(5): 195-201.

BIOGRAPHICAL SKETCH

Jesse DeSimone obtained his Bachelor of Kinesiology with honours from Brock University (St. Catharines, ON, Canada) and Master of Science in kinesiology with a research focus in visuomotor behavior from the University of Western Ontario (London, ON, Canada). He received doctoral training in motor control and neuroimaging at the University of Florida (Gainesville, FL, USA) and was awarded his Ph.D. in August 2019. Jesse's primary research interests include the neuronal mechanisms underlying executive function and goal-directed motor planning and control, and how these mechanisms are affected by neurological disease.